OVEREXPRESSION OF CHITOTRIOSIDASE-1 MODULATES MACROPHAGE FUNCTION AND ALTERS PLAQUE MORPHOLOGY IN HYPERLIPIDEMIC MICE

A THESIS SUBMITTED TO THE GRADUATE DIVISION OF THE UNIVERSITY OF HAWAII AT MĀNOA IN PARTIAL FULFILLMENT FOR THE DEGREE OF

DOCTOR OF PHILOSOPHY

IN

CELL AND MOLECULAR BIOLOGY

MAY 2019

BY

JONATHAN YAP

Dissertation Committee:

William Boisvert, Chairperson

Mariana Gerschenson

Takashi Matsui

Ben Fogelgren

Saguna Verma

ACKNOWLEDGMENTS

I would like to acknowledge my doctoral advisor, Dr. William Boisvert for giving me the opportunity and guidance not only to explore my scientific endeavors, but also to develop my character and a genuine sense of belonging and self-worth. I would like to further extend my gratitude to Dr. Takashi Matsui, Dr. Mariana Gerschenson, Dr. Ben Fogelgren, and Dr. Saguna Verma for your mentorship, encouragement, and dedication as members of my committee.

I would like to acknowledge the incredible faculty, colleagues, and fellow students at JABSOM. Words cannot express how truly grateful I am to have been surrounded by such outstanding individuals. I've never felt more welcomed and empowered. I sincerely thank all of those who have been part of my unique journey. I would like to mention Dr. Ralph Shohet in appreciation of his optimistic inclusiveness and pragmatic solutions to further my career.

As long as I have been at this institution, I have felt like a family member in the Boisvert Lab. I'm thankful to have worked and studied alongside Dr. Sara McCurdy. She has been an exemplary role model. Thanks to her selfless dedication, I'm truly a better person. I would especially like to thank the technicians that have been so integral in allowing me to conduct scientific research. Both in and away from the lab, Monica Montgomery, Whitney Regan, Jan Garo, and Jason Irei have each provided me with treasured friendships and have lent themselves to the pursuit of my happiness.

I would like to thank Dr. Shiro Kitamoto for his time and willingness to assist me in the completion of this project. His insight and patience were invaluable to the progress of my work. Further, this work would not have been possible without funding from the NIH. I would like to thank the NIH for funding my time as a student both as a trainee and pre-doctoral fellow.

Lastly, to my family and friends; words cannot describe how grateful I am for your unrelenting encouragement and support. Thank you for keeping it real and for helping me to live life like a "real boy". I would like to thank my brothers for always reassuring me that I am on the right path. And most importantly, my mom Chiquita Chow whose unwavering devotion enabled me to overcome impossible odds in becoming the person I'm supposed to be.

ABSTRACT

Cardiovascular diseases (CVD) are the leading cause of mortality in the world. Responsible for nearly 1/3 of all deaths globally, CVD poses extreme public health challenges and a growing economic burden. Atherosclerosis is fundamental to CVD, and is characterized by the accumulation of plaque within arterial blood vessels. Atherosclerotic plaques are the result of lipid deposition in the subendothelial space, which initiates monocyte infiltration and formation of lipid-laden foam cells derived from macrophages. The inflammatory cascade that follows, promotes plaque formation and development. Disease progression ultimately leads to a number of atherosclerotic pathologies including myocardial infarction and ischemic stroke. Clearly, our greatest efforts are required in exploring novel therapeutic perspectives that ameliorate inflammation and prevent dysfunctional cholesterol metabolism.

My work has been directed at investigating the potential role of macrophage chitotriosidase-1 (CHIT1) overexpression in dampening production of pro-inflammatory cytokines and inhibiting macrophage foam cell formation. We generated an atherosclerotic mouse model constitutively overexpressing CHIT1 by crossing hyperlipidemic *Ldl-r*$^{-/-}$ mice with transgenic, CHIT1 overexpressing mice. We carried out *in vitro* experiments aimed at elucidating the effect of CHIT1 overexpression on macrophage inflammatory mechanisms, cholesterol metabolism, and invasion. *In vitro*, macrophage overexpression resulted in diminished mRNA transcription of important pro-inflammatory mediators and increased expression of cytokines involved in immune cell migration and anti-inflammatory processes. We also observed that CHIT1 overexpression in BMDM enhanced macrophage invasiveness. The CHIT1-overexpressing, atherosclerotic mouse model (*Ldlr*$^{-/-}$-CHIT1-OE) facilitated a long-term *in vivo* mouse study. Animals in the study were fed a high-fat diet for 12 weeks which resulted in robust atherosclerotic progression. Although CHIT1 overexpression in *Ldlr*$^{-/-}$ mice did not affect plaque development when compared to control mice, we were able to observe significant differences in plaque morphology related to the deposition of ECM components. This unexpected finding may suggest that CHIT1 overexpression

affects plaque stability in atherosclerotic mice. The possibility of CHIT1 mediated athero-protection may in fact lie in its ability to augment ECM composition in atherosclerotic plaques.

LIST OF FIGURES

LIST OF TABLES

LIST OF ABBREVIATIONS

CHIT1: Macrophage chitotriosidase-1

BHABP: Biotinylated hyaluronic acid binding protein

HA-tag: human influenza hemagglutinin sequence

Tg: Transgenic

°C: degree Celsius

PBS: phosphate buffered saline

BSA: Bovine serum albumin

HRP: Horse radish peroxidase

EDTA: ethylenediaminestetraacetate

FBS: fetal bovine serum

HEPES: 2-[4-(2-hydroxyethyl)piperazin-1-yl]ethanesulfonic acid

DMSO: dimethyl sulfoxide

PVDF: polyvinyl difluoride

Ac-LDL: Acetylated low density lipoprotein

Ox-LDL: Oxidized low density lipoprotein

BCA: Bicinchoinic acid

SMA: Smooth muscle actin

TABLE OF CONTENTS

CHAPTER 1: INTRODUCTION

1.1 Cardiovascular disease burden

Cardiovascular disease (CVD) is a term that describes a group of pathologies affecting the heart and blood vessels. Diseased and damaged blood vessels supplying the heart muscle, the brain, arms and legs, as well as myocardial and valvular damage manifests in specific etiologies. Coronary heart disease, cerebral vascular disease, peripheral artery disease, and others are extremely complex maladies associated with the more general CVD.

CVD is the leading cause of mortality worldwide. In 2015, CVD claimed an estimated 17.7 million lives accounting for nearly 1/3 of all global deaths [1, 2]. In the United States alone approximately 801,000 Americans die from heart disease each year. Responsible for 1 in every 3 deaths, CVD is the leading cause of death for both men and women in America [3].

1.1.2 Economic burden

In 2015 the estimated global cost of CVD's in terms of lost productivity and healthcare expenses reached $906 billion [1]. According to the same metrics, the American Heart Association estimates that in 2017 the economic burden of CVD in the United States is $306 billion. Advancements in medical technology, pharmaceuticals, and education have been integral to the declining CVD-related mortality rates among industrialized countries. The trend continues domestically where total mortality decreased 3.79% between 2000-2011. However, this decline in mortality decelerated during 2011-2014 to just 0.23% [3]. It appears likely that while awareness of major cardiovascular risk factors like elevated cholesterol, hypertension, and smoking is increasing, they are also being replaced with other risk factors including obesity and diabetes. This disturbing trend is only compounded from an epidemiological fact that prevalence of CVD mortality is increasing among developing and low income countries. By 2030 the total economic burden felt worldwide is expected to meet or exceed $1 trillion [4].

Through novel pharmaceutical therapies, innovative medical interventions, and greater awareness of personal risk factors, much progress has been made in the way of slowing mortality rates. Yet even now, the unprecedented cost of CVD in economic terms and more importantly in lives, implores us to seek a more profound and lucid comprehension of the molecular mechanisms involved in these diseases. Extensive research is required in the effort to ameliorate the extensive impact of CVD.

1.2 Atherosclerosis-causes and risk factors

Atherosclerosis describes a condition caused by the hardening of blood vessels due to the accumulation of lipids and immune cells within the lining of the vasculature [5]. These deposits develop into plaque over time which reduce blood vessel elasticity, compromise blood flow to the heart and brain, and are risk factors for thrombotic events [6, 7]. Occlusion of blood vessels can cause ischemia in the heart and brain as well as hypertension throughout the circulatory system. Elevated blood pressure loosens and dislodges parts of vulnerable plaques. When these fragments enter the circulation they can cause a blockage of vital arteries that supply the heart and brain resulting in myocardial infarction (MI) and stroke respectively [8, 9]. Although thrombolytic agents can be administered to patients experiencing stroke and MI in an effort to restore blood flow, it is often too late to avoid serious tissue or brain damage due mostly in part to lack of oxygen for extended periods of time [10].

Risk factors for atherosclerosis are generally classified into 2 categories: modifiable and non-modifiable. Modifiable risk factors are environmental components which contribute to the development and progression of atherosclerosis [11, 12]. This type of risk factor includes: tobacco use, excessive alcohol consumption, sedentary lifestyle, hypercholesterolemia, hypertension, and metabolic conditions like diabetes mellitus and obesity [13-15]. Modifiable risk factors can be mitigated by the individual to prevent onset of atherosclerosis and/or impede its progress. Some risk factors however, cannot be altered with behavioral and lifestyle changes. Such risk factors are referred to as non-modifiable. Age, sex, and genetic traits comprise the category of non-modifiable risk factors. It has been well documented that risk for CVD,

and more specifically atherosclerosis, increases with age [16, 17]. Furthermore, men are more likely to be diagnosed with atherosclerosis at an earlier age than women [18, 19]. Studies suggest that at least some portion of gender-related risk factors for atherosclerosis can be attributed to physiological differences between men and women. For example, women tend to have a smaller carotid arteries exhibiting less plaque but a greater degree of stenosis possibly affecting angiogenesis and vascular remodeling [20]. Protective effects of hormones, like progesterone in women, may also contribute to the overall disparity in disease prevalence between the sexes [21, 22]. Others have demonstrated age-dependent effects of estrogen on atherosclerosis.. Administration of 17β-estradiol (E2) exhibited atheroprotective effects in young female mice and postmenopausal women. However, the same effect was not observed in older animals or postmenopausal women [23]. Preliminary studies with human macrophages show that estrogen receptor-α (ERα) is diminished in postmenopausal women compared to premenopausal women. Moreover, E2 hormone therapy beginning at menopause maintained ERα expression levels equivalent to premenopausal women. E2 also attenuated CRP dependent inflammatory responses in macrophages from premenopausal women but not in those derived from premenopausal women [24, 25].

The genetic basis of CVD and coronary artery disease (CAD) is exhibited in rare Mendelian disorders that cause premature onset of the disease. The mutations mostly affect cellular lipid and cholesterol handling mechanisms. Examples of these heritable conditions are: familial hypercholesterolemia, familial defective APOB, APOA1 deficiency, and Tangier disease [26]. In recent years, genome-wide association studies (GWAS) have produced robust data and profound new insight into the genomic architecture of susceptibility to CVD [27]. Innovative genetic-epidemiological research utilizing GWAS has demonstrated an association between the regulation of specific genes like SORT1, which is implicated in the production of very low-density lipoprotein (VLDL), and ANRIL, a long non-coding RNA that appears to regulate genes that are adjacent to it [28]. A deficiency in one of these genes, Cdkn2a,

caused atherosclerotic lesion development and monocyte proliferation in a mouse model for atherosclerosis.

1.3 Molecular mechanisms of atherosclerosis

The development of atherosclerosis is initiated by elevated levels of circulating lipids in the vasculature. These lipids subsequently accumulate in the subendothelial space, beneath the intima where they become trapped within the extracellular matrix [29, 30]. Immobilized lipids can be modified by reactive oxygen species (ROS) and various enzymes [31]. Modified LDL activates smooth muscle cells (SMC) and endothelial cells (EC) lining the arteries, which under normal conditions are resistant to immune cell attachment, but begin to express adhesion molecules [32, 33]. Cell-surface proteins like vascular cell adhesion molecule (VCAM) and intracellular cell adhesion molecule (ICAM) facilitate monocyte tethering and diapedesis. Activated ECs also secrete chemokines like monocyte chemoattractant protein-1 (MCP-1), and the growth factors: macrophage-colony stimulating factor (M-CSF) and granulocyte-macrophage colony stimulating factor (GM-CSF) [34].

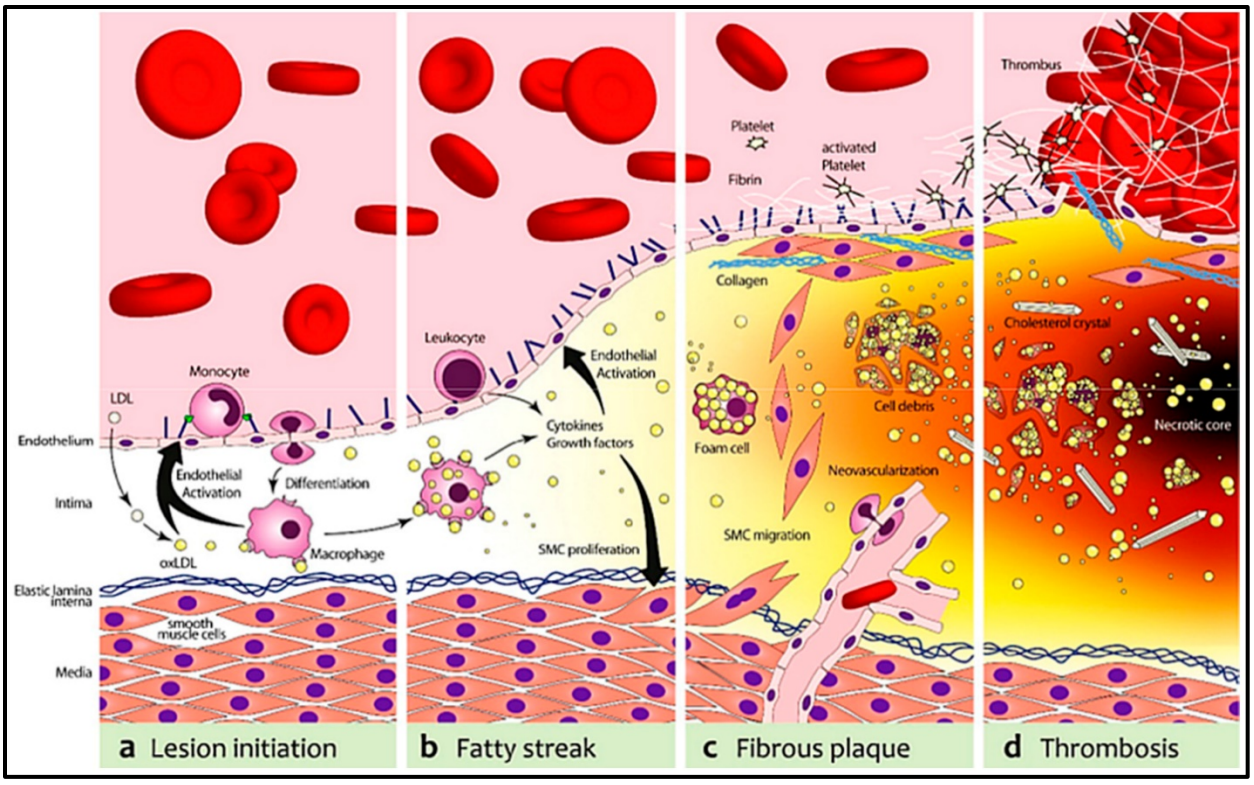

(Gargiulo et al., 2016 International Journal of Molecular Sciences)

Figure 1: Development and progression of atherosclerosis.

(A) *The initial stages of atherosclerosis are characterized by lesion formation, during which circulating LDL becomes trapped in the subendothelial ECM.* ***(B)*** *While sequestered, modification of LDL by reactive oxygen species (ROS) and various enzymes result in pro-inflammatory LDL particles. Endothelial cell activation, mediates the expression of adhesion molecules: P-selectin, VCAM-1, and ICAM-1. Activated endothelial cells subsequently initiate tethering and rolling of circulating monocytes through expression of P-selectin. After infiltrating the vascular intima, monocytes differentiate into macrophages that uptake and accumulate modified LDL. Macrophages, unable to maintain homeostatic cholesterol metabolism, become lipid-laden foam cells. Foam cell aggregation is referred to as a "fatty streak".* ***(C)*** *Migration and proliferation of smooth muscle cells assist in the formation of a fibrous cap around the luminal side of the plaque, contributing to stability. Vulnerable plaques are prone to rupture and are characterized by defective efferocytosis, necrotic core development, and fibrous cap thinning.* ***(D)*** *Metabolically dysfunctional macrophages together with necrosis, release proteolytic enzymes thinning the protective fibrous cap. Matrix metalloproteinases (MMPs) produced by macrophages degrade various types of ECM protein resulting in fibrous cap erosion and plaque rupture.*

In concert with adhesion molecules, chemokines and growth factors initiate recruitment, infiltration, and proliferation of immune cells in the subendothelial space. A “fatty streak” is the earliest visual indication of lesion formation. Its appearance is the result of an innate immune response that recruits monocytes to regions of lipoprotein deposition [36]. Monocytes differentiate into macrophages within the intima and uptake modified lipoproteins. Enhanced phagocytosis and dysfunctional cellular metabolism of modified lipoproteins causes macrophages to become lipid-laden foam cells [37]. Foam cells and macrophages secrete inflammatory and cytotoxic substances as well as chemotactic cytokines thereby contributing to a chronic state of inflammation and macrophage activation [38]. The accumulation of modified lipoproteins, macrophage-derived foam cells, leukocytes, ECs and, SMCs over time results in atherosclerotic plaque formation [39]. Atheromatous plaques are initially stabilized by vascular smooth muscle cells. SMCs migrate and proliferate on the luminal aspect of the plaque where, over time, they form a fibrous cap [40]. In a stable plaque, the fibrous cap is reinforced with molecules that comprise the ECM like collagen and elastin [41]. Stability, however, can be compromised in vulnerable plaques where persisting high levels of circulating LDL exacerbates the inflammatory environment. Apoptosis and secondary necrosis of SMCs and lipid-laden foam cells signify early stages of necrotic core formation within the vulnerable plaque [42]. Dead cells, cell debris, and modified lipid deposits continue to promote necrotic core development eventually leading to acellular, lipid-rich regions in the plaque [43, 44]. The cytotoxic milieu contained within, continues to activate infiltrating macrophages which, in turn, produce high levels of matrix-metalloproteinases (MMP). Thinning of the fibrous cap encapsulating vulnerable plaques are further destabilized by MMPs secreted by classically activated macrophages (M1), which degrades the collagen matrix leading to extreme weakening of the protective cap [45, 46]. MMPs are capable of completely degrading collagen and ECM, they are also implicated in modifications to soluble, cell surface proteins like cytokines and chemokines responsible for processes related to migration, proliferation, and death of immune cells [47]. Numerous publications have consistently

demonstrated the colocalization of MMPs with vulnerable plaques. MMP-knockout mice and transgenic mouse models that overexpress tissue inhibitors of MMPs (TIMP) exhibit diminished atherosclerosis [48, 49]. Mechanical stress related to vascular stenosis, along with shear stress, and reduced elasticity can cause rupture of vulnerable plaques resulting in severe downstream pathologies including ischemic stroke and myocardial infarction [45, 50].

1.4 Macrophages in Atherosclerosis

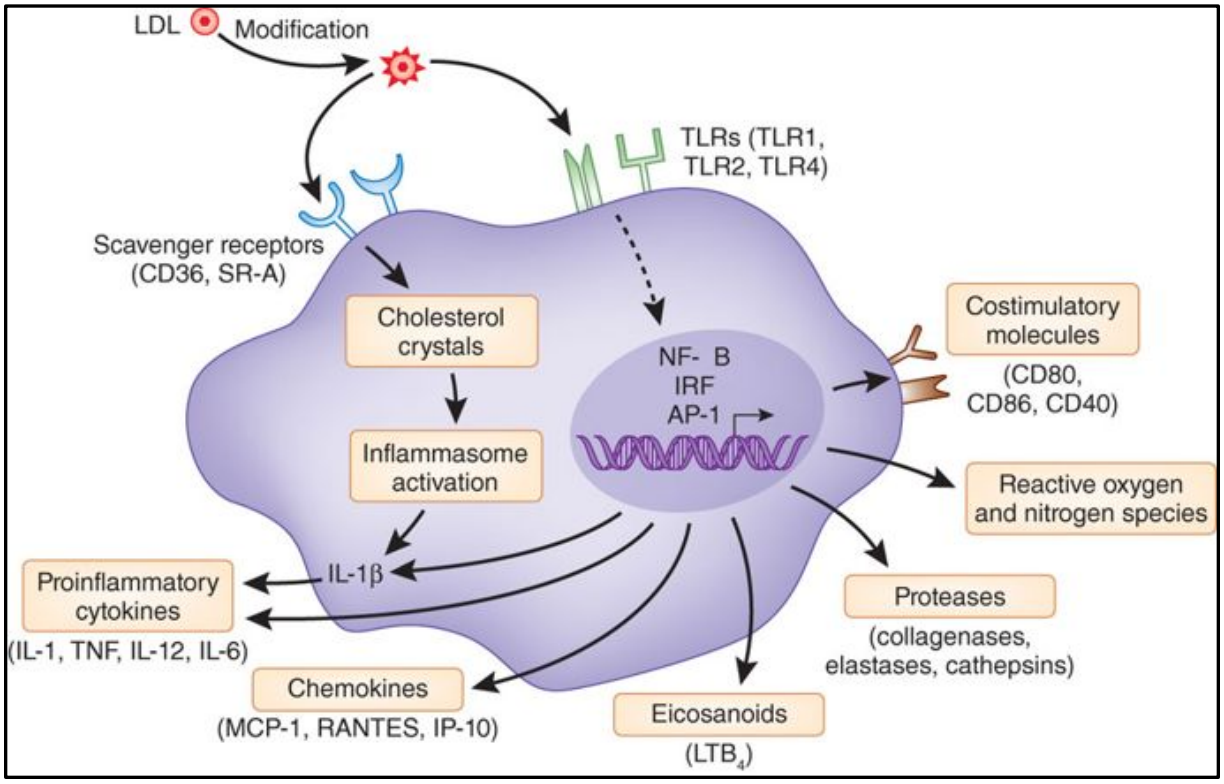

(Hansson et al., 2011, Nature Immunology)

Figure 2: Modified LDL uptake and inflammation.

Modified LDL interacts with cell surface receptors triggering an inflammatory cascade. This results in the activation of various inflammatory pathways. Secretion of pro-inflammatory cytokines via IL-1β signaling and transcription of chemokines are examples of the downstream effects of modified LDL uptake by macrophages. Gene transcription of proteases contribute to plaque instability, while reactive oxygen species and nitrogen species accelerate the development and progression of atherosclerosis.

Macrophage is the determinate cell type in all phases of atherosclerosis. During a typical immune response, recognition and phagocytosis of pathogens are the primary roles for resident and recruited macrophages. Clearance of the inflammatory stimuli and cessation of immune cell activity marks the resolution of acute inflammation. In atherosclerosis, however, macrophages display significantly altered functionality and behavior. Chronic inflammation is a hallmark of atherosclerosis. As a result of constant activation, macrophages exhibit extreme phenotypes of M1 polarization. So-called M1 macrophages display elevated lipid uptake by scavenger receptors; CD36 and SRA1. At the same time, activated macrophages secrete exaggerated amounts of cytokines and chemokines leading to further recruitment and polarization. Phagocytosis of modified LDL exposes the detrimental effects of improper lipid handling of macrophages in and around atherosclerotic plaques. Without adequate clearance of inflammatory LDL particles, dysfunctional macrophages, dead cells, and cell debris, accumulate in the microenvironment of an atherosclerotic plaque and promotes chronic inflammation largely through continuous infiltration, activation, and functional modification of macrophages.

1.4.1 Macrophages Polarization

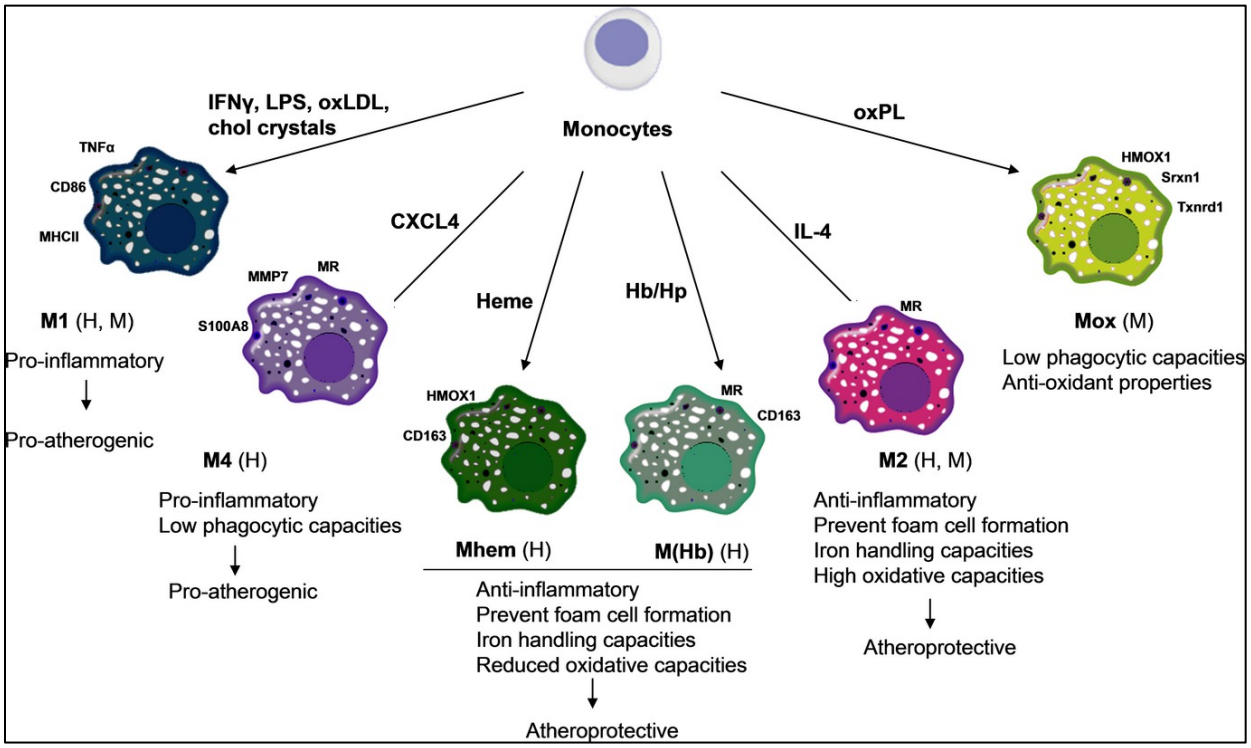

(Colin et al., 2014, Immunol Rev.)

Figure 3: Macrophage polarization in atherosclerosis.

Under atherosclerotic conditions, monocytes are recruited to lesions sites where they differentiate into macrophages. Phenotypic heterogeneity of macrophages is dependent on their activation states. Classically activated, pro-inflammatory macrophages (M1) are the predominant cell type in atherosclerotic plaques. On the other hand, M2, Mhem, and M(Hb) macrophages are alternatively activated, exhibiting anti-inflammatory properties that are indicative of their atheroprotective nature.

Macrophage polarization is a dynamic process that describes phenotypic changes in macrophage function related to inflammatory stimuli. The generalized M1/M2 nomenclature given to macrophages in differential inflammatory mechanisms was derived from the Th1 and Th2 lymphocyte classification relating to their respective pro-inflammatory and anti-inflammatory properties. *In vitro* polarization of macrophages is achieved through stimulation of toll like receptors (TLRs) by LPS and IFN-γ. M1-activated macrophages express a myriad of pro-inflammatory mediators. For example, inducible nitric oxide synthase (iNOS), tumor necrosis factor-alpha (TNF-α), proteolytic enzymes (i.e. MMPs), and cytokines of

the interleukin family: IL-1β, IL-6, and IL-12 [53]. Chemokines like Granulocyte-Macrophage-Colony Stimulating Factor (GM-CSF) and Monocyte Chemoattractant Protein-1 (MCP-1) are also secreted by M1 macrophages, thereby contributing to the continued recruitment and retention of immune cells [54, 55]. Experimental evidence suggests that chronic overabundance of M1 macrophages alters inflammatory conditions in and around the atherosclerotic plaque micro-environment. M1 activated macrophages are associated with enhanced plaque progression, necrotic core development, and destabilization of the fibrous cap due to degradation of collagen and other ECM constituents [56-58].

At the other end of the macrophage polarization spectrum are M2-activated macrophages. M2 macrophages most often exhibit anti-inflammatory properties. Differentiation of M2 macrophages is achieved, *in vitro*, by stimulation with Th2 cytokines; IL-4 and IL-13, and the T regulatory cell (Treg) cytokine; IL-10 [53, 59]. The expression of anti-inflammatory mediators characterizes M2 activated macrophages. Increased expression of transforming growth factor-β (TGF-β), arginase-1 (Arg-1), mannose receptor-1, and IL-10 distinguish M2 macrophages from their pro-inflammatory, M1 counterpart [60, 61]. Increased collagen production is also a function of M2 activation as it contributes to wound healing and tissue repair [62]. Despite being largely antagonistic in function to M1 macrophages, the M2 phenotype is still in a state of “activation”. An M2 immune response is elicited by pathogens-associated molecular patterns (PAMPs), I.e. Allergic reactions and other instances of host defense against PAMP-containing pathogens as is the case in fungal infection and parasitic invasion [63, 64]. M1 and M2 immune functions differ in that the latter is typically less severe on host tissues and more chronic in duration, while the former is more acute, less discriminating, and under normal conditions resolves itself resulting in wound healing and tissue repair. It has been well-reported that populations of both M1 and M2 macrophages are present in and around the atherosclerotic plaque, and that phenotypic switching regularly occurs during plaque progression [65-67]. Over time, a disproportionate fraction of the macrophage population favors proliferation of M1 activation, increasing the risk for plaque rupture and thrombosis. M2 macrophages

are more prevalent in the early atheroma stages, however, in advanced plaques M2 macrophage abundance is directly related to plaque stability and asymptomatic plaque development [46, 68]. The polarization of macrophages, *in vitro*, using Th1 and Th2 cytokines effectively illustrates the plasticity of this cell type. Yet, it is also clear that, *in vivo*, the complex pathophysiology of atherosclerosis results in differentiation of diverse macrophage phenotypes. For example, a macrophage with an entirely unique activation profile from either M1 or M2 is induced by oxidized phospholipids. Termed Mox, it is a macrophage phenotype that is associated with increased expression of nuclear respiratory factor 2 (NRF2)-dependent genes and reactive oxygen species [69]. In another phenotypically divergent instance, targeted deletion of Kruppel-like factor 4 (KLF4) resulted in enhanced Nf-κB activity and VCAM1 [70]. Significant downstream effects include inhibition of M2 and promotion of M1 activated macrophages, over-stimulated differentiation of M1 macrophages, and accelerated atherosclerosis progression in apoe$^{-/-}$ mice. Understanding macrophage biology in the context of atherosclerosis is fundamental to ameliorating the development and progression of this metabolic inflammatory disease. Therefore, given the atherogenic conditions that ultimately become the chronic state of inflammation associated with atherosclerosis, there is a clearly relationship with perhaps the earliest determinant of inflammation; hypercholesterolemia, or elevated levels of circulating cholesterol.

1.4.2 Lipid Homeostasis in Macrophages

Plaque formation and development in atherosclerosis is driven by an inflammatory response to LDL particles trapped within the subendothelial space of the intima. While sequestered in the extracellular matrix, the LDL can be modified in such a way that macrophages are unable to properly metabolize the modified lipids. Increased uptake coupled with impaired efflux of cholesterol by macrophages disrupts reverse cholesterol transport (RCT) resulting in lipid-laden foam cells. Accumulation of foam cells is indicative of the pathophysiology associated with atherosclerosis [37].

Macrophage internalization of cholesterol is achieved through several different pathways. Modified lipoproteins are an inflammatory stimulus, which causes macrophages to express high levels of scavenger receptors that facilitate phagocytosis of oxidatively modified LDL. Moreover, macrophages possess receptors that also promote intracellular cholesterol accumulation [71, 72]. Scavenger receptors are located on the cell surface and mediate the functional mechanisms of phagocytosis, endocytosis, adhesion, and signaling [73]. Class A-1 scavenger receptor (SR-A1) was identified based on its ability to induce foam cell formation, and is highly expressed in macrophage-derived foam cells within atherosclerotic plaques [74]. Ligands for SR-A1 derive from a wide range of polyanionic macromolecules. SR-A1 receptors preferentially bind acetylated LDL (Ac-LDL) *in vitro*. Macrophage-mediated uptake of modified LDL is achieved in part by SR-A1 [75]. Knockdown of the SR-A1 scavenger receptor in both LDLr-/- and Apoe$^{-/-}$ led to a reduction in foam cell formation and atherosclerosis progression [76, 77]. Similar pro-atherogenic results observed in LDL$^{-/-}$ mice reconstituted with SR-A1$^{-/-}$ hematopoietic fetal liver cells demonstrates an important role for macrophage expression of SR-A1 with atherosclerosis [78]. Another scavenger receptor, CD 36, as a high affinity for oxidized LDL (ox-LDL) and has also been shown to bind minimally modified LDL species [79].

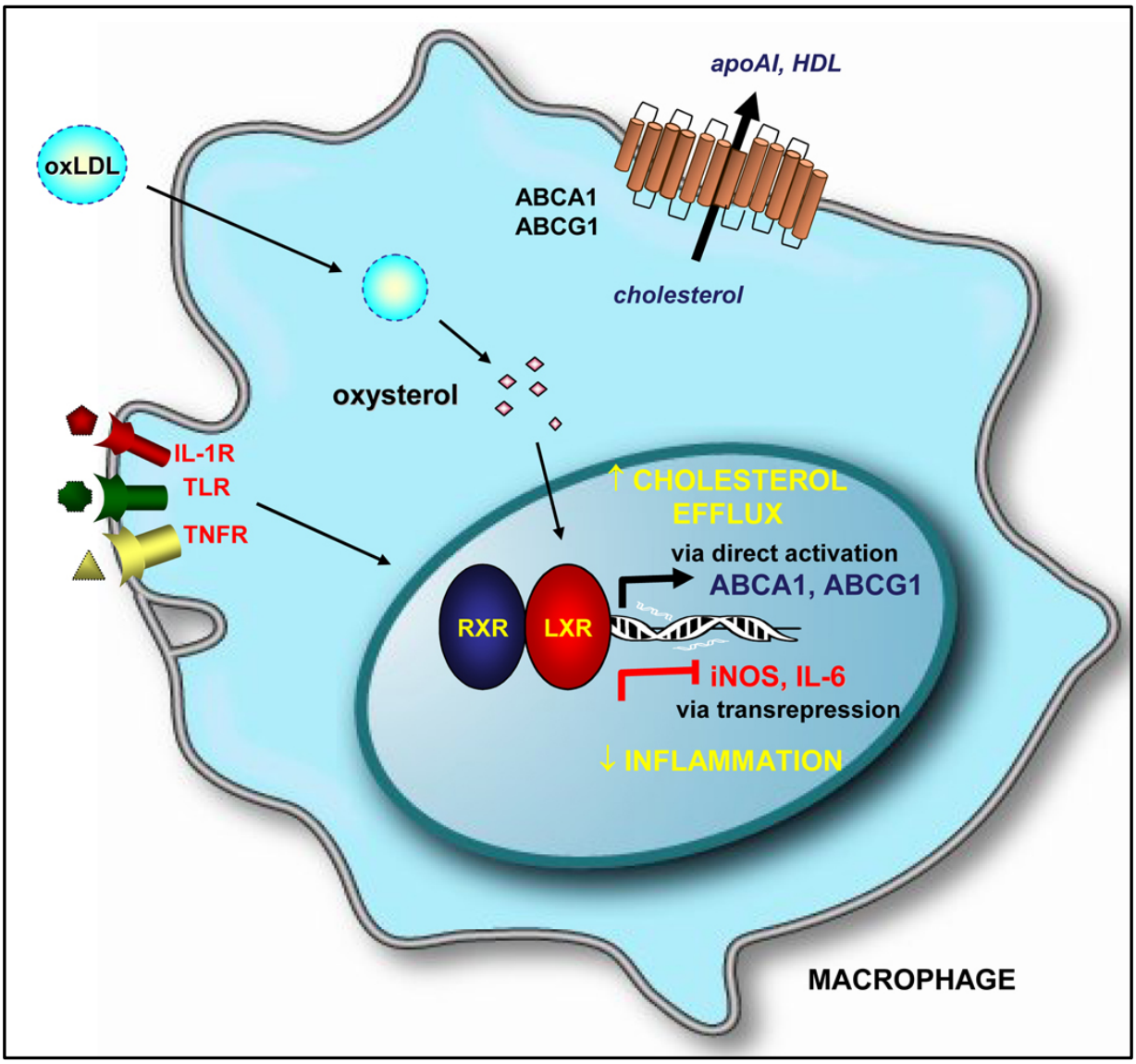

(Hong et al., 2008, Curr Opin Gen Dev)

Figure 4: Cholesterol homoeostasis in macrophages.

Atherosclerosis is characterized by dysfunctional cholesterol metabolism of modified LDL. Receptor-mediated lipid accumulation in macrophages is initiated by PRRs that bind to PAMPs/DAMPs. Cholesterol transport proteins ABCA1 and ABCG1 are down regulated in atherosclerosis, thereby preventing proper efferocytosis. Activation of LXR also dampens the expression of inflammatory genes. Dysfunction in the cellular processes eventually leads to foam cell formation and cell death.

A member of the pattern-recognition receptor family (PRR), toll-like receptors (TLRs) also participate in macrophage-mediated lipid uptake. During an innate immune response, TLRs recognize

molecular patterns related to pathogenicity and/ or cell damage. Pathogen-associated molecular patterns (PAMPs) and damage-associated molecular patterns (DAMPs) typically derive from exogenous stimuli like lipopolysaccharide (LPS) and peptidoglycans. However, ox-LDL, ECM fragments, and HMGB1 are examples of endogenous PAMPs and DAMPs which activate signal transduction pathways that mediate atherogenic inflammation and plaque progression [81, 82].

Receptor-mediated lipid accumulation in macrophages and subsequent foam cell formation is a characteristic feature of atherosclerosis. At the same time, other mechanisms that govern the release of excess cholesterol and its transport by extracellular acceptors counteract atherogenic lipid uptake. ATP binding cassette A1 (ABCA1) is an intracellular transport protein found in macrophages that is upregulated by lipid loading. ABCA1 activity results in efflux of unesterified, free cholesterol (FC) and phospholipids (PL) to lipid-poor and/or lipid-free apoA-1 which is the major protein component of HDL [83, 84]. FC and PL efflux occurs simultaneously through an additional pathway that relies on ATP-binding cassette G1 (ABCG1). ABCG1 releases FC and PL to mature HDL as a lipid acceptor but not to lipid-poor or lipid free apoA-1. The compensatory action of ABCA1 and ABCG1 have been attributed to the varied effects observed while studying either single knockout [85]. However, research has demonstrated that bone marrow (BM) generated from ABCA1/ABCG1 double knockout mice transplanted into LDL receptor knockout ($LDLr^{-/-}$) mice exhibited accelerated atherosclerosis when fed a high-fat diet [86]. Further, [87] macrophage specific $ABCA1^{-/-}$ and $ABCG1^{-/-}$ ($MAC\text{-}ABC^{DKO}$) BM transplanted into $LDL^{-/-}$ hosts not only had disproportionate atherosclerosis compared to wild type controls, but lesional macrophages displayed enhanced inflammatory gene expression as well.

1.4.3 Therapeutics:

Monocytes/macrophages are present in all stages of atherosclerosis and are the determinate cells throughout the atherosclerotic inflammatory response and plaque development. As such, therapeutic

interventions targeting monocyte/macrophage-related processes is imperative in prevention, cessation, and regression of atherosclerotic pathophysiology.

Monocyte/macrophage recruitment and infiltration of the vascular endothelium are the initial steps in early lesion formation. Vascular adhesion molecule-1 (VCAM-1) plays an important part in this process through endothelium-leukocyte interactions. Antibody-derived VCAM-1 inhibition prevented leukocyte adhesion and transmigration *in vitro*, and reduced atherosclerosis in Apoe$^{-/-}$ mouse models [87]. Activated macrophages within the atherosclerotic plaque express interleukin-1 (IL-1) as 2 distinct isoforms IL-1α and IL-1β. While IL-1α generally remains associated with the cell surface, IL-1β has effector functions in several different cell types including: increased proliferation and MMP release by smooth muscle cells, degradation of vascular endothelial cells, and increased expression of MMPs and other proteolytic enzymes by macrophages [88]. Canakinumab is a monoclonal anti-human IL-1β antibody which is currently being evaluated in the Canakinumab Anti-inflammatory Thrombosis Outcomes Study (CANTOS). Evaluation of Canakinumab efficacy in human patients revealed a dose -dependent reduction of greater than 50% for IL-6 and C-reactive protein [89, 90]. Several reports have indicated that IL-6 accelerates atherosclerosis. Under atherosclerotic conditions, activated macrophages produce IL-6 which stimulates expression of CRP, contributes to further macrophage activation, and exerts chemotactic effects that result in increased recruitment and accumulation of leukocytes [91, 92]. It has also been demonstrated that IL-6 administered to Apoe$^{-/-}$ mice via injection enhanced atherosclerosis progression [93].

In recent years, the use of micro RNAs (miRNA) as a therapeutic agent has provided a novel intervention for a myriad of diseases and disorders. miRNAs are short sequences of non-coding RNA, located within the introns or intergenic regions of protein coding genes. Co-transcription of miRNAs and their host genes is a function of their genomic proximity. Initially transcribed as pre-miRNAs, they are processed by enzymatic proteins (i.e. DROSHA, PASHA, DICER) which convert them into their bioactive form that is capable of binding to target mRNA sequences via the RNA-induced silencing complex (RISC)

[94-96]. MicroRNA-155 (MiR-155) is upregulated in the serum of atherosclerotic patients and in PMA-stimulated THP-1 cells treated with ox-LDL. Moreover, transfection of THP-1 macrophages with a synthesized miR-155 mimic or inhibitor was performed to explore the effect of miR-155 overexpression and knockdown respectively [97]. Following treatment with ox-LDL, macrophage overexpression of miR-155 resulted in attenuated lipid uptake, suppression of foam cell formation, and decreased TNF-α expression. Inhibition of miR-155 led to inverse effects on lipid uptake, foam cell formation, and TNF-α expression.

Therapeutic intervention aimed at macrophage function remains a vast opportunity for novel approaches to disease prevention, cessation, and regression. New techniques that are unprecedented in their sophistication and elegance have given researchers the tools to search for a more expansive understanding of disease states and macrophage-related pathogenesis.

1.5 Chitotriosidase

Chitin is among the most abundant biopolymers in nature, second only to cellulose. It is a linear polysaccharide made up of repeating N-acetyl-D-glucosamine (GlcNAC) monomers. Chitin functions as the primary structural component in the exoskeleton of arthropods, and is produced by mollusks, crustaceans, fungi, and nematodes as well [98].

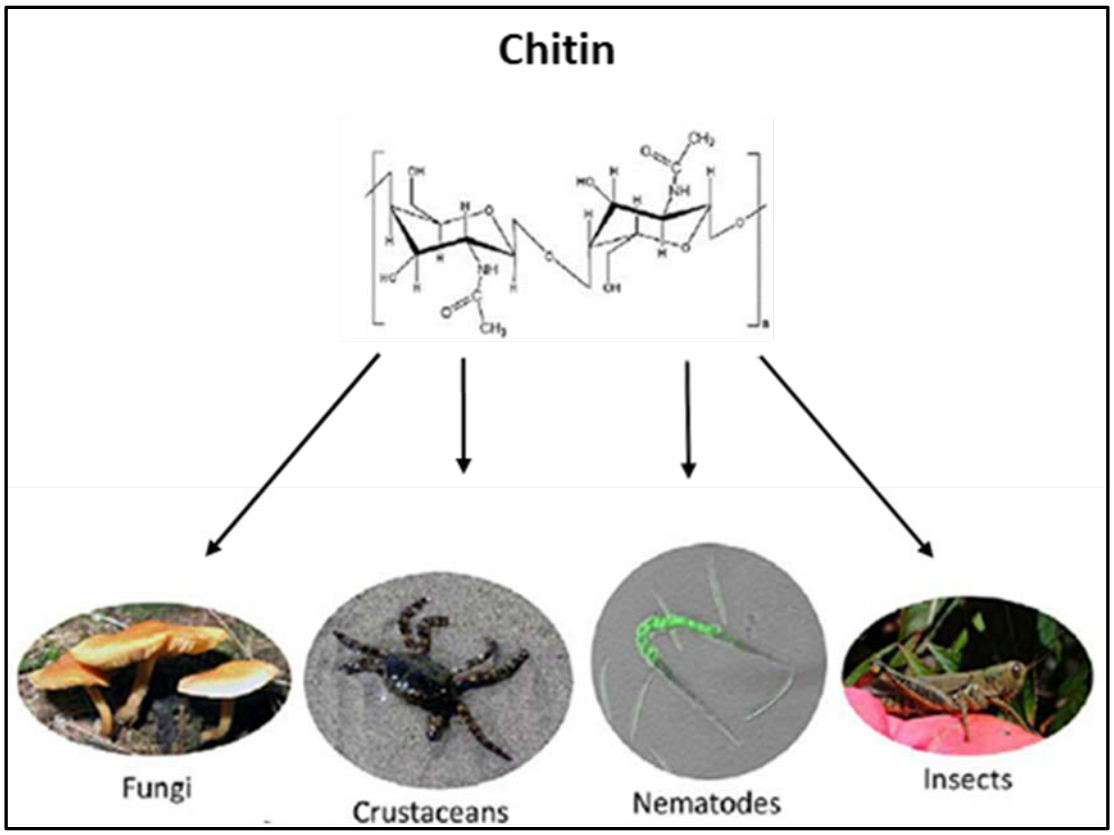

(Bueter et al., 2013, PLOS)

Figure 5: Chitin in nature.

Chitin is a linear biopolymer made up of repeating N-acetyl-D-glucosamine (GlcNAC) moieties. Structurally resilient, chitin can be found in the cell walls of fungi and parasitic helminths, it is also the main constituent of arthropod exoskeletons. Chitin itself is a dynamic regulator of inflammation in that chitin recognition by TLRs elicits various inflammatory cell functions.

Endogenous chitin is not present in vertebrates and is, in fact, recognized by macrophage TLRs as a PAMP. Activation of the TLR signaling pathway elicits an innate immune response. Macrophage activation by chitin is characterized by release of inflammatory cytokines and chemokines. Chitinases are enzymes that degrade chitin into fragments small enough for phagocytosis as a host defense against chitin-containing pathogens [100]. Humans express two distinctly different chitinases: acidic mammalian chitinase (AMCase) and macrophage chitotriosidase-1 (CHIT1). AMCase is found largely in the stomach and lungs, and is most enzymatically active at pH 2.0. It is especially prevalent in bronchial asthma and

allergic airway inflammation [101, 102]. CHIT1 is highly expressed in activated macrophages. Named for its ability to cleave chitotrioside residues, the enzyme was the first human chitinase to be discovered.

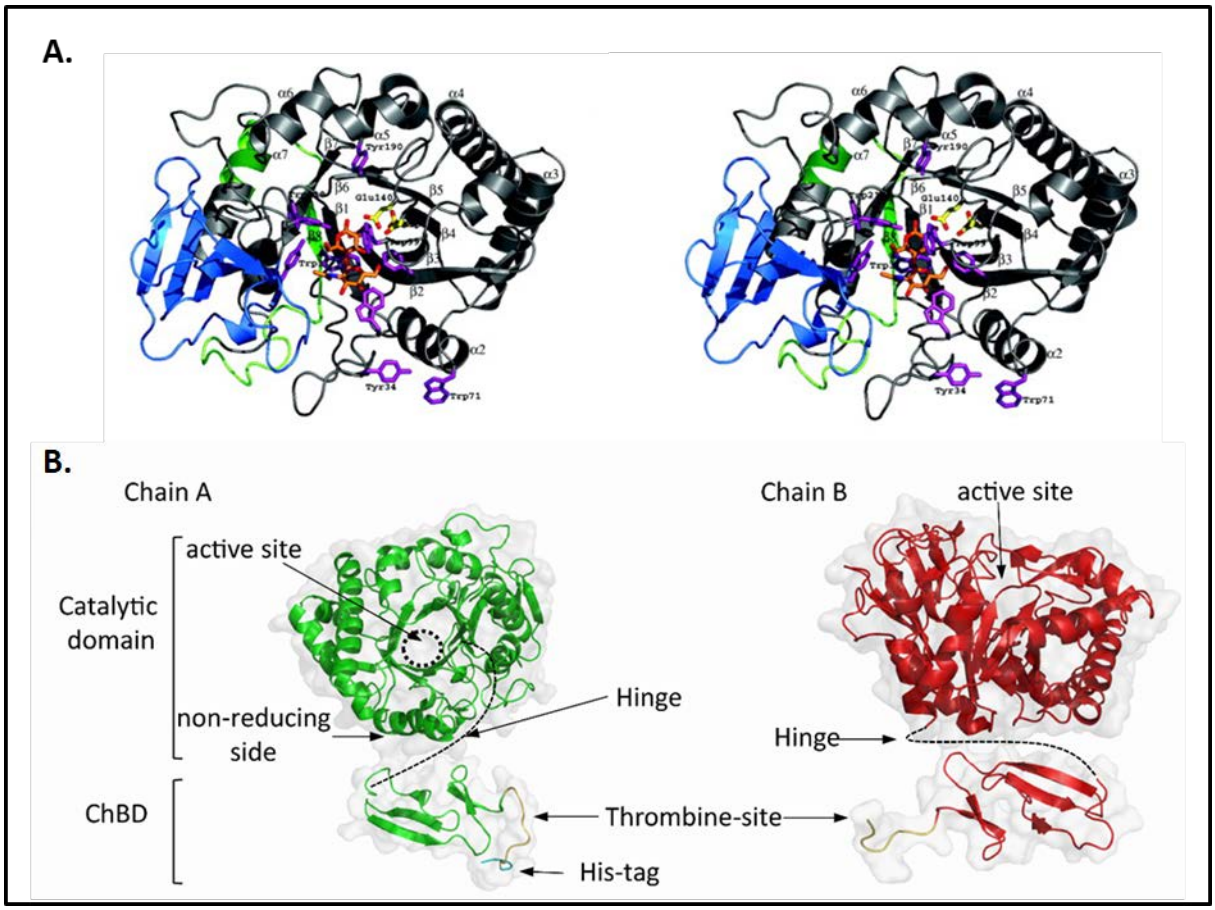

(Fusetti et al., 2002, Journal of biological chemistry and Fadel et al., 2016, PLOS)

Figure 6: X-ray crystal structure of CHIT1 isoforms.

(A) *Stereo images of the Crystal structure of the 39 kDa CHIT1 isoform. It is a result of post-translational modification from the full-length enzyme. The truncated isoform still retains full enzymatic activity and is sequestered in specialized vesicles within the cell.* ***(B)*** *The full-length, 50 kDa isoform of CHIT1 includes the CBD (ChBD, chitin/carbohydrate binding domain) which potentiates enzymatic processivity. The hinge region that connects the enzyme to the CBD allows for multiple directionality of both subunits.*

Like most mammalian chitinases, CHIT1 is a member of the glycosyl-hydrolase enzymatic family 18 (GH18). Cleavage of substrate is achieved through hydrolysis of β(1→4) glycosidic bonds. There are 2 major isoforms of CHIT1 that arise from post-translational modification. In macrophages, CHIT1 is initially

synthesized as a 50 kDa protein. This isoform is either secreted in response to an inflammatory stimulus or packaged in lysosomes and lysosome related organelles (LRO) where the acidic environment within is believed to promote cleavage into a, still fully enzymatically active, 39 kDa isoform [105, 106]. A third isoform exists as a rare splice variant due to a point mutation that results in a 40 kDa protein that is essentially identical to the 39 kDa isoform. Recent discoveries have revealed that the difference in size between the 50 kDa and 39 kDa isoform is due to the presence of a carbohydrate-binding domain (CBM) [107, 108]. The CBM allows for processivity, which increases efficiency of hydrolysis by maintaining a close proximity between the enzyme and substrate during subsequent hydrolytic reactions. It should be noted that while CHIT1 expression has been observed in neutrophils very little is known about its mode of action. Data has provided evidence that CHIT1 is present in specialized vesicles that are unique from lysosomes. However, a mechanism to describe neutrophil-derived CHIT1 function has yet to be elucidated [109].

1.5.1 CHIT1 in disease

A growing body of evidence describes the relevance of CHIT1 in a wide array of pathophysiologic conditions. Aside from acting as an effective defense mechanism against fungal infection or parasitic invasion, CHIT1 expression and secretion is unexpectedly increased in non-pathogen related, human diseases. Lysosomal storage disorders like Gaucher's disease and Niemann-Pick disease are characterized by an extreme preponderance of lipid-laden, macrophage-derived foam cells. And while Gaucher's patients present liver and spleen enlargement, patients afflicted with Niemann-Pick disease also display neurological abnormalities (i.e. cognitive decline, progressive ataxia, and seizures) [110, 111]. In both diseases, lipid-laden macrophages exhibit a steep rise in CHIT1 expression and secretion.

Wound healing and tissue repair are natural physiological responses to injury. However, augmentation of these mechanisms can result in pathologic fibrosis. This is the case in chronic inflammatory conditions where persistent injury causes extracellular matrix (ECM) components to accumulate in excessive amounts. A role for CHIT1 in fibrosis is an intriguing assertion and this pathology

has been investigated in a number of pathologic conditions. Systemic sclerosis (SSc) is a disease that affects multiple systems and is characterized by cutaneous and visceral sclerosis. Pulmonary involvement is observed in approximately 70% of patients with SSc, and in many cases is manifested as interstitial lung disease (SSc-ILD) where normal lung tissue is replaced with inflamed fibrotic tissue [112]. In one study, the authors found that fibrosis was significantly diminished in CHIT1$^{-/-}$ following bleomycin-induced pulmonary fibrosis [113]. Also, they demonstrated that pulmonary fibrosis was significantly enhanced in transgenic mouse models that overexpress CHIT1. This effect was not bleomycin-specific, as a similar decrease in fibrosis was observed in transgenic CHIT1$^{-/-}$ mice that overexpress IL-13. IL-13 is capable of eliciting CHIT1 expression, and the cytokine is involved in Th2-mediated inflammation and fibrogenesis. The authors go on to describe that human fibroblast MRC5 cells incubated with recombinant CHIT1 and TGF-β showed enhanced expression of TGFR1 and diminished TGFR2 suppression which ultimately led to an increase in SMAD signaling.

In cases of non-alcoholic steatohepatitis (NASH), TGF-β signaling is upregulated leading to steatosis, inflammation, and fibrosis. Research exploring a potential role of CHIT1 in NASH has provided evidence that CHIT1 was highly expressed exclusively by Kupffer cells in subjects with NASH [114]. CHIT1 expression levels were significantly higher in patients, and this correlated with TNF-α release from hepatocytes and Kupffer cells, α-smooth muscle actin (α-SMA) from hepatic stellate cells, and pathogenic fibrosis. Additional studies will be required to determine whether CHIT1-mediated TGF-β signaling is involved in fibrogenic liver disorders. Research investigating the effects of CHIT1 on immune cells in neuromyelitis optica and multiple sclerosis revealed that monocytes isolated from patients with either disease expressed enhanced levels of MCP-1, RANTES, and IL-8 upon stimulation with CHIT1. Increased migratory capacity for macrophages was also observed *in vitro* [115].

A number of different sources described elevated serum CHIT1 activity in atherosclerotic patients and animals [116-118]. Previously published data from our group has shown that CHIT1 inhibition using a

chitinase inhibitor, allosamidin, promotes atherosclerosis in ApoE$^{-/-}$ mice [119]. We observed significant alterations in macrophage cholesterol efflux and secretion of inflammatory cytokines and chemokines. RAW 264.7 macrophages were treated with allosamidin or medium alone. Transcripts for ABCA1, ABCG1, CD36, SR-A1, PPARγ, and LXRα were all significantly down regulated upon allosamidin treatment. Similar results were achieved in bone marrow-derived macrophages (BMDM). Pro-inflammatory cytokines and chemokines associated with M1 macrophage polarization: MCP-1, TNF-α, iNOS, IL-6, IL-12, IL-1β were significantly upregulated in both cell types when treated with allosamidin and IFN-γ compared to those treated with IFN-γ alone. Both lipid uptake and cholesterol efflux were decreased in RAW 264.7 macrophages when treated with allosamidin. Perhaps most intriguing was data that indicated promotion of atherosclerosis in ApoE$^{-/-}$ mice fed a Western diet and administered allosamidin compared to vehicle control via surgically implanted pump. After 6 weeks on high-fat diet, histological analysis depicted a significantly larger lesion in the aortic arch of animals with CHIT1 inhibition. Moreover, we found that lesion area was also significantly larger in the aortic sinus, and that macrophage deposition was also significantly greater.

1.6 Hypothesis and Aims:

Inflammation and dysfunctional cholesterol metabolism are fundamental components in the pathogenesis of atherosclerosis. CHIT1 is a highly-expressed protein in activated macrophages. It's production and secretion are elicited during both M1 and M2 inflammatory responses. Furthermore, Chitinase inhibition has been shown to stimulate pro-inflammatory cellular functions, decreased transcription of lipid-handling genes *in vitro*, and promoted atherosclerosis in hyperlipidemic mice. In light of these findings we tested the hypothesis that CHIT1 overexpression has athero-protective qualities that diminish disease progression. The following aims were pursued:

Aim 1) Investigate the effect of CHIT1 over-expression on the inflammatory response and invasiveness by macrophages

Aim 2) Determine whether over-expression of CHIT1 modulates cholesterol uptake and efflux in macrophages

Aim 3) Explore the effects of CHIT1 over-expression in atherosclerosis mouse model

CHAPTER 2: MATERIALS AND METHODS

2.1 Mouse strains

Wild-type C57BL/6 mice and LDLR null mice generated on a C57BL/6 background animal were purchased from Jackson Laboratories (Bar Harbor, Maine). CHIT1-OE mice were developed in cooperation with Kyushu University and Riken research Institute (Saitama, Japan). Briefly, the transgene depicted in figure 7 was microinjected into fertilized mouse embryos. To confirm transgene expression, gel electrophoresis was used to detect the presence of primer sequences specific to the CHIT1 transgene. *Ldlr*$^{-/-}$were crossbred with CHIT1-OE mice to produce *Ldlr*$^{-/-}$-CHIT1-OE animals. Mice between 8-12 weeks of age were used for isolation of bone marrow derived macrophages. Male *Ldlr*$^{-/-}$-CHIT1-OE mice between 8-10 weeks were utilized for the *in vivo* atherosclerosis study. All animal studies and protocols were approved by the University of Hawaii Institutional Animal Care and Use Committee.

2.2 Bone marrow-derived macrophage cell isolation and *in vitro* cell culture:

Experimental and control mice were sacrificed by CO_2 asphyxiation at 8-10 weeks of age. 70% EtOH was sprayed on the animals to disinfect the skin. Each femur and tibia were surgically removed under a biosafety hood. Using a 30-gauge needle, the marrow within the exposed bones were flushed out with ice cold PBS into a 50-mL falcon tube while on ice. The isolated bone marrow was broken up by vigorous pipetting with a 10-mL pipette. It was then passed through a 40-µm cell strainer into a 50-mL falcon tube, and centrifuged at 1300 RPM (≈300 x g) for 5 minutes to form a pellet. PBS was aspirated and the remaining pellet was resuspended in BMDM differentiation medium (DMEM/F12, [Gibco, Dublin, Ireland], 10% FBS, 20% L929 conditioned medium, and 1% penicillin-streptomycin (pen/strep) [Gibco, Dublin, Ireland]). Cell viability was determined by staining a 10 µL sample of cells in suspension with trypan blue. Cells were cultured at a density of 1×10^6 cells per mL and plated in 15-cm tissue-culture treated plates (Corning, Tewsbury, Massachusetts) with 25 mL of medium. 5-10 mL of media was added to the plate every other day for 7 days. Differentiated macrophages adherent to the plate were detached using non-

enzymatic Cell Stripper solution (Gibco, Dublin, Ireland). The cells were then counted and re-plated as specified in each experiment.

2.3 Preparation of L929-conditioned media:

L929-conditioned media was prepared by culturing 4.7×10^5 L929 cells (ATCC, Manassas, Virginia) in T-75 flasks containing 50-mL of media (DMEM/F12, 10% FBS, 1% HEPES (Gibco, Dublin, Ireland), and 1% pen/strep) for 7 days before collecting and sterile filtering the supernatant. The conditioned media was kept in 50-mL aliquots at -80° C for long-term storage and 20° C for short-term storage.

2.4 Western blot

2.4.1 Preparation of lysates from cells and tissues

RIPA buffer (10 mM Tris-Cl [pH 7.6], 1 mM EDTA, 1% Triton X-100, 0.1% sodium deoxycholate, 0.1% SDS, 140 mM NaCl) and 1X Halt protease and phosphatase inhibitor cocktails (Thermo Fisher, Waltham, Massachusetts) was used in preparation of lysates. Adherent cells in 6-well plates were washed with PBS which was then aspirated from each well before adding 100 µL of 4°C cold lysis buffer with protease/phosphatase inhibitor cocktails (diluted 1:1000) (Roche). Plates were kept on ice for 15 minutes before scraping the wells with a cell scraper and transferring the lysates to 1.5 Milliliter Eppendorf tubes on ice. Samples were then sonicated by pulsing 10 times with a probe sonicator (Thermo Fisher, Waltham, Massachusetts) at power level 2.5, and centrifuged at 400 x g for 5 minutes at 4° C. Lysates were transferred to a new Eppendorf tube and the pelleted cell debris was discarded. Pierce BCA protein assay kit (Thermo Fisher, Waltham, Massachusetts) was used to determine protein concentrations of lysates in a 1:10 dilution of samples.

2.4.2 Polyacrylamide gel electrophoresis and Western blot transfer

Precast NuPAGE® Novex® 4-12% Bis-Tris Mini or Midi protein gels (Invitrogen, Carlsbad, California) with 12 or 20-lanes respectively, were used in conjunction with the appropriate mini or midi electrophoresis gel box. 4x SDS loading buffer (0.1 M Tris-HCl pH 6.8, 0.7% SDS, 33% glycerol, 0.01%

bromophenol blue, 8% β-mercaptoethanol) was added to 10-20 µg of protein and this mixture was heated and maintained at 95° C for 5 minutes. Samples were loaded into each lane and 4 µL of Li-cor 1-color protein marker was added as a size reference latter. Gels were run in 1X NuPAGE® MES SDS Running Buffer (Invitrogen, Carlsbad, California) at a constant voltage of 150 V until the loading dye has completely migrated to the bottom of the gel. The gel is removed from its casing and placed on a low florescence PVDF membrane that has been activated in 100% methanol and immersed in 1x Efficient™ Western Transfer Buffer (G-Biosciences® #786-019 St. Louis, Missouri) with 20% methanol for 5 minutes. The gel and membrane together were placed between sheets of filter paper soaked in transfer buffer, and compressed tightly within the transfer cassette. The transfer cassette was placed in the transfer chamber along with an ice pack and stir Rod. The chamber was then put on ice. Protein was transferred to the membrane after running for 1 hour at 100 V.

2.4.3 Membrane incubation with antibodies and scanning

The membranes were blocked in 1:1 Li-cor blocking buffer and PBS for one hour with gentle agitation on an orbital shaker. The blocked membranes were incubated with primary antibodies diluted in Li-cor blocking buffer at room temperature for one hour or at 4° C overnight. Membranes were subsequently washed 3 times with 0.1% Tween20 in PBS. Secondary antibodies diluted in Li-cor blocking buffer were incubated with membranes at room temperature for one hour in the dark. After washing 3 times for 5 minutes each with 0.1% PBST, membranes were scanned with a Li-cor Odyssey infrared scanner and images were analyzed with Li-cor Image Studio (Li-cor Biosciences, Lincoln, Nebraska).

Table 1: List of antibodies used for Western blotting

Name	Species	Company	Dilution
CHIT1	Goat α Mouse	Santa Cruz Biotechnology	1:500
β-actin	Rabbit α Mouse	Sigma	1:2000
MAPK (ERK1/2)	Mouse α MAPK	Cell Signaling	1:1000
pMAPK ser (pERK1/2)	Rabbit α Mouse	Cell Signaling	1:1000
pAKT ser	Rabbit α Mouse	Cell Signaling	1:1000
PIκB-α	Rabbit α Mouse	Cell Signaling	1:1000
IRDye 800CW	Donkey α Rabbit	Licor	1:10,000
IRDye 800CW	Donkey α Goat	Licor	1:10,000
IRDye 680CW	Donkey α Mouse	Licor	1:10,000

2.5 Reverse transcriptase quantitative PCR (RT-qPCR)

Total RNA was extracted by adding 500 µL-1 mL TRIzol reagent (Life Technologies, Carlsbad, California) to each sample in a 1.5 mL Eppendorf tube. The sample was then vortexed until completely dissolved and chloroform was added to TRIzol in a 20% v/v ratio, and inverted vigorously to mix. The samples were centrifuged at 12,400 RPM for 15 minutes in a pre-cooled centrifuge at 4° C. Once phase separation occurs, the aqueous fraction was carefully pipetted into a separate tube and combined with an equal volume of nuclease-free, 70% ethanol. Samples were mixed thoroughly and put through RNA purification columns provided in the Qiagen RNeasy RNA extraction kit. DNA digest was performed, on-column, for 15 minutes at room temperature. After the appropriate wash steps, columns were allowed to completely dry. Elution of RNA from the columns was performed using 30-50 µL nuclease-free water. RNA concentration and quality was determined with a NanoDrop 2000. RNA was used immediately for RT-qPCR or stored at -80° C. 1 µg of total RNA per sample would be used to transcribe cDNA using the qScript

cDNA synthesis kit (Quanta Biosciences, Beverly, Massachusetts). 80 µL of nuclease-free water was added to each cDNA sample, bringing the total volume to 100 µL. In performing the RT-qPCR, 4 µL of cDNA was added to each well along with a master mix of 12.5 µL SYBR Green 2X master mix containing ROX (Roche), 0.5 µL of both forward and reverse primers (10 µM), and 7 µL of nuclease-free water. Ten µL of the reaction mixture was pipetted in triplicate to a 384-well qPCR plate and analyzed with an Applied Biosystems 7900HT Fast Real-Time PCR System.

Table 2: List of qPCR primers

Gene	**Forward sequence (5'-3')**	**Reverse sequence (3'-5')**
Gapdh	GGC AAA TTC AAC GGC ACA GT	CGC TCC TGG AAG ATG GTG AT
CHIT1	GAT GTG GAT CCC AAC CTG TGT ACC	GGG TCT TGA GCT TGG GGT TCT TAG
ABCA1	CCC AGA GCA AAA AGC GAC TC	GGT CAT CAT CAC TTT GGT CCT TG
ABCG1	CAA GAC CCT TTT GAA AGG GAT CTC	GCC AGA ATA TTC ATG AGT GTG GAC
CD36	CAA GCT CCT TGG CAT GGT AGA	TGG ATT TGC AAG CAC AAT ATG AA
IL-1β	TCC AGG ATG AGG ACA TGA GCA	GAA CGT CAC ACA CCA GCA GGT TA
IL-6	GAC AAC CAC GGC CTT CCC TA	CTG CAA GTG CAT CAT CGT TGT TC
iNOS	TGC ATG GAC CAG TAT AAG GCA AGC	GCT TCT GGT CGA TGT CAT GAG CAA
LXRα	CTC CTG ATT CTG CAA CGG AGT TGT G	TCC AAC CCT ATC CCT AAA GCA ACC C
PPARγ	CGG AAGCCC TTT GGT GAC TTT ATG G	GGG CGG TCT CCA CTG AGA ATA ATG A
MCP-1	TCA CTG AAG CCA GCT CTC TCT	GTG GGG CGT TAA CTG CAT
TNF-α	CCT CCA GAA AAG ACA CCA TGA G	CAC CCC GAA GTT CAG TAG ACA G
SR-A1	TTA AAG GTG ATC GGG GAC AAA	CAA CCA GTC GAA CTG TCT TAA G

2.6 Immunoprecipitation

2.6.1 Immunoprecipitate preparation

BMDM from wild type and CHIT1-OE mice were cultured for 6 hours with or without LPS + IFN-γ. The supernatant was then collected and 850 µL were transferred to microcentrifuge tubes. 2 µg of goat, anti-mCHIT1 primary antibody was added to the tube. The supernatant-antibody mixture was incubated for 1 hour at 4° C. Twenty µL of Protein G PLUS-Agarose beads (Santa Cruz Biotechnology, Dallas, Texas) were then added to the tubes and incubated at 4°C overnight. The immunoprecipitates were collected by centrifugation and washing with 20 mM Tris-HCl, pH 7.4. Protein elution is carried out by resuspending the pellet in glycine buffer and incubatinfg for 10 minutes at 4° C. The solution is centrifuged and the eluate is collected, it is then immediately neutralized by adding 1 molar Tris, pH 8.5. This step is repeated 3 times and each resultant elution is analyzed with Western blot and SDS-PAGE.

2.6.2 Coomassie Blue staining (total protein control)

The same PVDF membranes used for immunoprecipitation were stained using Coomassie Brilliant Blue "G" (Sigma-Aldrich, St. Louis, Missouri). The Western blot membrane was washed for 5 minutes at room temperature and then stained with 65% Coomassie stained solution and incubated for 5 minutes at room temperature. The membrane was washed with 50% methanol, 10% acetic acid the staining solution. The membrane is visualized using the Li-cor CLx Odyssey imaging system at 700 nm.

2.7 CHIT1 activity assay

Chitinase activity in cell lysates was performed as described above, however in place of RIPA buffer, a non-denaturing lysis buffer was prepared in order to preserve enzymatic activity of CHIT1. The lysis buffer cocktail contained: 50 mM Tris-HCL, 200 mM NaCl, 10% glycerol, and for 0.5% Triton X-100. CHIT1 activity was detected using 4-methylumbelliferyl-N, N', N"-triacetyl chitotrioside [4MU-$(GlcNAc)_3$, Sigma-Aldrich] as a substrate. A 20 µM working solution of 4MU-$(GlcNAc)_3$ was prepared by dissolving in N, N-dimethylformamide. This was added to 8 µg of protein sample prepared from cell lysates and allowed

to incubate for one hour at 37° C in 50 mM citric acid/$NaPO_4$ incubation buffer. The reaction was stopped using 1M glycine/NaOH stop buffer. Florescence of liberated 4-Methylumbelliferone was measured with a fluorescence spectrometer (excitation: 360 nm, emission: 450 nm). A 4-MU standard solution curve was used to calculate absolute chitinase activity (U/mL)

2.8 Cytokine array

The Proteome Profiler Array: Mouse Chemokine Array Kit (R&D Systems, Minneapolis, Minnesota) was used to determine relative levels of 40 different mouse Cytokines and Chemokines. Cell lysates were prepared by rinsing BMDM cultures with PBS and then adding 100 to 150 µL of lysis buffer to each well. The cells and lysis buffer are incubated for 30 minutes before harvesting with a cell scraper. Protein concentration was determined using BCA assay. Two mL of array buffer 6 (blocking buffer) is added to each well and the pre-blotted, nitrocellulose membranes that were provided in the kit are added to the wells. The membranes were incubated for 1 hour at room temperature. Fifteen µL of reconstituted Mouse Cytokine Array Panel A Detection Antibody Cocktail was added to each sample containing 100 µg total protein. The wells were emptied of Array Buffer 6 and the samples/antibody mixtures were added to the wells and allowed to incubate overnight at 2-8° C on a rocking platform shaker. Each membrane was washed and then 2 mL of IRDye 800CW Streptavidin (LI-COR, Catalog #926-32230) diluted 1:2000 using the Array Buffer 6 was added to each well of the dish. After incubating for 30 minutes at room temperature, each membrane was removed and images were collected with an Odyssey CLx imaging system.

2.9 Cholesterol homeostasis assays

2.9.1 Cholesterol uptake using fluorescently labeled cholesterol

Cholesterol uptake was measured in bone marrow-derived macrophages from CHIT1-OE mice and littermate controls. BMDM were plated at a density of 1×10^6 cells per well in 12-well plates for flow cytometry analysis. Cells were treated with 50 µg/mL DiI-labeled acetylated-LDL (Ac-LDL), BODIPY-labelled

Ac-LDL, DiI-labelled oxidized-LDL (ox-LDL), and BODIPY-labelled ox-LDL as separate treatments with or without 20 ng/mL IFN-γ + 100 ng/mL LPS. Experiments were carried out for 4, 6, 12, and 24 hours of incubation. The cells were then detached with cell stripper and fixed for 10 minutes with 4% PFA in preparation for flow cytometry analysis of fluorescence intensity corresponding with DiI- and BODIPY-labelled lipids. The immunoprecipitates are collected by centrifugation and the pellet is resuspended with 20 mM Tris-HCl, pH 7.4. Following the immunoprecipitation process the pellet is resuspended with 50 µL of glycine buffer and incubated for 10 minutes at 4° C. The sample solution is centrifuged and the eluate is immediately neutralized with one molar TRIS, pH 8.5. The elution step is repeated 3 times2.9.2

2.9.2 Cholesterol efflux using [H]^3-cholesterol

BMDM from both CHIT1-OE mice and littermate controls were plated at a seeding density of 1×10^6 cells per well in 24 well plates. Cells were incubated overnight to promote adhesion. After incubation cells are washed with PBS and then labeled with loading medium which containing: DMEM, glutamine, penicillin, streptomycin, 0.2% fatty acid-3 bovine serum albumin, AcLDL (50 µg/ml), and 1 µCi/µl [^{3}H] cholesterol (NEN Life Science products Santa Clara, California), for 24 hours. The cells were washed twice with PBS and equilibrated for 2 hours in efflux media (DMEM and 0.2% BSA). Cells were washed again with PBS and then incubated in 0.5 mL efflux media alone or with either 20 µg/mL ApoA1 (indicates ABCA1-mediated efflux) or 50 µg/mL HDL (indicates ABCG1-mediated efflux) added to the well. The BMDM were incubated for 6 hours at which time the supernatant was collected and analyzed with a scintillation counter to determine the amount of radiolabeled cholesterol efflux by the macrophages via HDL or ApoA1.

2.10 Macrophage invasion assay

Cultured BMDM were washed once with PBS and 15 mL of 1% pen strep serum free media was added, and cells were incubated at 37° C for 3 hours to starve cells. Cells were washed once with PBS and detached by incubation with cell stripper for 5 to 10 minutes. Using a cell lifter, BMDM were collected

from the plate and spun down for 5 minutes at 1300 RPM in a falcon tube. ECM Matrigel (Sigma-Aldrich St. Louis, Missouri) was diluted 1:1 with DMEM to a 6 mg/mL working solution. Using chilled pipette tips, 50 µL of matrigel was added to transwell inserts in 24 well plates. Each insert contained a membrane with 0.8 µm pores through which the macrophages migrate after invasion of ECM. After matrigel has solidified for 10-30 minutes, 100 µL of cell suspension (1×10^5 BMDM) was pipetted onto the solidified matrigel layer. 600 µL of either serum free media or experimental cell culture media alone and experimental cell culture media supplemented with MCP-1, reconstituted chitin from shrimp shells, or IL-13 was added to the well below the transwell inserts. Macrophages were incubated for 24 hours at 37° C and supplemented with 5% CO^2 to observe cellular invasion. In order to visualize macrophages that invaded ECM layer the inserts were removed and the top of each membrane was carefully swabbed with a cotton-tipped applicator to remove media and noninvasive cells. Transwell inserts were submerged in 70% alcohol for 10 minutes to fix cells. Membranes were subsequently stained with 0.2% crystal violet at room temperature. Each transwell insert was then carefully dipped into distilled water as to avoid washing off fixed cells while removing excess crystal violet stain. The insert with the membrane still attached was then viewed under an inverted microscope and stained sections were quantified using ImageJ software.

2.11 Mouse atherosclerosis study

2.11.1 Blood collection and sacrifice of study animals

Blood from each mouse was collected at the start and end point of the study using a submandibular bleeding technique. A portion of the whole blood collected was centrifuged at 1500 x g for 15 minutes to achieve plasma separation. Plasma samples were used to measure lipid levels. At the study's conclusion, animals were euthanized by CO_2 asphyxiation and total blood was collected through cardiac puncture of the left ventricle. Liver, spleen, lymph nodes and kidneys were removed and each mouse was perfused with ice cold PBS followed by 4% PFA/5% sucrose. The hearts and your orders were removed and analyzed as described below.

2.11.2 Analysis of blood cell populations by flow cytometry

Blood collected in EDTA tubes was agitated by gently tapping the tubes and then put on ice. 5 mL of red blood cell lysis buffer (eBioscience Santa Clara, California) was used was applied to whole blood for 15 minutes at room temperature. 5 mL of PBS was then added to the tubes and centrifuged at 350 x g for 5 minutes. A second treatment with RBC lysis buffer was performed if the cell pellet showed signs of RBC contamination. This was done by adding 1 mL of lysis buffer for an additional five minutes before adding PBS and centrifuging. To re-suspend the cell pellet, 200 µL of Hank's complete buffer (recipe below) was added and then transferred to a round-bottom 96-well plate and centrifuged. The remaining supernatant was decanted by inverting the plate. An antibody master mix was prepared with 0.5 µL of each required antibody and brought to a total volume of 50 µL using 50% flow blocking buffer (recipe below) and 50% Hank's complete buffer per sample. The cell pellet was resuspended in 50 µL of the antibody master mix and incubated for 20 minutes on ice, in the dark. 150 µL of Hank's complete buffer was used to wash the cells which were then centrifuged.

Table 3: The list of flow cytometry antibodies

Antigen	Fluorophore	Company	Dilution
Ly6G	PE	Biolegend	1:100
Gr-1	APC	Invitrogen	1:800
CD45	APC-Cy7	Biolegend	1:100
CD11b	PerCP-Cy5.5	Biolegend	1:100
CD11c	PE-Cy7	Biolegend	1:100
CD3	AlexaFluor700	Biolegend	1:100
CD4	PE-Texas Red	Biolegend	1:100
CD8	eFluor450	eBioscience	1:100
CD19	BV605	Biolegend	1:1600

2.11.3 Analysis of serum cholesterol and triglyceride levels

At the end of the atherosclerosis study blood cholesterol and triglyceride measurements were gathered from serum samples of all mice in each group. A fluorometric assay kit (Cayman Chemical) was used to determine total cholesterol. Samples were diluted 1:200 with assay buffer in duplicates prepared in a 96-well plate. Serum samples were also analyzed for triglyceride levels. A colorimetric assay (Cayman Chemical Ann Arbor, Michigan) allowed for the measurement of fluorescence or absorbance using a SpectraMax Microplate Reader. Standard curves were derived from standard solutions provided in the kit.

2.11.4 Analysis of lesion area of whole aortas and aortic root cryosections

Upon dissection of the animal, adventitial fat was cleared away from aorta and branching arteries. The entire aorta was then cut open longitudinally, excised, and pinned to a wax lined dissecting tray. Oil-Red-O Stock (ORO) solution was prepared with 1 gram of ORO powder (Sigma-Aldrich St. Louis, Missouri) dissolved in 300 mL of 99% isopropanol. A working solution of the stain was prepared fresh by mixing 180 mL of stock solution with 120 mL Milipore water. The solution was allowed to equilibrate for one hour before filtration with Whatman filter paper into a clean glass bottle. 60% isopropanol was used to wash the pinned aortas which were then completely submerged in ORO working solution for 15 minutes. The aortas were washed with 60% isopropanol until the stain was no longer visibly being removed (3-4 washes). Aortas were photographed and the images were analyzed to measure plaque area using the ImageJ software.

Fixed hearts were collected from the study mice and mounted in Optimal Cutting Temperature (OCT) compound (Tissue-Tek Torrance, California) which were then frozen at -80° C. Embedded hearts were sectioned in a sagittal orientation through the aortic valve were all 3 leaflets are visible. Cryo-sectioning was achieved with a cryostat and serial sections of 10 µm increments were made, and 5

representative sections were selected from each mouse. These sections would be used to visualize lesion area as represented with ORO staining. Newly prepared cross-sections were incubated in PBS for 5 minutes and then air dried. They were dipped 10 times in 60% isopropanol and then stained with fresh ORO working solution for 15 minutes. The staining solution was removed and the slides were again dipped 10 times in isopropanol and washed for 5 minutes under running tap water. Slides were covered using mounting media (Sigma-Aldrich) and dried overnight. Photos were taken of the sections at 5X zoom and the ORO stained area was quantified using ImageJ and represented as a percentage of total aortic area.

Table 4: List of antibodies used for immunohistochemistry staining

Antigen	**Company**	**Dilution**
Rat α MOMA	Abcam	1:1000
Goat α CHIT1	Santa Cruz Biotechnology	1:500

2.11.5 Immunohistochemical staining of aortic root cryosections

Immunohistochemical (IHC) staining was used to characterize and quantify CHIT1 expression, macrophage populations, necrotic core area, ECM deposition, and collagen formation in WT and CHIT1-OE mouse, aortic cryosections. Slides with mounted cryosections were prepared for IHC by fixing in ice cold, 100% acetone for 1 minute and then washed with PBS using dip-style glass chamber. Tissue sections were circled with a PAP pen and then washed with PBS-Tween. Antigen retrieval was carried out using 0.05% trypsin/0.1% calcium chloride solution (trypsin/CA). Slides were incubated with trypsin CA in a humidified chamber at 37° C for 15 minutes, and allowed to cool at room temperature for 10 minutes. Antigen retrieval solution was removed and slides were washed 3 times with PBS-Tween. 0.1% Triton X-100 was then applied for 20 minutes, removed, and slides were washed again with PBS-Tween.

Hydrogen peroxide block was performed by adding enough 3% hydrogen peroxide to cover each section and incubate until bubbles can no longer be observed emanating from the tissue. Slides were then

rinsed with PBS and placed in a dip chamber containing PBS for 2 minutes. Sections were blocked with 5% donkey serum dissolved in 2% BSA with 1X PBS. Slides were incubated in block solution for 1 hour at room temperature.

Primary antibodies for CHIT1 (Santa Cruz Biotechnology Dallas, Texas) and macrophages (MOMA-2, Abcam Cambridge, United Kingdom) were added to the sections and allowed to incubate overnight at 4° C. Sections were washed with PBS-Tween followed by addition of the horseradish peroxidase (HRP), conjugated secondary antibody. Slides were incubated in a dark humidified chamber for 1 hour at room temperature. Sections were washed with PBS-Tween and kept wet until mounted. One drop of reagent a was diluted in 1 mL of distilled water as described in the AEC staining kit instructions (Invitrogen, Carlsbad, California). One drop of reagent be and reagent C were then added and the solution was kept away from light and incubated with the cryosections for 30 minutes (or until color development is satisfactory). Slides were then rinsed with distilled water. Mayer's hematoxylin counter stain was applied using a dip chamber for no more than 10 seconds. The slide was then washed and rinsed under running tap water for 5 minutes. Next, the slides were put into a dip chamber containing Scott's Bluing solution for 30 seconds and dipped once in tap water to wash. Dako fluorescent mounting media was added to the top of each section, which was then covered with a coverslip and stored at 4° C.

Visualization of hyaluronic acid was achieved using biotinylated hyaluronic acid binding protein (BHABP, EMD/Millipore/Calbiochem Burlington, Massachusetts). After acetone fix, hydrogen peroxide block, and blocking (2% BSA in 1X PBS), streptavidin/biotin blocking was performed according to the instructions provided by the kit (Vector Laboratories Burlingame, California): incubate section with Avadin D solution for 15 minutes at room temperature rinse with PBS-Tween, next incubate section with biotin solution for 15 minutes at room temperature and rinse again with PBS-Tween. BHABP was diluted 1:100 in blocking solution and applied to sections. These were allowed to incubate at room temperature for one hour. BHABP was aspirated away and slides were washed 3X with PBS. The streptavidin-conjugated HRP

was then applied to the cells for 1 hour at room temperature before washing 3X with PBS. AEC chromogen and Mayer's hematoxylin counter stain was added as described above.

Hyaluronidase negative controls sections were prepared in the same way as sample sections. However, no detection stain was added. Instead, cryosections were incubated with hyaluronidase (StemCell Technologies Vancouver, Canada) for 2 hours at room temperature.

Picro-Sirius Red staining was used to visualize collagen in the aortic root. Cryosections were acetone fixed and trypsin/CA antigen retrieval was applied. As described in the instruction manual (Abcam Cambridge, United Kingdom), Picro-Sirius red solution was added to completely cover the section, and incubated for 60 minutes. The slide was rinsed with 2 changes of acetic acid solution, and then rinsed once in absolute alcohol. The cryosections were then dehydrated into changes of absolute alcohol and the slide was mounted in resinous mounting media.

2.12 Statistical analyses

A minimum of 3 biological replicates run in duplicate or triplicate were analyzed for *in vitro* experiments as indicated. Statistical power of 0.8 was utilized for determination of significance and sample size, such that variation as represented by standard deviation within groups did not exceed an acceptable threshold for sample size n=3. For qPCR analysis, transcript abundance was determined from cDNA isolated from samples. CT values were initially normalized to GADPH and expressed as the average fold change relative to controls for each treatment. Error bars represent the SEM. These cytokine array used protein samples from 3 biological replicates and was performed in duplicate for each treatment. Values are representative of an average of the duplicate measurements ± SEM.

Using flow cytometry we determined cholesterol uptake *in vitro*. The intensity of DiI florescence/cell was ascertained with 10,000 counts for each sample in duplicate. Mean fluorescence intensity (MFI) of DiI was measured in 3 biological replicates and depicted as an average MFI of CHIT1-OE cells compared to controls ± SEM. Cholesterol efflux measurements taken *in vitro* were performed in

triplicate from 3 separate experiments. Basal cholesterol efflux level (no acceptor), efflux to ApoA1, or HDL is shown as a percentage of the total cholesterol loaded by cells. Bar graphs represent the average values derived from experiments ± SEM.

Invasion assay was performed 3 times in duplicate. For imaging, a total of 5 photos were taken from each insert and analyzed with ImageJ. Macrophage invasion is represented by the average of stained areas from all 5 photos as a percentage of the total area captured in each photo. Statistical analysis with prism for all *in vitro* experiments was carried out using the two-tailed Welches *t*-test with $p<0.05$ as threshold for significance.

The *in vivo* mouse study compared 2 groups with 14 mice in each group therefore resulting in a df of 26, a student T value of 2.06, and a significance value $\alpha=0.05$ (two-tailed). A minimum of 6 mice per group was used to determine statistical significance. P values for all experiments were calculated with the Prism software (Graph Pad), * = $p<0.05$, ** = $p<0.005$, *** = $p<0.0005$, **** = $P<0.0001$.

CHAPTER 3: RESULTS

3.1 Verification of CHIT1 overexpression in macrophages

Initial experiments were performed in order to observe CHIT1 overexpression in BMDM harvested from CHIT1-OE mice. As mentioned above, CHIT1-OE mice were crossbred with ldlr$^{-/-}$ mice, thereby providing us with a atherosclerotic, CHIT1 overexpressing mouse model. Moreover, CHIT1 overexpression is achieved using the Cre-Lox system whereby the removal of a LoxP-flanked stop sequence allows for conditional overexpression of CHIT1 in lysozyme producing macrophages. Conditional overexpression with LysMCre is made possible because the Cre recombinase gene is inserted after the promoter of the LysM gene and as lysozyme is constitutively expressed so too is Cre recombinase, and with that CHIT1. Thus, the genetic description of our experimental mouse models can be described as follows: ldlr$^{-/-}$- CHIT1-OE-LysM^{Cre}.

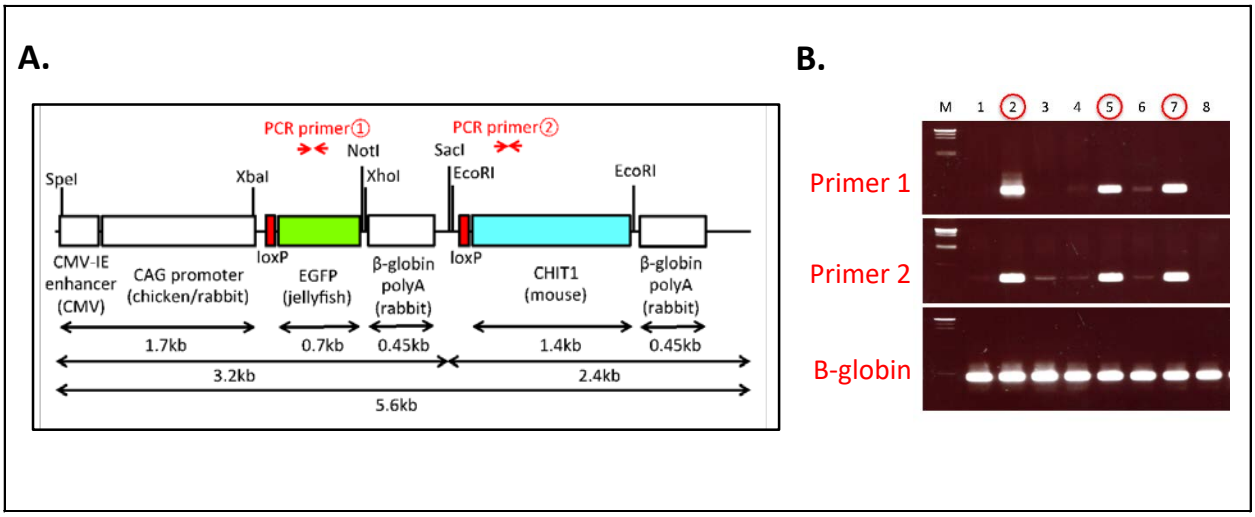

Figure 7: CHIT1 overexpression transgene design

(A) *The transgene was designed with an EGFP stop sequence (green) that is removed in the presence of Cre recombinase. When Cre recombinase is expressed in lysozyme producing cells, the CHIT1 gene (blue) is constitutively expressed by macrophages.* ***(B)*** *Results from genotyping F0 mice indicate the presence of both primers and confirm transgene insertion. B-globin gene was used as internal control.*

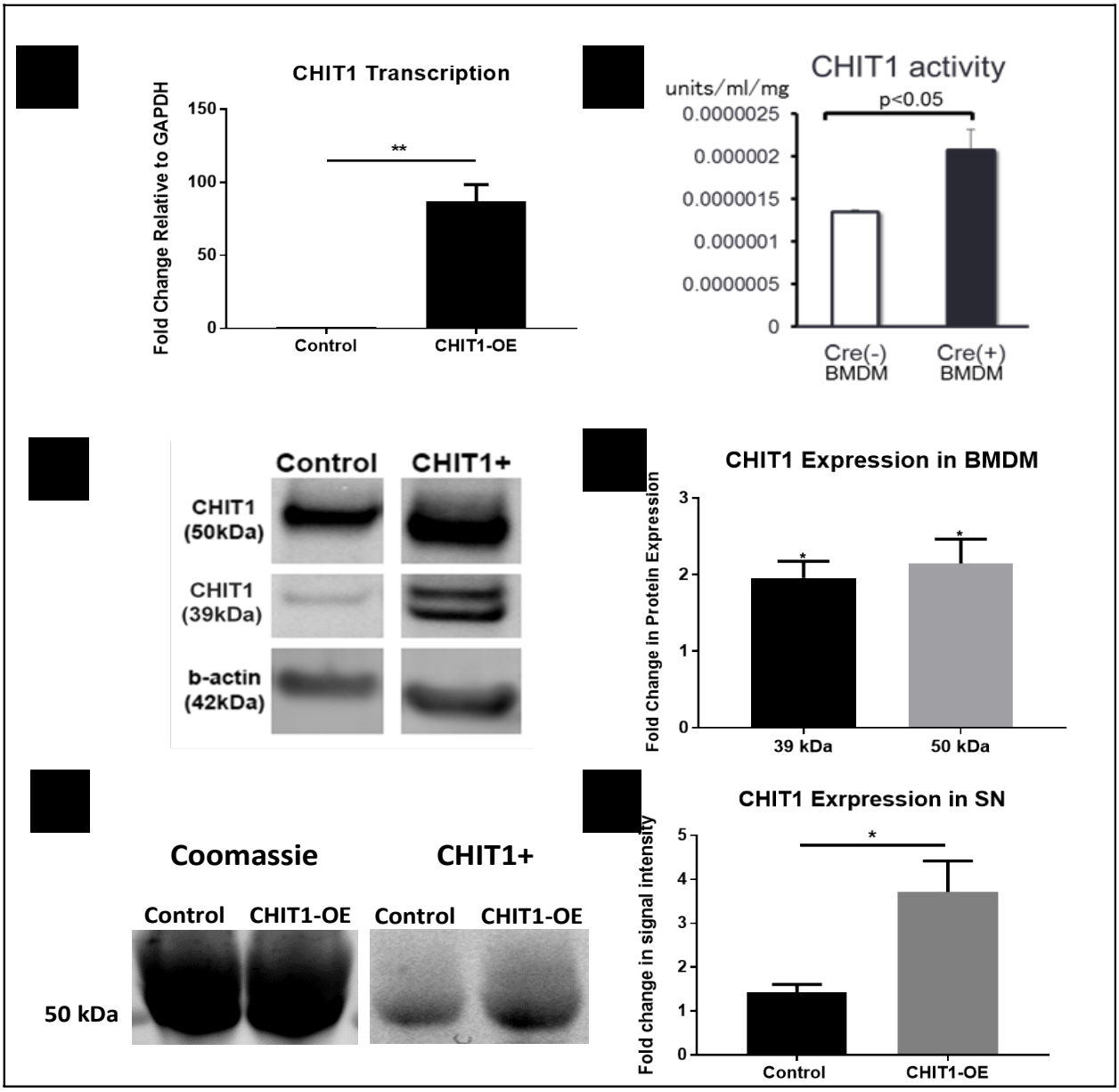

Figure 8: CHIT1 overexpression in vitro

(A) *Transcription of CHIT1 mRNA was quantified using qPCR. cDNA was isolated from control and CHIT1-OE BMDM.* ***(B)*** *CHIT1 activity was analyzed in BMDM from control (Cre-) and CHIT1-OE (Cre+). Liberated 4-MU emission was measured with a plate reader to determine enzymatic activity.* ***(C)*** *Western blot imaging of CHIT1 protein expression. Both isoforms (50 kDa and 39 kDa) were significantly increased in BMDM from CHIT1-OE mice compared to controls.* ***(D)*** *Membranes after Western blot were imaged using Licor Odyssey CLx and analyzed with image studio software measurements reflect the fold change in florescence intensity.* ***(E)*** *immunoprecipitation was performed on supernatants of BMDM harvested from CHIT1-OE mice and control animals. Coomassie staining of the membrane was used as a total protein*

control. ***(F)*** *Analysis of Western blot images with image studio software showed a significant increase in CHIT1 protein expression. N=3 *P<0.05 **P<0.01*

To verify the overexpression of CHIT1 in macrophages, BMDM were harvested from both experimental and littermate control animals. Isolated RNA was analyzed with "quantitative" PCR (qPCR). We found that CHIT1 transcription was not affected in control BMDM as the transcript detected was similar to our internal control, GADPH (figure 8A). CHIT1 transcription was significantly increased in CHIT1-OE BMDM when compared to control BMDM. Cell lysates were prepared from BMDM and visualized using Western blot analysis. Figures 8C and 8D show protein expression was enhanced in CHIT1-OE BMDM as evidenced by the presence of one distinct band at 50 kDa and one at 39 kDa, which are characteristic of the predicted molecular weight of both CHIT1 isoforms. The 39 kDa isoform of CHIT1 is a product of the post-translational modification of the 50 kDa isoform, and was only visible in CHIT1-OE BMDM. Due to the fact that only the 50 kDa isoform of CHIT1 is secreted while the 39 kDa isoform is sequestered in specialized vesicles, analyzed the supernatant of macrophage cell cultures for the presence of CHIT1. As expected, we found that the 50 kDa, secreted isoform of CHIT1 was robustly expressed in the supernatant of CHIT1-OE BMDM (figure 8E and 8F). Lastly, we determined that CHIT1 enzymatic activity is elevated in both cell lysates and the supernatant of CHIT1-OE BMDM as exhibited by the cleavage of 4-MU-conjugated substrates.

3.2 effects of CHIT1 overexpression on macrophage function

3.2.1 Overexpression of CHIT1 modulates inflammatory responses in macrophages

We examined the effects of CHIT1 overexpression on macrophage inflammatory response by treating BMDM from CHIT1-OE mice with a combination of IFN-γ and LPS. Incubation of cells for 6 hours, followed by RNA isolation, and qPCR analysis revealed exaggerated transcription levels of CHIT1 as well as suppressed transcription of inflammatory cytokines compared to BMDM from littermate control animals (figure 9A-D).

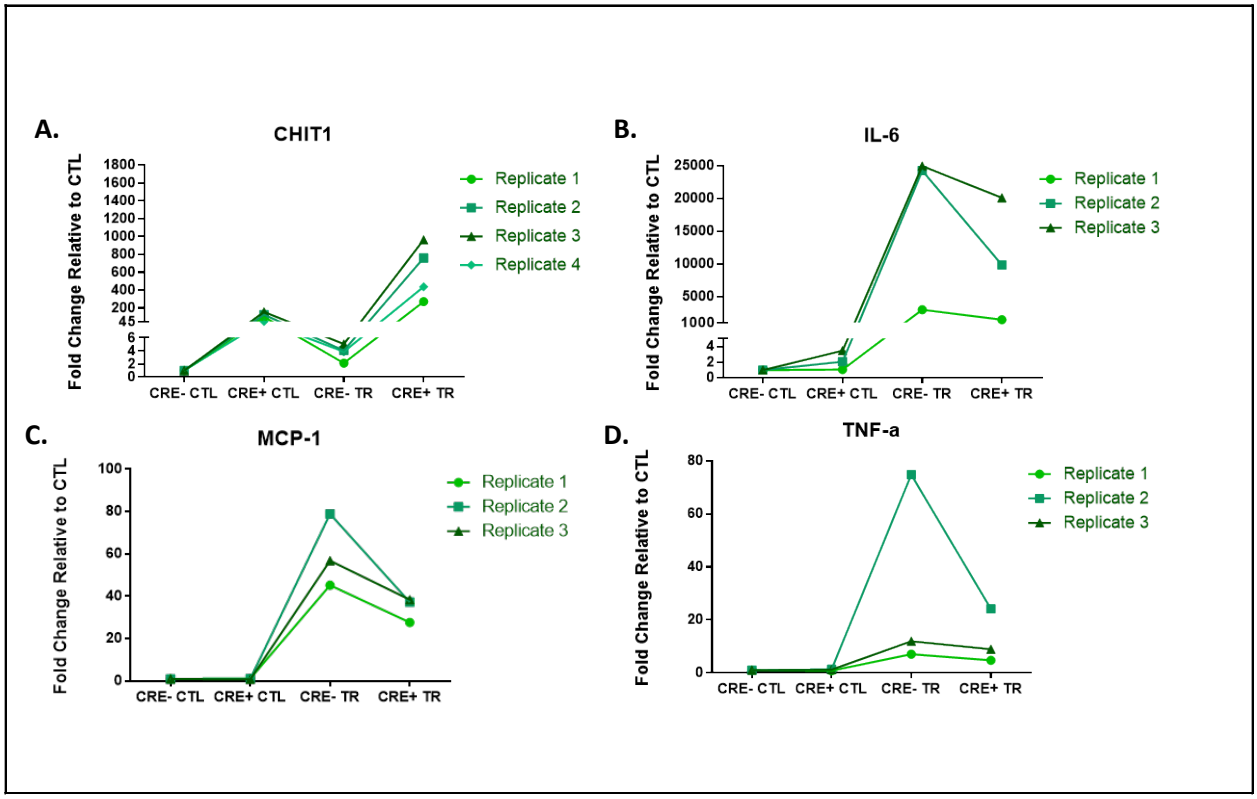

Figure 9: Macrophage overexpression of CHIT1 reduces pro-inflammatory gene expression

BMDM from CHIT1-OE (CRE+) and control mice (CRE-) were treated with 20 ng/mL IFN-γ + 100 ng/mL LPS for 6 hours or left untreated as experimental control. Cellular RNA was extracted to prepare cDNA for qPCR analysis. Gapdh, a well-known housekeeping gene was used as internal control. ***(A)*** *CHIT1 gene expression was strongly enhanced in CHIT1-OE mice when subjected to inflammatory stimuli.* ***(B-D)*** *Treatment with IFN-γ + LPS for 6 hours resulted in a marked decrease in transcription of pro-inflammatory genes in CHIT1-OE BMDM when compared to control BMDM. N=3, values represent fold change in transcript abundance.*

In order to better understand the effects of CHIT1 overexpression, a cytokine antibody array was performed using nitrocellulose membranes spotted with capture antibodies for a variety of cytokines and chemokines. The assay analyzed cell lysates prepared from BMDM, treated with the same inflammatory stimuli used in qPCR experiments. Membranes were incubated with cell lysates from both CHIT1-OE BMDM and control BMDM for 8 hours prior to application of biotin-labeled detection antibodies. Results in figure 10A-C showed a significant up regulation of G-CSF, the anti-inflammatory cytokine IL-4, and KC

(the murine homolog of IL-8) which is involved in immune cell recruitment, macrophage phagocytosis, parasitic invasion defense, and is expressed during both M1 and M2 inflammatory conditions [120-123].

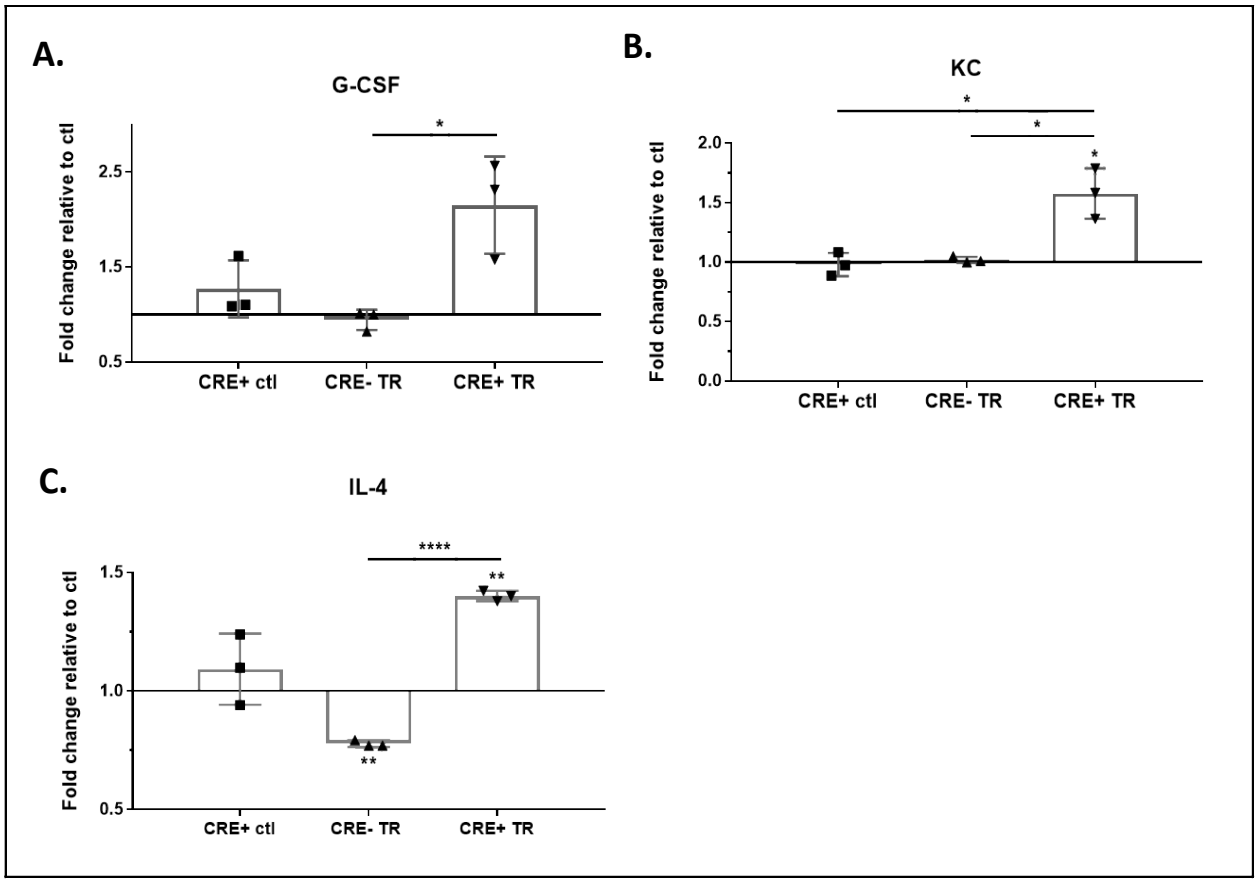

Figure 10: CHIT1 overexpression alters macrophage protein expression

Protein expression in CHIT1-OE BMDM and control BMDM was detected with a mouse cytokine array. Cell lysates were prepared from experimental and control BMDM which were untreated or exposed to 20 ng/mL IFN-γ + 100 ng/mL LPS for 8 hours. **(A-C)** BMDM treated with pro-inflammatory stimuli exhibited a significant increase in protein expression of **(A)** G-CSF, **(B)** KC, and **(C)** IL-4. N=3 biological replicates, each run in duplicate. Values represent fold change in florescence. *p<0.05, **** p<0.0001

3.2.2 Inflammatory signaling pathways are inhibited by CHIT1 overexpression

Phosphorylation is a fundamental component of intracellular signal transduction. To further explore the cell signaling potential of CHIT1, we treated both CHIT1-OE and control BMDM with IFN-γ + LPS for 0, 0.5, and 1 hour. Cell lysates were prepared and analyzed via Western blot for specific

phosphorylated signaling molecules: ERK 1/2, Akt, and IκB. While pIκB was not changed, pAkt (ser) and pERK 1/2 (ser) was significantly down regulated depicting a decrease in phosphorylated signaling in this pathway. This is consistent with diminished transcription of pro-inflammatory cytokines that we observed (figure 11C-D).

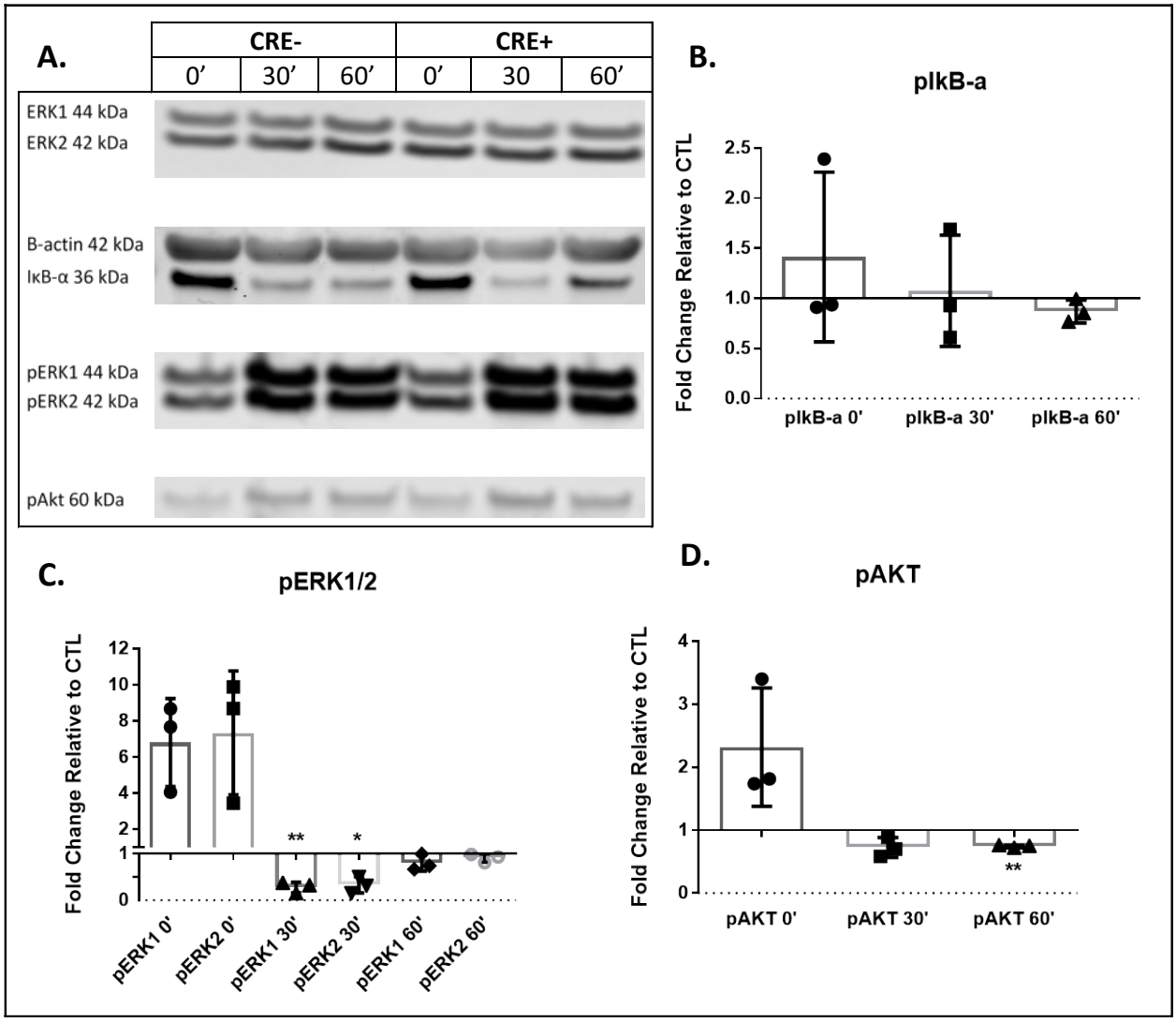

Figure 11: CHIT1 overexpression affects signaling pathways in macrophages

BMDM from CHIT1-OE mice and control animals were treated with 20 ng/mL IFN-γ + 100 ng/mL LPS for 0, 0.5, and 1 hour. ***(A)*** *Cell lysates were incubated with florescent antibodies for phosphorylated signaling molecules, and analyzed with Western blot. Florescence intensity was measured using the Licor Odyssey cLx.* ***(B)*** *No significant results were obtained in the presence of pIκB-α.* ***(C)*** *Exposure to pro-inflammatory*

stimuli led to depressed ERK1/2 signaling in CHIT1-OE BMDM after 0.5 hour and ***(D)*** *Akt signaling after one hour when compared to control BMDM. N=3 *p<0.05 **p<0.01,*

3.2.3 Macrophage invasiveness is enhanced by IL-13 in CHIT1 overexpressing macrophages

Infiltration of immune cells is facilitated in part by chemoattractants. MCP-1 is widely recognized as a macrophage chemoattractant that promotes invasion through the endothelium and plays a significant role in macrophage invasion of atherosclerotic plaques. A transwell invasion assay was performed to determine whether CHIT1 overexpression by macrophages affect their ability to penetrate ECM (figure 12).

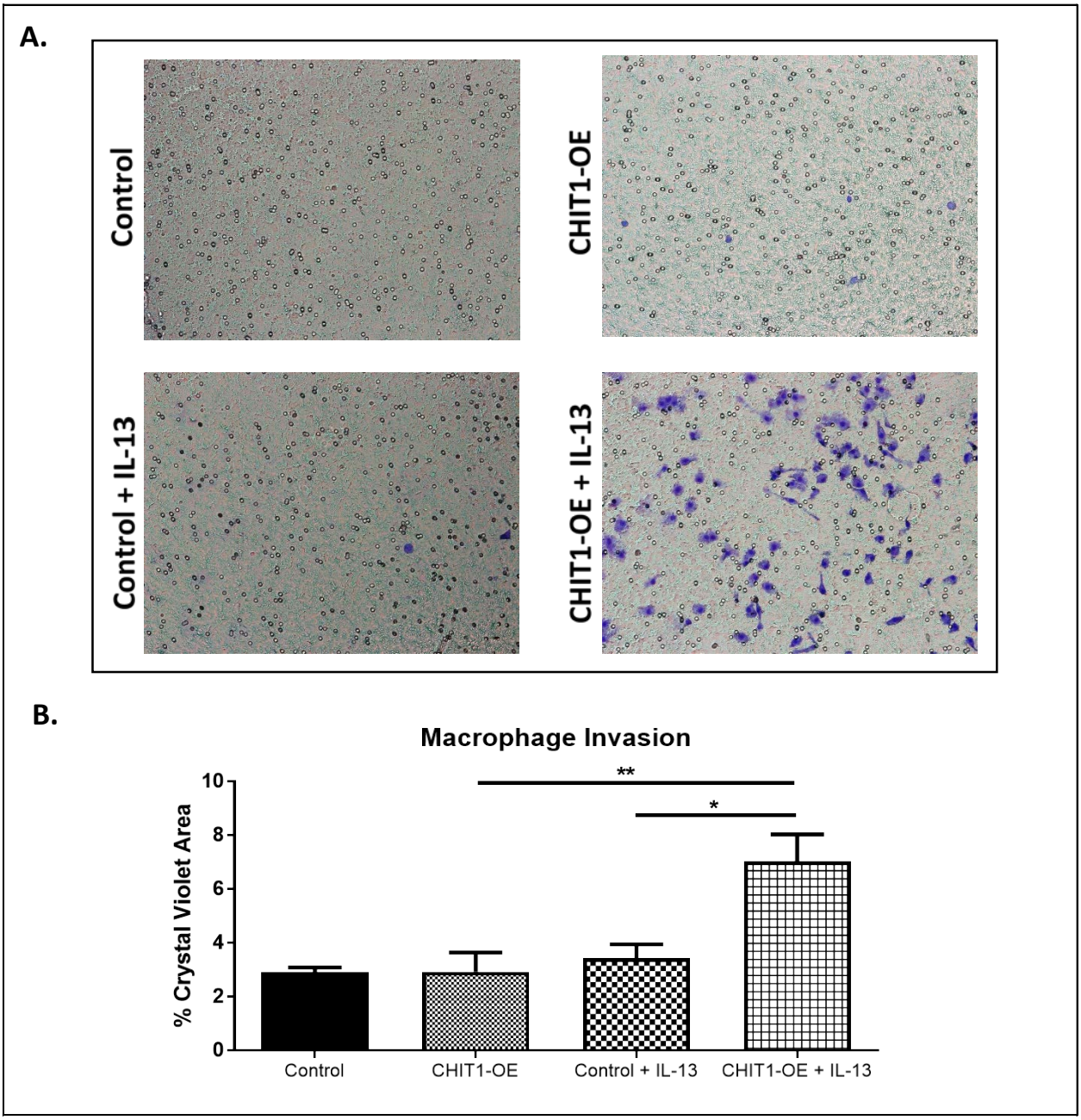

Figure 12: Macrophage invasiveness is enhanced by IL-13 in CHIT1-OE BMDM

A transwell invasion assay was performed with ECM matrigel serving as a basal substrate over a 0.8 µm membrane within the transwell insert. ***(A)*** *BMDM from control mice and CHIT1-OE mice were seeded on the matrigel and were treated with 10 ng/mL IL-13 or left untreated for 24 hours. Cells that migrated to the underside of the membrane were stained with crystal violet and quantified.* ***(B)*** *While CHIT1 expression or treatment with IL-13 alone had no effect on macrophage invasion, invasiveness was clearly amplified in*

CHIT1-OE BMDM treated with IL-13. ***(B)*** *Crystal violet staining was quantified using ImageJ software as % area stained compared to total area. N=3, *P<0.05 **P<0.01*

CHIT1-OE and control BMDM were seeded onto a layer of ECM matrigel in the top chamber of 0.8 µm filter membranes and allowed to migrate overnight in the presence of different chemoattractants. As an experimental control, MCP-1 was added to the bottom chamber of the transwell. IL-13 was explored as a possible chemoattractant due to its putative non-enzymatic interactions with CHIT1 (figure 12A). After 24 hours, the infiltrated cells were stained on the underside of the insert membrane with crystal violet. The images were analyzed with ImageJ software to quantify the macrophages that invaded the matrigel (figure 12B). No significant difference in invasiveness was detected with MCP-1. However, with IL-13 as the chemoattractant, CHIT1-OE BMDM displayed a significant increase in macrophage invasion in contrast to control BMDM.

3.2.4 Cholesterol metabolism was not affected by CHIT1 overexpression in BMDM

Uptake and efflux of low-density lipoproteins (LDL) by macrophages are extremely important mechanisms that have a profound effect on inflammation, foam cell formation, plaque development, etc. In direct lipid uptake experiments, we conducted a lipid uptake assay by incubating macrophages from CHIT1-OE mice and littermate controls with DiI-labeled, acetylated LDL or oxidized LDL for 6, 12, and 24 hours. Levels of cellular LDL accumulation were measured with flow cytometry by detection of the mean fluorescence intensity (MFI) of DiI. figure 13 shows MFI values for both conditions in experimental and control BMDM**.**

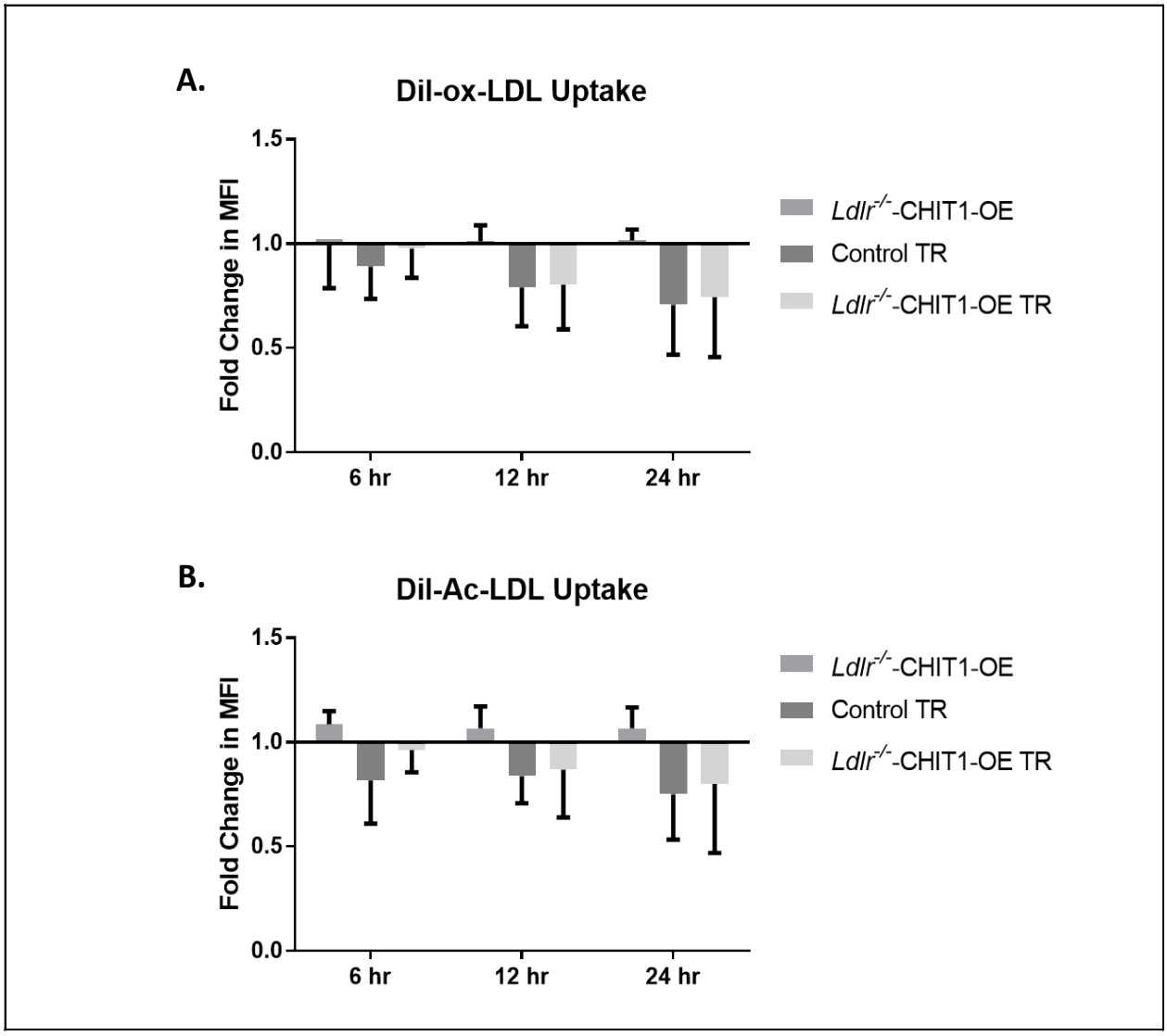

Figure 13: Macrophage overexpression of CHIT1 does not affect the lipid uptake in vitro

BMDM from CHIT1-OE mice and littermate controls were either left untreated or stimulated with 20 ng/mL IFN-γ + 100 ng/mL LPS and incubated with ***(A)*** *DiI-labeled ox-LDL or* ***(B)*** *Ac-LDL for 6 hours, 12 hours or 24 hours. The lipid uptake was measured with flow cytometry. No significant difference was observed between groups. N=3*

Proper regulation of cholesterol efflux in macrophages is imperative to cellular homeostasis and biological function. Further, dysfunctional cholesterol efflux is fundamental to the development and progression of atherosclerosis as lipid accumulation leads to deleterious downstream effects. To investigate whether overexpression of CHIT1 in BMDM affects transcription of genes involved in lipid

metabolism, we employed qPCR analysis (figure 14). Treatment of BMDM from CHIT1-OE mice with acetylated LDL (ac-LDL) for 6 hours resulted in diminished transcription of ABCA1 mRNA and enhanced transcription of ABCG1 compared to control BMDM *In vitro*. We utilized a cholesterol efflux assay to investigate whether CHIT1 overexpression affects cholesterol homeostasis by labelling Ac-LDL with [^{3}H]-cholesterol and incubating BMDM from CHIT1-OE and control mice for 24 hours. While we observed significant differences in ABCA1 and ABCG1 transcription (figure 14A and B), cholesterol efflux was not significantly different between groups (figure 14C).

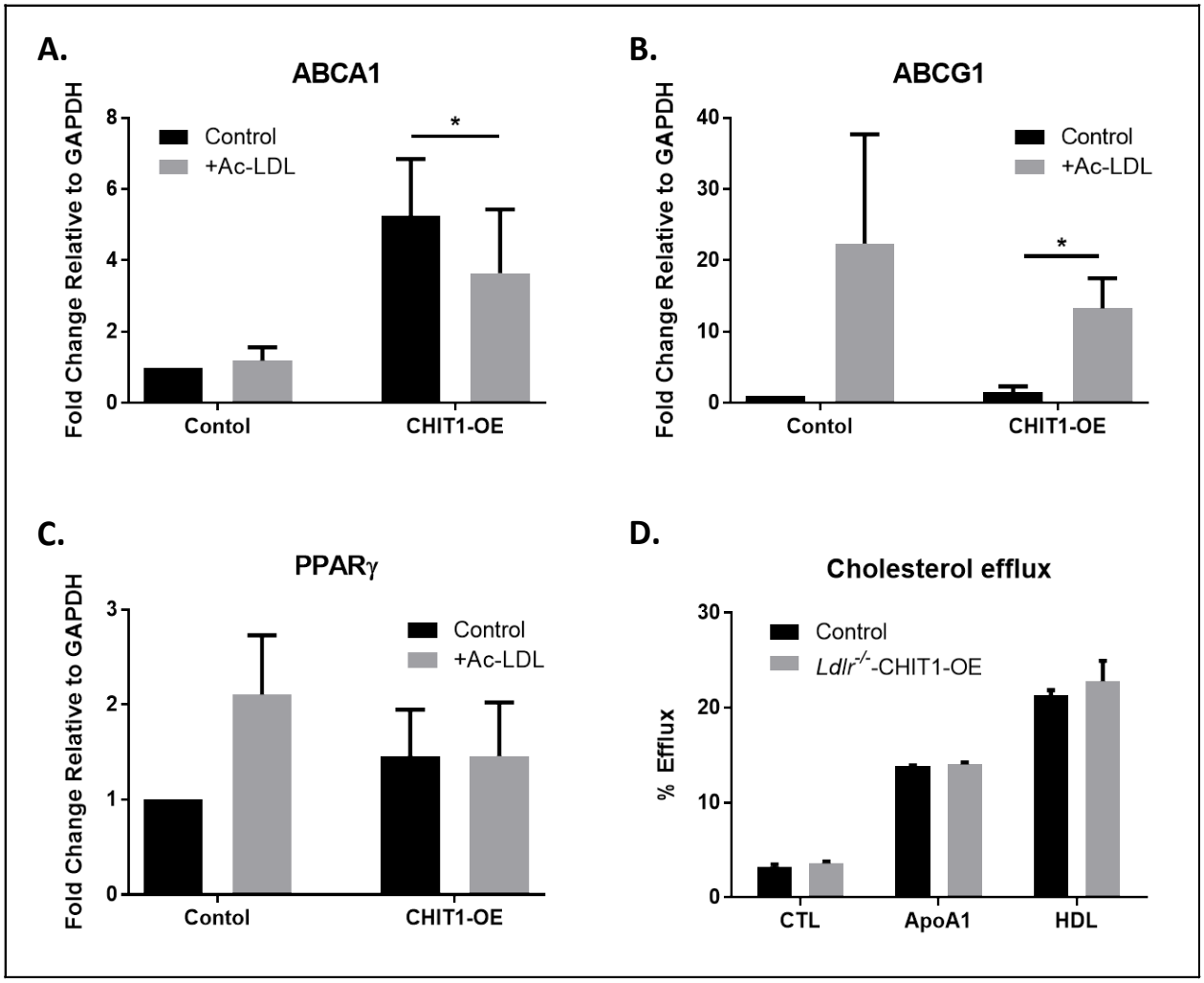

Figure 14: Overexpression of CHIT1 does not affect cholesterol efflux

mRNA transcription of genes involved with macrophage cholesterol efflux was determined using qPCR. BMDM from control and CHIT1-OE mice were incubated with or without Ac-LDL for 6 hours. (A) Transcription of ABCA1 was significantly down regulated in CHIT1-OE BMDM incubated with Ac-LDL. (B) ABCG1 transcription was significantly upregulated when CHIT1-OE BMDM were exposed to Ac-LDL in comparison to control BMDM. (C) PPARγ was not significantly affected by treatment with Ac-LDL in either experimental or control BMDM. (D) Cholesterol efflux was carried out by incubating BMDM from CHIT1-OE and control mice with [^{3}H]-Cholesterol-labeled Ac-LDL for 24 hours. Efflux was generally unchanged between groups. N=3, *P<0.05

3.3 Macrophage overexpression of CHIT1 affects atherosclerotic plaque morphology *in vivo*

Taken together, *in vitro* data that CHIT1 inhibited transcription of pro-inflammatory cytokines and chemokines, elevated protein expression of anti-inflammatory cytokines, and participated in macrophage

invasion of ECM are suggestive of a protective role for CHIT1 in atherosclerosis. To test whether our *in vitro* data indeed support this assertion, an atherosclerosis mouse study was designed. For this *in vivo* model we crossbred *Ldlr*$^{-/-}$ mice with CHIT1-OE mice in order to generate an atherosclerosis-prone, CHIT1 overexpressing mouse model. After 8 weeks male mice were placed on HFD containing 15.8% (wt/wt) fat and 1.25% cholesterol (wt/wt) (diet 94059; Harlan Teklad Laboratories, Indianapolis, IN, USA) for 12 weeks to induce atherosclerosis.

3.3.1 Initial characterization of *Ldlr*$^{-/-}$- CHIT1-OE mice post-HFD

Upon termination of the HFD regimen, blood was collected from all study mice in each group before sacrifice. Serum cholesterol and triglyceride levels were analyzed with commercially available fluorometric and colorimetric kits (Cayman Chemical). No difference in cholesterol or triglycerides was detected between experimental and control groups. Measurement of body weight before and after 12 weeks of HFD revealed significant weight gain in both groups at the end of the experiment, with no differences observed between groups (figure 15).

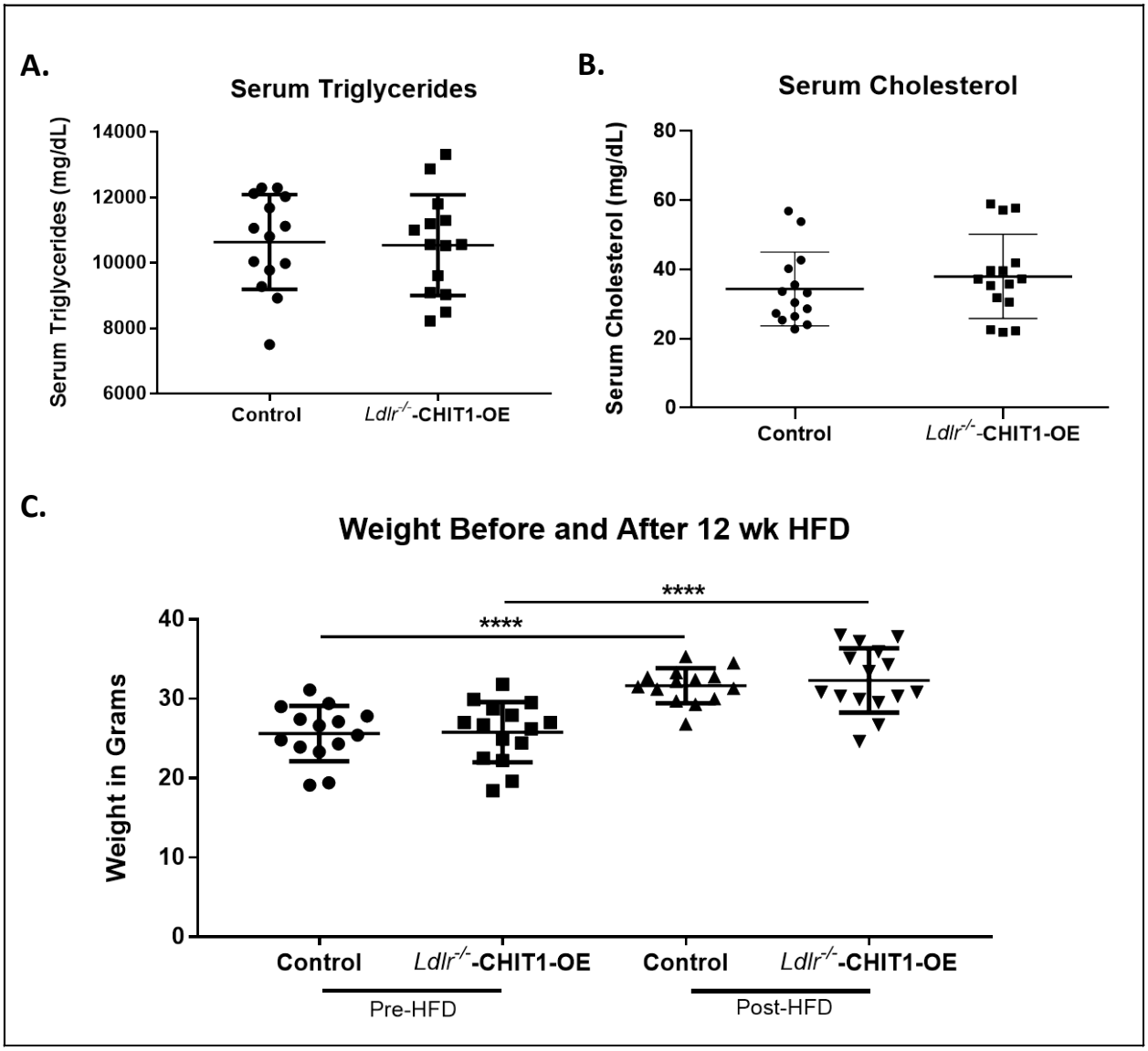

Figure 15: Initial characterization of study mice

After 12 weeks of HFD both control mice and Ldlr$^{-/-}$- CHIT1-OE mice were analyzed for differences in serum triglycerides and cholesterol levels. ***(A-B)*** *Using a colorimetric and fluorometric kit revealed no significant differences in serum triglycerides or cholesterol between groups.* ***(C)*** *Animal body weight was also measured before and after administration of HFD. No significant differences were observed between groups only before and after HFD within groups. N=14 per group, ****P<0.0001*

Analysis of circulating leukocyte populations following 12 weeks of HFD was carried out using flow cytometry. 100 µL of whole blood was stained with antibodies specific to flow cytometry as previously described. Figure 15 depicts leukocyte populations of T cells, monocytes, and neutrophils (figure 16). No significant difference in these populations was observed between groups suggesting that CHIT1 does not affect leukocyte survival or proliferation.

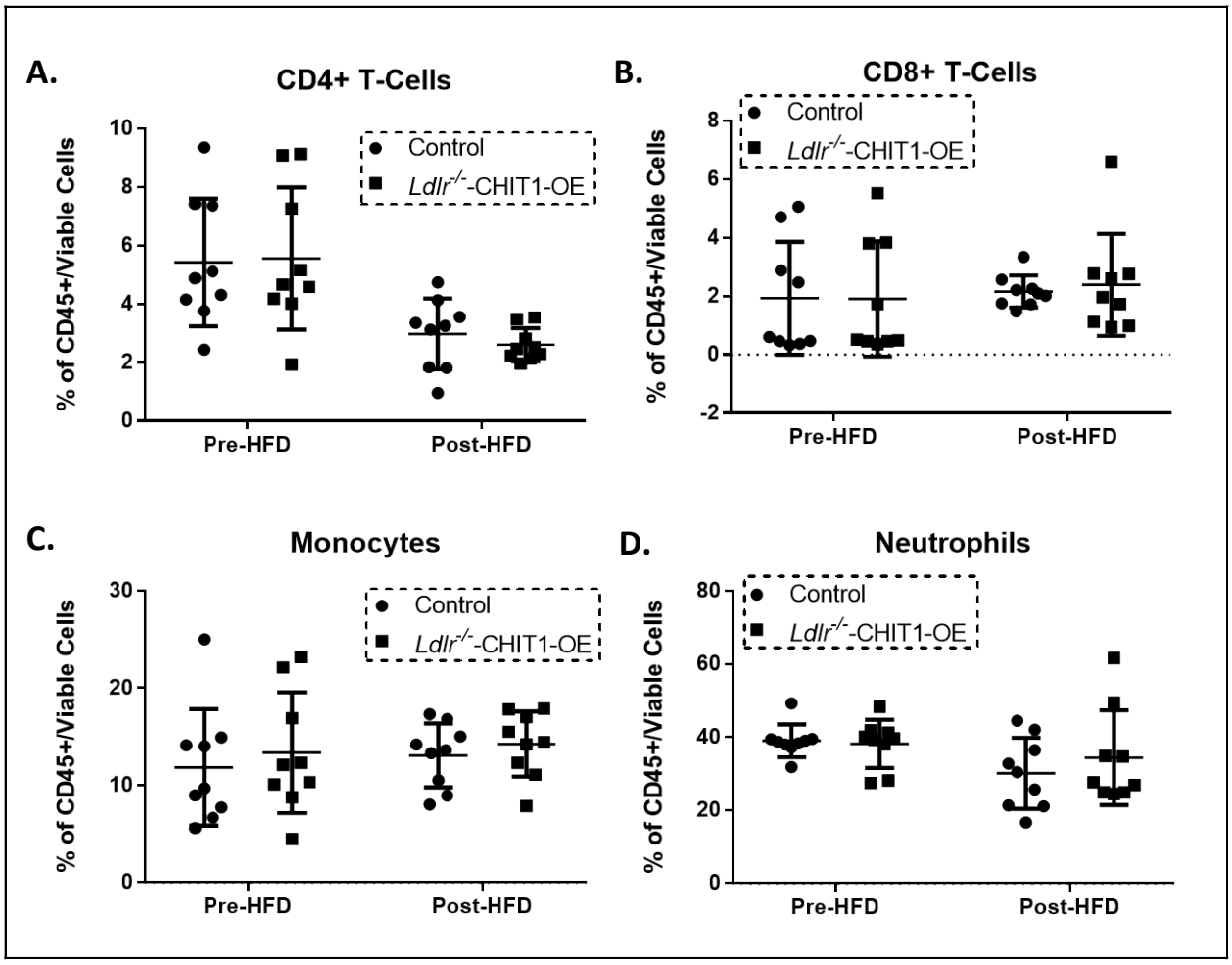

Figure 16: Populations of circulating leukocytes after 12 weeks of HFD

Blood collected from study mice at sacrifice was processed, stained, and analyzed using flow cytometry in order to determine the relative percentage of each population compared to viable/CD45+ cells. ***(A-D)*** *Monocytes, neutrophils, CD4 T cells, and CD8 T cells were identified via differential gating based on antibody staining selection. No significant difference in leukocyte populations was observed between groups. N=9*

3.3.2 CHIT1 overexpression in atherosclerotic mice does not affect plaque area

Areas of the cardiovascular system that are subject to high flow volumes and shear stress for vulnerable regions for the development of atherosclerotic plaque. The aortic sinus, aortic arch, and abdominal aorta are widely accepted as being indicative of atherosclerosis *in vivo*. In an effort to determine the effects of CHIT1 overexpression in *Ldlr*$^{-/-}$ mice, mouse hearts were perfused with 4% PFA/5% sucrose before being removed from the animal. Hearts were subsequently embedded in OCT compound, and frozen at -80° C. Serial cryosections were prepared at a thickness of 10 µm using a cryostat, and were then mounted on to glass slides. Cryosections were made specifically of the aortic sinus where all 3 leaflets are visible. Samples from both groups were stained in ORO for 30 minutes before being washed with 60% isopropanol (figure 17A). Quantification was performed using ImageJ software and measurements are represented as the percentage of stained area in relation to total plaque area (figure 17B). To further analyze plaque content *in vivo* we also quantified plaque accumulation in the whole aorta. This was accomplished by cleaning and excision of the entire aorta from the aortic arch to the iliac bifurcation.

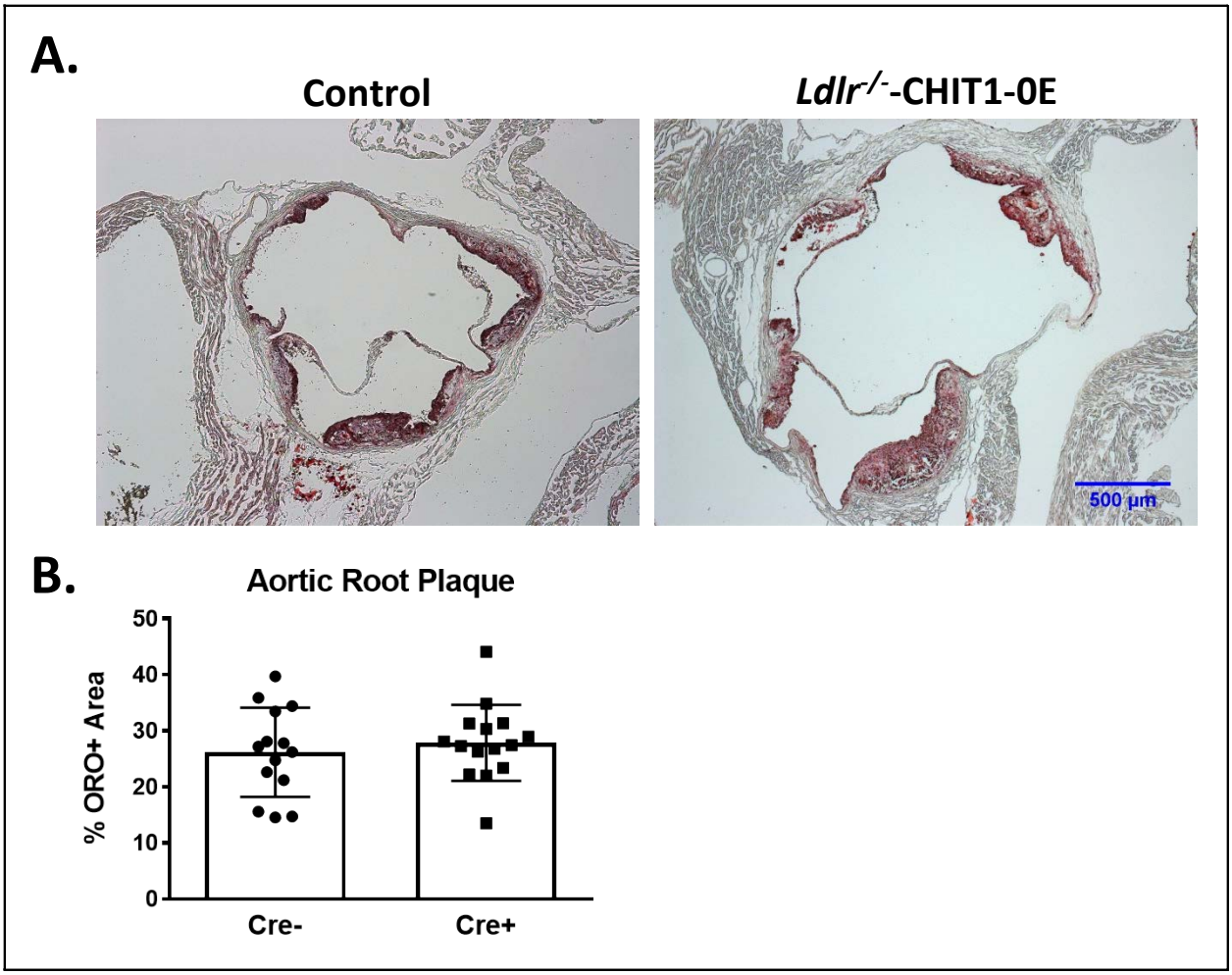

Figure 17: Aortic plaque size is not affected by CHIT1 overexpression in vivo

(A) *Cryosections of the aortic sinus from both Ldlr$^{-/-}$- CHIT1-OE (CRE+) mice and littermate controls (CRE-) after 12 weeks of HFD were stained with Oil-Red-O to determine plaque size.* ***(B)*** *Analysis of plaque area as a function of % total area. Measurement with ImageJ software showed no significant differences in plaque size between experimental and control animals. N=14 per group*

An incision was made longitudinally along the length of the aorta such that it could be separated, pinned, and stained with ORO for 30 minutes (figure 18A). Again, plaque aggregation was measured with ImageJ software and in this case results are represented as percentage of stained area in relation to total aortic area (figure 18B).

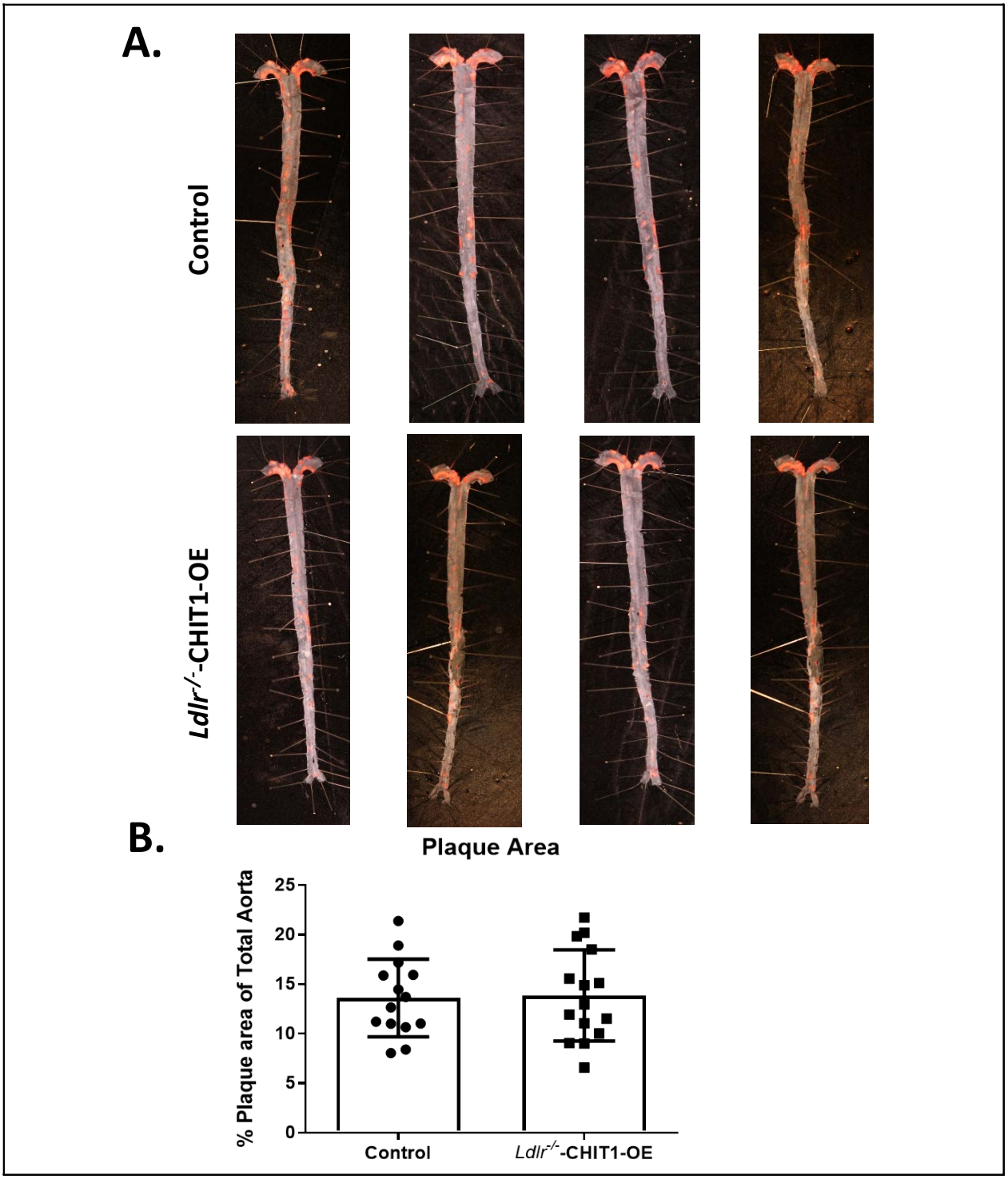

Figure 18: CHIT1 overexpression by macrophages does not affect aortic atherosclerotic lesion size

(A) Whole aortas were removed from both Ldlr-/--CHIT1-OE and control mice after 12 weeks of HFD. The specimens were pinned and stained with Oil-Red-O. (B) No difference was observed between groups upon quantification of plaque area as a percentage of total aortic area. N=14 per group

3.3.3 Macrophage content in atherosclerotic plaques is unaffected by CHIT1 overexpression

Macrophages play multifaceted roles in the development of atherosclerosis. Recruitment and accumulation of macrophages is associated with increased plaque size and weakening of the fibrous cap. We sought to determine whether CHIT1 overexpression in *Ldlr*$^{-/-}$ mice alters macrophage accumulation in atherosclerotic plaques. To this end, slides were prepared from serial cryosections of the aortic sinus at 10 µm increments. Figure 19 depicts samples from each group that were incubated for 24 hours with MOMA primary antibody and then and HRP conjugated chromogen was applied. MOMA is a macrophage specific stain and therefore, it was utilized to determine macrophage content and plaques. No significant difference was observed between groups after analyzing percent MOMA stained area relative to total plaque area (figure 19B).

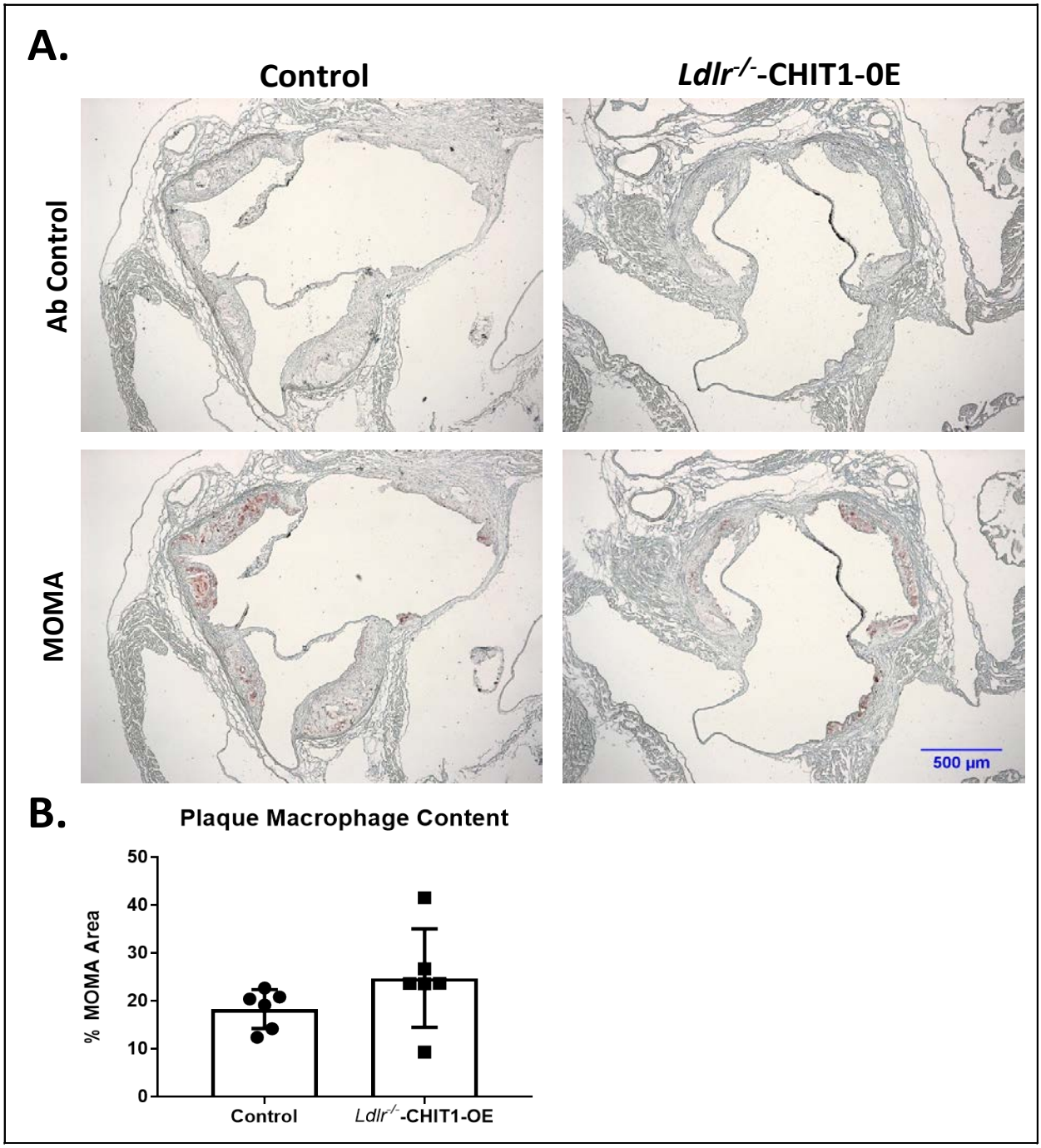

Figure 19: Macrophage content in aortic plaques is not affected by CHIT1 overexpression in vivo

(A) Cryosections of the aortic sinus from both Ldlr$^{-/-}$- CHIT1-OE mice and littermate controls after 12 weeks of HFD were stained with MOMA to determine macrophage content. **(B)** Analysis of stained area versus % total plaque area. Measurement with ImageJ software showed no significant differences in macrophage content between experimental and control animals. N=6 per group

3.3.4 CHIT1 is highly expressed in atherosclerotic plaques of *Ldlr*$^{-/-}$-CHIT1-OE mice post-HFD

Given the importance of macrophages in every stage of atherosclerosis and the fact that CHIT1 is among the most abundantly expressed proteins by activated macrophages, we stained serial cryosections prepared at a thickness of 10 µm of the aortic sinus with a murine CHIT1 antibody (figure 20). Ensuing 24 hours of incubation, a secondary HRP conjugated chromogen was applied and CHIT1 was visualized using light microscopy. IHC revealed significantly greater expression of CHIT1 in the atherosclerotic plaques of *Ldlr*$^{-/-}$- CHIT1-OE mice in comparison to littermate controls. CHIT1 staining was quantified using ImageJ software and expressed as the CHIT1 stained area as a percentage of the total plaque area.

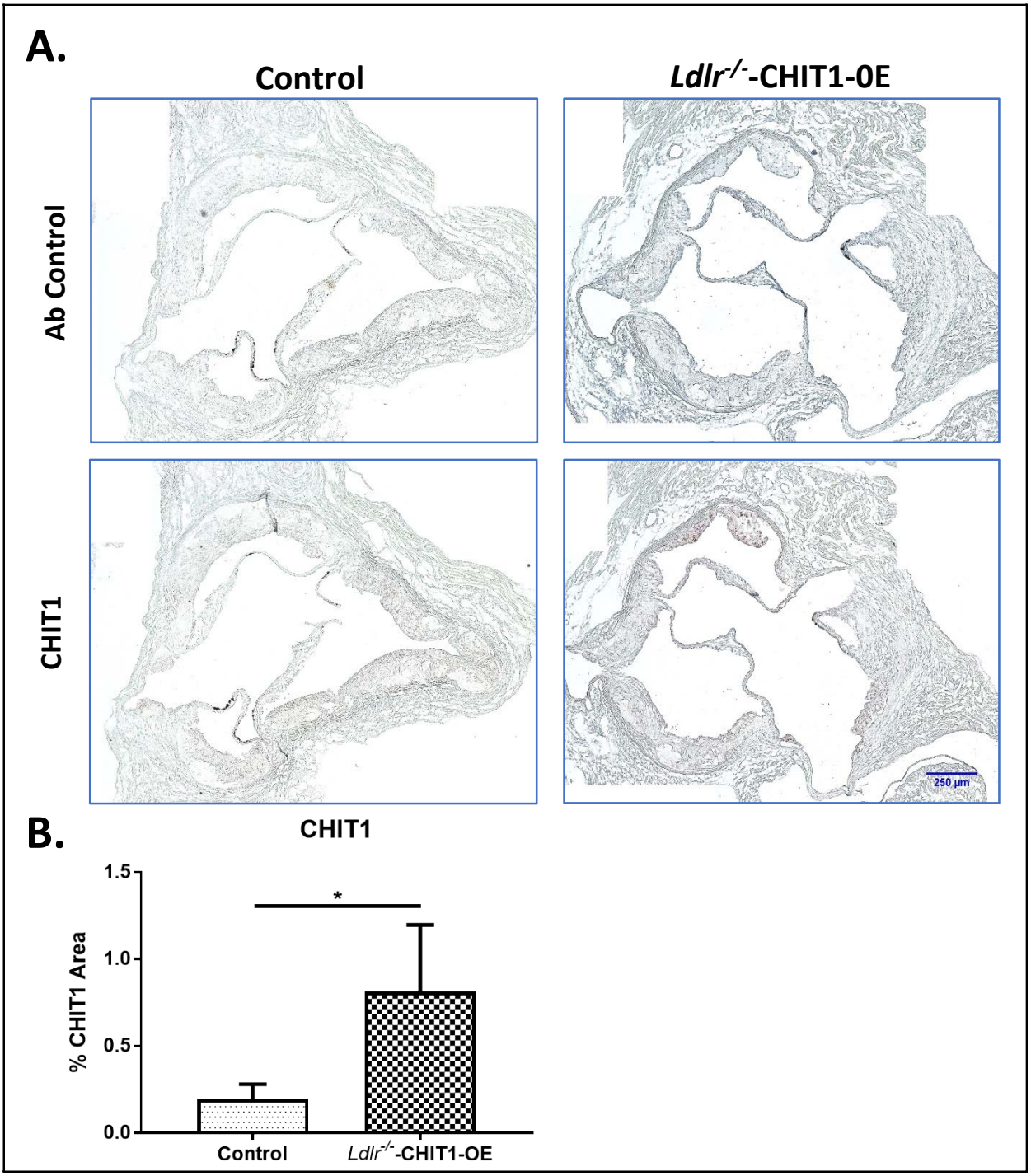

Figure 20: CHIT1 is abundant in atherosclerotic plaques of Ldlr$^{-/-}$-CHIT1

(A) *Cryosections of the aortic sinus from both Ldlr$^{-/-}$- CHIT1-OE mice and littermate controls after 12 weeks of HFD were stained with biotinylated antibodies against CHIT1.* ***(B)*** *Analysis of stained area versus % total plaque area. Measurement with ImageJ software showed no significant differences in macrophage content between experimental and control animals. N=6 per group, *P<0.05*

3.3.5 CHIT1 overexpression alters ECM content in the aortic sinus of *Ldlr*$^{-/-}$ mice

At sacrifice, mice were perfused with PBS followed by 4% PFA/5% sucrose. The hearts were collected and embedded in OCT compound to be frozen and cryosectioned at a thickness of 10 µm. Serial sections were made at the aortic sinus where 3 valve leaflets were visible. The heart sections were stained for hyaluronic acid (HA) using a biotinylated hyaluronic acid binding protein (BHABP) and collagen using picrosirius red. The sections were analyzed using ImageJ software to determine the area of HA and collagen deposition as a percentage of overall plaque area (Figure 21). Our findings were that both HA and collagen were significantly more abundant in CHIT1 overexpressing mice.

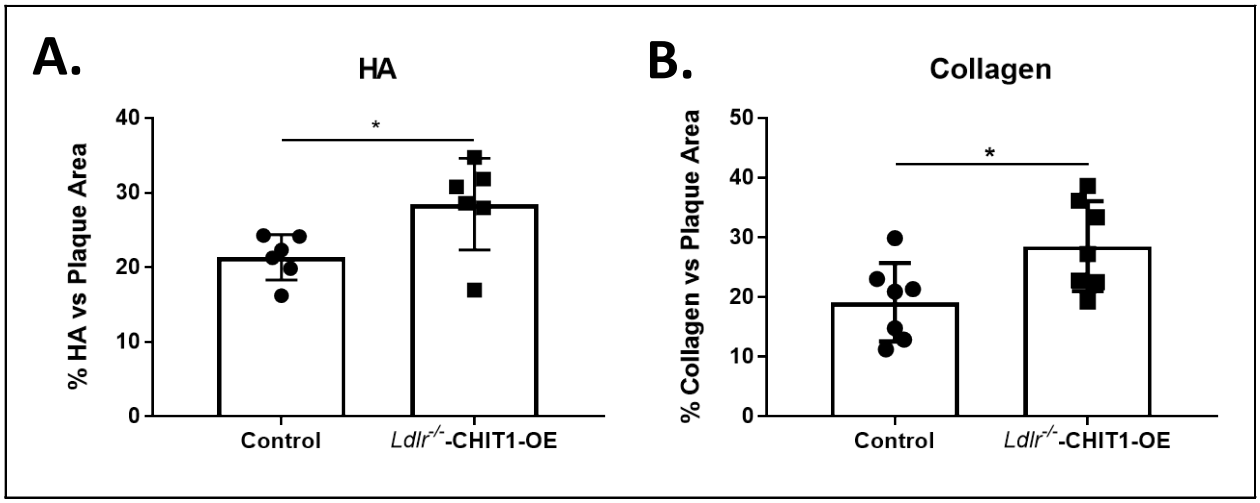

Figure 21: CHIT1 overexpression significantly increases HA and collagen in atherosclerotic plaques

(A-B) *Analysis of stained collagen and HA area as a function of % total plaque area. Measurement with ImageJ software revealed significant differences in collagen stained area between experimental and control animals. HA: N=6 per group, Collagen: N=7 per group*

Further, the pattern of HA and collagen accumulation had observational differences in distribution between CHIT1-OE mice and littermate controls (figures 22 and 23). We found that while HA expression was generally limited to the periphery of atherosclerotic plaques in control mice, while in CHIT1-OE mice HA staining could be seen within almost all aspects of the plaque (figure 22E).

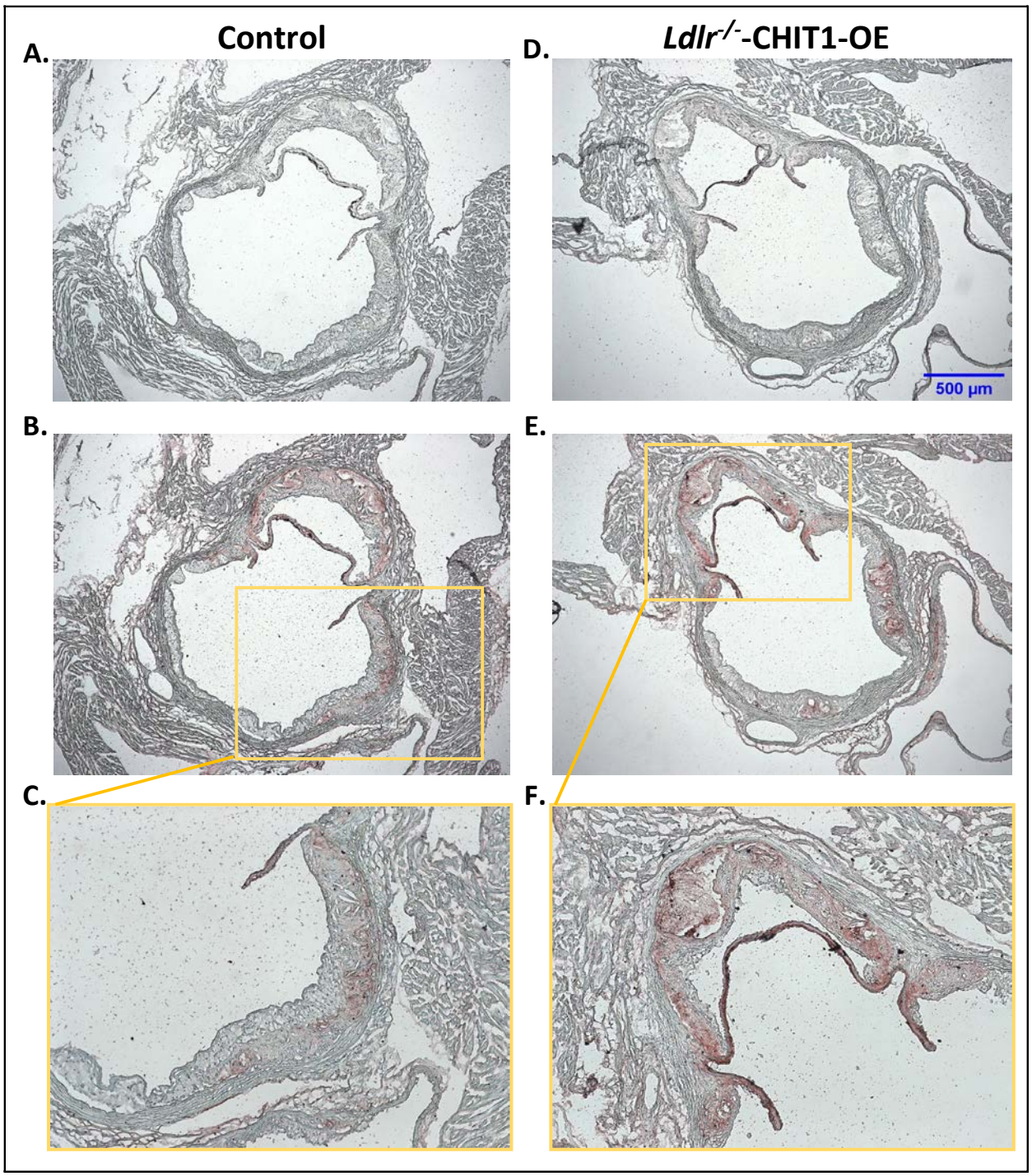

Figure 22: Overexpression of CHIT1 alters the distribution of HA in atherosclerotic plaques

(A and D) *antibody control.* ***(B and E)*** *HA stained with BHABP can be seen localized in the periphery of the aortic sinus in control cryosections, whereas HA appears throughout the plaque and within the necrotic cores of Ldlr$^{-/-}$- CHIT1-OE mice.* ***(C and F)*** *10 X magnification reveals the extensive HA staining in plaques of Ldlr$^{-/-}$- CHIT1-OE mice particularly within the necrotic core. N=6 per group*

Distribution of collagen in plaques from control mice was similar to that of HA, whereas in CHIT1-OE mice collagen staining was most prevalent on the luminal aspect of atherosclerotic plaques and could be found encircling necrotic cores (figure 23).

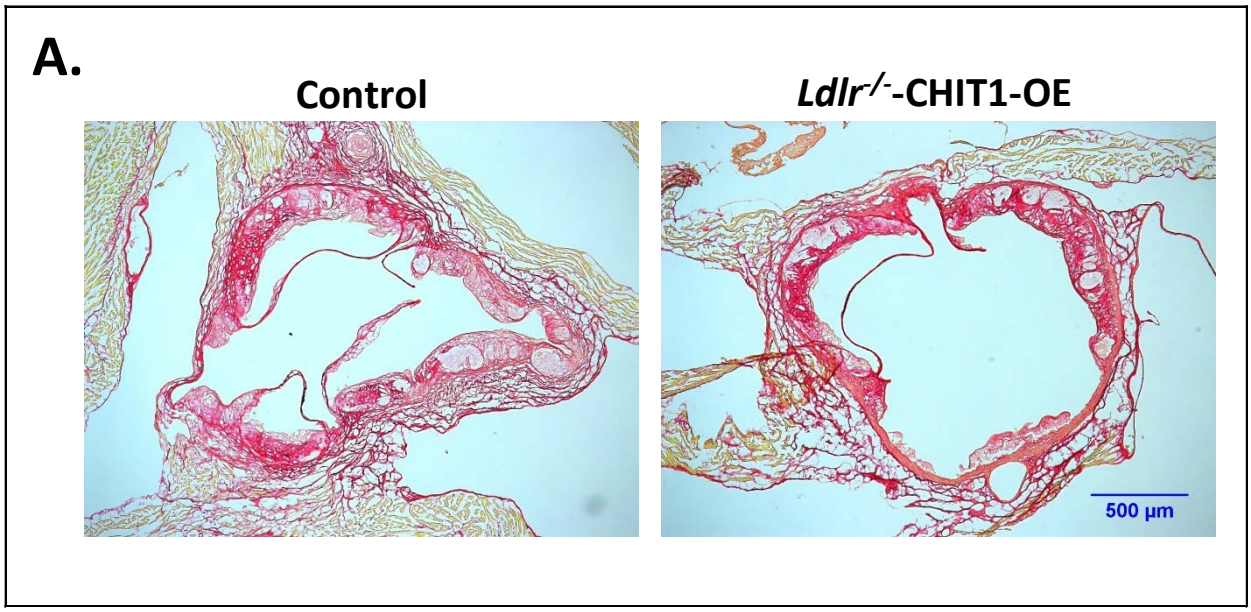

Figure 23: CHIT1 overexpression augments collagen distribution in atherosclerotic plaques

(A) *Cryosections of the aortic sinus from both Ldlr$^{-/-}$- CHIT1-OE mice and littermate controls after 12 weeks of HFD were stained with picrosirius red to visualize type I collagen. While collagen appears unorganized and lightly stained especially on the luminal aspect of necrotic cores in control sections, collagen had a more organized "lattice" appearance and was distributed around necrotic cores and specifically on the luminal aspect. N=7 per group*

CHAPTER 4: DISCUSSION

4.1 Summary and interpretation of results

In previously published work, we reported that CHIT1 mRNA was present in atherosclerotic lesions within the descending aorta of cynomolgus monkeys. CHIT1 mRNA expression was also closely correlated with macrophage infiltration in atherosclerotic plaques of abdominal aortas. Our research further demonstrated that inhibition of CHIT1 with allosamidin promoted atherosclerosis in hyperlipidemic mice [119]. Here we show *In vitro* evidence using CHIT1-OE macrophages that overexpression of CHIT1 modulates the inflammatory response in an anti-inflammatory manner when subjected to an inflammatory stimulus of IFN-γ with LPS. A non-resolving inflammatory response promotes the development of atherosclerosis through continuous recruitment and activation of immune cells, perhaps most importantly, macrophages. As CHIT1 is abundantly produced by activated macrophages, it is likely that it's expression contributes to anti-inflammatory cell functions. Macrophage invasion through the ECM was also quantified *in vitro* and revealed that IL-13 significantly enhanced the invasiveness of CHIT1-OE BMDM. In developing a *Ldl*$^{-/-}$- CHIT1-OE mouse model we were able to conduct an *in vivo* mouse study to investigate the effects of CHIT1 overexpression in an atherosclerotic animal model. While we were unable to observe significant differences in macrophage content or lesion size, we found significant alterations in plaque morphology. The accumulation and distribution of HA and collagen allude to a possible interaction between CHIT1 and the ECM.

4.1.1 Macrophage inflammatory functions

Dysregulation of the innate immune response drives atherogenesis, and the resultant stages of atherosclerosis are largely attributable to the recruitment and infiltration of monocytes into the intimal layer of the vessel wall. Chemokines like macrophage chemoattractant protein-1 (MCP-1) are well known contributors to atherosclerosis [124, 125]. MCP-1 has been shown to accelerate atherosclerosis in ApoE-deficient mice. MCP-1 overexpression in ApoE-deficient mice resulted in increased to lipid staining,

oxidized lipid, and immunostaining for macrophage cell surface markers. Our own experiments revealed a trend of transcriptional down-regulation of MCP-1 in CHIT1-OE BMDM compared to littermate controls when exposed to IFN-γ with LPS. Given the importance of MCP-1 in the development of atherosclerotic plaques and disease progression, the relationship it shares with CHIT1 expression is certainly intriguing. Recruitment of macrophages toward atherosclerotic lesions and plaques is effectively achieved in large part by the chemoattractant properties of specific cytokines. Interestingly, we found protein expression of the chemotactic cytokine KC (the murine homolog of IL-8) is significantly upregulated in CHIT1-OE macrophages when treated with inflammatory stimuli. KC and its receptor CXCR2 are secreted by activated macrophages and play a significant role in immune cell trafficking and infiltration of the vessel wall. In an effort to elucidate the mechanism of KC/CXCR2 in atherosclerosis, Boisvert et al. utilized $LDLR^{-/-}$, atherosclerosis-prone mice with KC/GRO-$\alpha^{-/-}$ and $CXCR2^{-/-}$ mice to demonstrate that overexpression of KC/GRO-α and CXCR2 are essential to macrophage accumulation into atherosclerotic lesions. Results also revealed that KC/GRO-α and CXCR2 do not play a critical role in macrophage recruitment into early atherosclerotic lesions [126]. While it is generally accepted that KC participates in development of atherosclerosis, other studies suggest a putative role of IL-8/KC in smooth muscle cell proliferation and recruitment as well as angiogenesis [127-129]. IL-8 was shown to be a potent macrophage-derived mediator of angiogenesis. Human recombinant IL-8 was administered in the rat cornea where it induced proliferation and chemotaxis of human umbilical vein endothelial cells. Also, blockade of IL-8 by antibodies decreased angiogenic activity of inflamed human rheumatoid synovial tissue macrophages [130]. Such findings suggest that IL-8 may be involved in tissue repair and wound healing.

IL-4 is a cytokine associated with alternative macrophage activation which potentiates Th2 inflammatory processes. We have demonstrated that IL-4 protein expression is significantly upregulated in CHIT1-OE BMDM. Experimental evidence demonstrates that IL-4 signaling involves SOCS1 to induce M2 macrophage polarization while inhibiting SOCS3 signaling and negatively regulating M1 polarization [131,

132]. IL-4 activation of alveolar macrophages has been shown to promote wound healing in the long after Helmand invasion or during gut inflammation in mice [133]. And in the context of atherosclerosis, IL-4 attenuated atherosclerosis in several different mouse models [134-136]. Given that IL-4 and IL-13 signaling includes a pathway requiring both cytokines, and the putative interactions of CHIT1 with IL-13, it is foreseeable that CHIT1 can participate in IL-4/IL-13 signal transduction.

A definitive role for macrophage-derived granulocyte colony stimulating factor (G-CSF) in atherosclerosis has yet to be established. However, several studies suggest protective roles for G-CSF in atherosclerotic animal models. We observed a significant increase in protein expression of G-CSF in BMDM harvested from CHIT1-OE mice compared to WT controls. Experiments with human peripheral blood mononuclear cells (PBMC) illustrated that G-CSF post-transcriptionally inhibits TNF-α secretion from PBMC. Suppression of TNF-α secretion was accomplished without affecting mRNA expression [137]. G-CSF also promotes generation of type-1 regulatory T cells (Treg) that secrete the anti-inflammatory cytokine IL-10, and TGF-β1 which is associated with tissue repair, wound healing, and fibrosis [138]. Several studies have described a protective role for G-CSF in atherosclerotic mouse and rabbit models. Daily treatment of ApoE deficient mice with G-CSF for nine weeks resulted in less atheromatous plaque area and a decrease in macrophage infiltration into atherosclerotic lesions. The authors also observed decreased serum cholesterol and LDL, which is suggestive of lipid-related effects of G-CSF [139]. In hyperlipidemic and cholesterol fed rabbit models, G-CSF administration prevented progression of atherosclerotic lesions and vascular stenosis, while encouraging plaque stability and reendothelialization. Moreover, it was shown that an appropriate dosage of G-CSF was required for these protective effects to manifest most efficiently [140, 141].

Pro-inflammatory cytokines like TNF-α and IL-6 perpetuate chronic inflammation associated with atherosclerosis. We found that transcripts of both were down regulated in BMDM from CHIT1-OE mice compared to those of littermate controls, *in vitro,* when stimulated with a combination of the

inflammatory stimuli; IFN-γ + LPS. TNF-α is a potent mediator of inflammatory signaling by influencing the activation state of leukocytes, the release of cytokines and chemokines, and expression of NO and ROS. Studies have indicated that TNF-α contributes to the development and progression of atherosclerosis. Using a TNFα-deficient mice crossbred with atherosclerosis prone APOE*3-Leiden mice, Boesten et al. demonstrated that TNF-α promoted the formation of advanced lesions and necrosis as apoptosis was decreased, although lesion area did not change [142]. Inhibition of TNF-α in ApoE deficient mice resulted in a 50% reduction of relative lesion size after 10 weeks of Western diet. And in ApoE knockout mice, administration of soluble TNF receptor I pellets reduced lesion size after 25 weeks [143].

IL-6 is another cytokine that contributes to propagating the inflammatory cascade associated with atherosclerosis. IL-6 modulates both acute and chronic inflammation. IL-6 is pleiotropic in nature and can enhance the given polarization state of macrophages. IL-6 is also capable of inhibiting Treg formation [144]. Injection of supra-physiological levels of IL-6 exacerbated early atherosclerosis in ApoE-deficient mice fed a high-fat diet. Upon injection, significant increases in IL-1β and TNF-α. Treatment with IL-6 resulted in increased lesion size in atherosclerotic, ApoE-deficient mice. The authors concluded that the presence of IL-6 ultimately exacerbated early atherosclerosis in mice [145]. The effect of CHIT1 in diminishing transcription of inflammatory cytokines like TNF-α and IL-6 require further study to determine what therapeutic potential if any may exist.

4.1.2 Inflammatory signaling pathways

To extend our understanding of the inflammatory mechanisms affected by CHIT1 overexpression, we investigated inflammatory signaling pathways associated with atherosclerosis. Our data revealed significant decrease in pERK1/2 protein expression in BMDM from CHIT1-OE mice compared to littermate controls when exposed to IFN-γ + LPS after 30 minutes *in vitro*. We also observed that Akt signaling was suppressed in CHIT1-OE BMDM after 60 minutes of treatment with the same inflammatory stimuli *in vitro*. The ERK1/2 signaling pathway is critical to the expression and secretion of various downstream effectors

that mediate inflammation. Experimental evidence demonstrates that LPS stimulation of murine peritoneal macrophages activated ERK1/2 signaling, causing the subsequent induction of TNF-α secretion [146]. IFN-γ stimulation of this pathway in human macrophages induced alterations in the expression of several key genes implicated in the progression of atherosclerosis, such as MCP-1 [147]. Akt signaling has various roles in macrophage function. Deficiency of Akt mediated signal transduction elicits M2 macrophage polarization and negative regulation of the TLR4 signaling pathway [148-150]. In relation to atherosclerosis, Zhai et al. found that inhibition of Akt signaling depressed autophagy *in vitro*, and atherosclerotic mouse models exhibited enhanced plaque stability as well as diminished inflammatory response was promoted by Akt/mTOR-mediated autophagy [151].

4.1.3 Macrophage invasion

Invasion of monocytes/macrophages is a continuous process throughout atherosclerosis that begins with the initiation of an inflammatory response by invading monocytes, illicit plaque formation via infiltration and accumulation of immune cells, and ultimately ends with fibrous cap weakening and thrombosis. Given the data presented in a number of studies describing the effects of CHIT1 and IL-13, we performed an ECM invasion assay to determine whether this interaction influences macrophage invasiveness [115, 152, 153]. We found that when IL-13 was used as a macrophage chemoattractant, invasion of CHIT1-OE BMDM through the ECM matrigel was significantly greater than those from littermate controls. Interestingly, Correale et al. showed that IL-13 significantly increased CHIT1 secretion from macrophages and that CHIT1 enhanced macrophage secretion of chemokines including IL-8, MCP-1, and RANTES. Further, IL-13 promoted macrophage transmigration through a blood-brain barrier model *in vitro* [115]. Induction of immune cell trafficking by CHIT1 in concert with IL-13 seems to be a novel interaction that may have relevant effects in atherosclerosis and other inflammatory diseases.

4.1.4 Overexpression of CHIT1 and atherosclerotic plaque morphology

The ECM is an important component for a wide array of cellular functions. In the cardiovascular system, ECM interactions serve as a cell signaling platform and maintain structural integrity of the heart and vasculature. Changes in ECM content related to atherosclerosis has been implicated in fibrous cap formation and plaque stability. Our results demonstrate a significant increase in key ECM components: hyaluronic acid (HA) and collagen in the plaques of $ldlr^{-/-}$, CHIT1-OE mice when compared to littermate controls. HA is a large, hydrophilic glycosaminoglycan (GAG) that is integral to wound healing and tissue remodeling [154]. Degradation of HA by hyaluronidases is upregulated in unstable atherosclerotic plaques, while the formation of a pericellular HA matrix supports smooth muscle cell proliferation and migration possibly enhancing plaque stability [155, 156]. It should be noted that no endogenous substrate for CHIT1 has been identified in vertebrates. However, studies have demonstrated that the DG42 gene in Xenopus and mouse models produces chitin-oligosaccharides as a precursor to HA chains [157, 158]. Also, due to the structural similarity of HA to its native substrate; chitin, the CHIT1 binding domain is capable of interactions with HA [107, 108]. It may be possible that chitin interactions with HA prevent its degradation, thereby promoting plaque stability.

Like HA, collagen contributes to the mechanical strength of atheromatous plaques. Collagen comprises up to 60% of the total plaque protein and engages a multitude of cell functions. Modulation of macrophage behavior, smooth muscle cell proliferation/migration, and plaque reinforcement exemplify the variety of functions and cell types that collagen can influence [159-161]. CHIT1 has also been implicated in collagen production as evidenced by fibrotic diseases in the liver and lungs. Interstitial lung disease with pulmonary fibrosis is representative of pulmonary systemic sclerosis. $CHIT1^{-/-}$ murine models demonstrate reduced fibrosis, and *in vitro* studies showed that CHIT1 interactions with TGF-β1 augment the expression of both TGF-β 1 and 2 receptors and subsequent TGF-β-induced ERK activation [113]. Human Kupffer cells were also implemented to investigate the role of CHIT1 in nonalcoholic

steatohepatitis. This data highlighted the ability of CHIT1 to activate hepatic stellate cells which, in turn, results in the overproduction of collagen and ultimately hepatic fibrosis [114].

In our assessment of plaque morphology, despite having no difference in macrophage content or size, collagen and hyaluronic acid deposition was markedly different between experimental and control animals. *Ldlr*$^{-/-}$-CHIT1-OE mice on an atherosclerotic diet, displayed hyaluronic acid staining throughout the plaque and around necrotic cores, whereas aortic sections from control mice showed accumulation of hyaluronic acid around the periphery of the vessel. Collagen staining revealed substantial accumulation on the luminal aspect of necrotic cores in *Ldlr*$^{-/-}$-CHIT1-OE animals. In contrast, collagen distribution in control animals did not show any particular patterning in atherosclerotic plaques. Taken together, overexpression of CHIT1 by macrophages augments ECM biosynthesis and organization in such a way that enhances plaque stability in *Ldlr*$^{-/-}$-CHIT1-OE mouse models.

4.2 Limitations and future directions

The data presented in this dissertation provide novel insight into the non-enzymatic signaling properties of CHIT1 in atherosclerosis. Macrophage overexpression and secretion of CHIT1 augmented the inflammatory response of BMDM exposed to inflammatory stimuli *in vitro*. CHIT1 overexpression in ldlr$^{-/-}$ mice resulted in alterations to ECM deposits and plaque morphology *in vivo.* In lieu of our previously published findings which demonstrated that inhibition of chitinase promotes atherogenic macrophage function *in vitro* and promotes atherosclerosis in ApoE$^{-/-}$ mice [119], we sought to understand the mechanism and therapeutic potential of CHIT1 overexpression in atherosclerosis. One underlying caveat in the comparison of our previous data is that chitinase inhibition was achieved through dietary administration of allosamidin; a competitive inhibitor of all chitinases that also binds to chitinase-like proteins (CLP). Chitinases and CLPs both contain a glycosyl-18 domain which is evolutionarily conserved among the 18 glycosyl hydrolase family. In the case of CLPs, mutations in the highly conserved enzymatic sites render them enzymatically inactive and thus they are also termed chitolectins. Despite their lack of

enzymatic activity, CLPs are still able to bind chitin through conformational changes dependent on the oligosaccharide length in the same fashion as true chitinases [162]. Breast regression protein-39 (BRP-39) and its human homolog YKL-40 (Chi3l1) are CLPs that are expressed in a variety of cells including macrophages, neutrophils, and vascular smooth muscle cells. YKL-40 has been shown to inhibit cellular responses to pro-inflammatory cytokines IL-1 and TNF-α [163]. YKL-40 is also able to bind specifically to type I collagen, modulating the rate of fibril formation [164]. Other studies have indicated that the CLPs: YM1 and YM2 alternatively activate macrophages, initiating Th2-mediated inflammation [165]. The authors went on to show that macrophages can express M2 surface markers upon activation with CLPs independently of neutrophils. In many ways, the very existence of CLPs is confounding and enigmatic. However, it has become clear that both true chitinases and CLPs have signaling properties beyond any enzymatic capacity. Furthermore, their abundant secretion as a part of both M1 and M2 macrophage polarization suggests varying roles for these molecules.

CHIT1 overexpression has been described in a number of chronic conditions affecting different tissues and organ systems. These include: lysosomal storage disorders like Niemann-Pick's and Gaucher's disease [166], asthma and airway inflammation/remodeling [153, 167], and non-resolving inflammatory diseases like diabetes, atherosclerosis, and liver disease [118, 168, 169]. And although the non-enzymatic interactions of CHIT1 are poorly understood, the close association it has with sterile inflammation and tissue remodeling in the absence of an endogenous substrate make it an intriguing target for augmenting innate immunity and management of chronic inflammation.

LITERATURE CITED

1. Roth, G.A., et al., *Global, Regional, and National Burden of Cardiovascular Diseases for 10 Causes, 1990 to 2015.* Journal of the American College of Cardiology, 2017. **70**(1): p. 1-25.
2. Pagidipati, N.J. and T.A. Gaziano, *Estimating Deaths From Cardiovascular Disease: A Review of Global Methodologies of Mortality Measurement.* Circulation, 2013. **127**(6): p. 749-756.
3. Writing Group, M., et al., *Heart Disease and Stroke Statistics—2017 Update: A Report From the American Heart Association.* Circulation, 2017. **135**(10): p. e146-e603.
4. Gheorghe, A., et al., *The economic burden of cardiovascular disease and hypertension in low- and middle-income countries: a systematic review.* BMC Public Health, 2018. **18**(1): p. 975.
5. Lusis, A.J., *Atherosclerosis.* Nature, 2000. **407**(6801): p. 233-241.
6. Zaman, A.G., et al., *The role of plaque rupture and thrombosis in coronary artery disease.* Atherosclerosis, 2000. **149**(2): p. 251-266.
7. Badimon, L. and G. Vilahur, *Thrombosis formation on atherosclerotic lesions and plaque rupture.* J Intern Med, 2014. **276**(6): p. 618-32.
8. Rothwell, P.M., *Atherothrombosis and ischaemic stroke.* BMJ : British Medical Journal, 2007. **334**(7590): p. 379-380.
9. Badimon, L., T. Padró, and G. Vilahur, *Atherosclerosis, platelets and thrombosis in acute ischaemic heart disease.* European Heart Journal. Acute Cardiovascular Care, 2012. **1**(1): p. 60-74.
10. Insull, W., Jr., *The Pathology of Atherosclerosis: Plaque Development and Plaque Responses to Medical Treatment.* The American Journal of Medicine, 2009. **122**(1): p. S3-S14.
11. Fruchart, J.C., et al., *New risk factors for atherosclerosis and patient risk assessment.* Circulation, 2004. **109**(23 Suppl 1): p. Iii15-9.
12. Hackam, D.G. and S.S. Anand, *Emerging risk factors for atherosclerotic vascular disease: A critical review of the evidence.* JAMA, 2003. **290**(7): p. 932-940.
13. Altman, R., *Risk factors in coronary atherosclerosis athero-inflammation: the meeting point.* Thrombosis Journal, 2003. **1**: p. 4-4.
14. Rafieian-Kopaei, M., et al., *Atherosclerosis: Process, Indicators, Risk Factors and New Hopes.* International Journal of Preventive Medicine, 2014. **5**(8): p. 927-946.
15. Smith, S.C., Jr., *Multiple risk factors for cardiovascular disease and diabetes mellitus.* Am J Med, 2007. **120**(3 Suppl 1): p. S3-s11.
16. Wang, J.C. and M. Bennett, *Aging and atherosclerosis: mechanisms, functional consequences, and potential therapeutics for cellular senescence.* Circ Res, 2012. **111**(2): p. 245-59.
17. Head, T., S. Daunert, and P.J. Goldschmidt-Clermont, *The Aging Risk and Atherosclerosis: A Fresh Look at Arterial Homeostasis.* Frontiers in Genetics, 2017. **8**: p. 216.
18. Lansky, A.J., et al., *Gender and the Extent of Coronary Atherosclerosis, Plaque Composition, and Clinical Outcomes in Acute Coronary Syndromes.* JACC: Cardiovascular Imaging, 2012. **5**(3, Supplement): p. S62-S72.
19. Spence, J.D. and L. Pilote, *Importance of sex and gender in atherosclerosis and cardiovascular disease.* Atherosclerosis, 2015. **241**(1): p. 208-210.
20. Dunlay, S.M. and V.L. Roger, *Gender Differences in the Pathophysiology, Clinical Presentation, and Outcomes of Ischemic Heart Failure.* Current heart failure reports, 2012. **9**(4): p. 267-276.
21. Pérez-López, F.R., et al., *Gender Differences in Cardiovascular Disease: Hormonal and Biochemical Influences.* Reproductive sciences (Thousand Oaks, Calif.), 2010. **17**(6): p. 511-531.
22. Rossouw, J.E., *Hormones, genetic factors, and gender differences in cardiovascular disease.* Cardiovascular Research, 2002. **53**(3): p. 550-557.

23. Bowling Meaghan, R., et al., *Estrogen Effects on Vascular Inflammation Are Age Dependent.* Arteriosclerosis, Thrombosis, and Vascular Biology, 2014. **34**(7): p. 1477-1485.
24. Novella, S., et al., *Effects of estrogen on vascular inflammation: a matter of timing.* Arterioscler Thromb Vasc Biol, 2012. **32**(8): p. 2035-42.
25. Giordano, S., et al., *Estrogen and Cardiovascular Disease: Is Timing Everything?* Am J Med Sci, 2015. **350**(1): p. 27-35.
26. Watkins, H. and M. Farrall, *Genetic susceptibility to coronary artery disease: from promise to progress.* Nature Reviews Genetics, 2006. **7**: p. 163.
27. Lusis, A.J., *Genetics of Atherosclerosis.* Trends in Genetics, 2012. **28**(6): p. 267-275.
28. Xu, C., et al., *Candidate Pathway-Based Genome-Wide Association Studies Identify Novel Associations of Genomic Variants in the Complement System Associated With Coronary Artery Disease.* Circulation: Cardiovascular Genetics, 2014. **7**(6): p. 887.
29. Wouters, K., et al., *Understanding hyperlipidemia and atherosclerosis: lessons from genetically modified apoe and ldlr mice.* Clin Chem Lab Med, 2005. **43**(5): p. 470-9.
30. Manjunath, C., et al., *Atherogenic dyslipidemia.* Indian Journal of Endocrinology and Metabolism, 2013. **17**(6): p. 969-976.
31. Steinberg, D., *The LDL modification hypothesis of atherogenesis: an update.* Journal of lipid research, 2009. **50 Suppl**(Suppl): p. S376-S381.
32. Blankenberg, S., S. Barbaux, and L. Tiret, *Adhesion molecules and atherosclerosis.* Atherosclerosis, 2003. **170**(2): p. 191-203.
33. Galkina, E. and K. Ley, *Vascular Adhesion Molecules in Atherosclerosis.* Arteriosclerosis, Thrombosis, and Vascular Biology, 2007. **27**(11): p. 2292.
34. Sprague, A.H. and R.A. Khalil, *Inflammatory cytokines in vascular dysfunction and vascular disease.* Biochemical pharmacology, 2009. **78**(6): p. 539-552.
35. Gargiulo, S., M. Gramanzini, and M. Mancini, *Molecular Imaging of Vulnerable Atherosclerotic Plaques in Animal Models.* 2016. **17**(9): p. 1511.
36. Libby, P., *Inflammation in atherosclerosis.* Arterioscler Thromb Vasc Biol, 2012. **32**(9): p. 2045-51.
37. Yu, X.H., et al., *Foam cells in atherosclerosis.* Clin Chim Acta, 2013. **424**: p. 245-52.
38. Galkina, E. and K. Ley, *Immune and Inflammatory Mechanisms of Atherosclerosis.* Annual review of immunology, 2009. **27**: p. 165-197.
39. Bentzon Jacob, F., et al., *Mechanisms of Plaque Formation and Rupture.* Circulation Research, 2014. **114**(12): p. 1852-1866.
40. Newby, A.C. and A.B. Zaltsman, *Fibrous cap formation or destruction--the critical importance of vascular smooth muscle cell proliferation, migration and matrix formation.* Cardiovasc Res, 1999. **41**(2): p. 345-60.
41. Halvorsen, B., et al., *Atherosclerotic Plaque Stability—What Determines the Fate of a Plaque?* Progress in Cardiovascular Diseases, 2008. **51**(3): p. 183-194.
42. van der Wal, A.C. and A.E. Becker, *Atherosclerotic plaque rupture – pathologic basis of plaque stability and instability.* Cardiovascular Research, 1999. **41**(2): p. 334-344.
43. Moore, K.J. and I. Tabas, *Macrophages in the pathogenesis of atherosclerosis.* Cell, 2011. **145**(3): p. 341-55.
44. Martinet, W., D.M. Schrijvers, and G.R. De Meyer, *Necrotic cell death in atherosclerosis.* Basic Res Cardiol, 2011. **106**(5): p. 749-60.
45. Newby, A.C., *Metalloproteinases promote plaque rupture and myocardial infarction: A persuasive concept waiting for clinical translation.* Matrix Biology, 2015. **44-46**: p. 157-166.

46. Newby Andrew, C., *Metalloproteinase Expression in Monocytes and Macrophages and its Relationship to Atherosclerotic Plaque Instability.* Arteriosclerosis, Thrombosis, and Vascular Biology, 2008. **28**(12): p. 2108-2114.
47. Newby, A.C., *Matrix metalloproteinases regulate migration, proliferation, and death of vascular smooth muscle cells by degrading matrix and non-matrix substrates.* Cardiovascular Research, 2006. **69**(3): p. 614-624.
48. Visse, R., H. Nagase, and G. Murphy, *Structure and function of matrix metalloproteinases and TIMPs.* Cardiovascular Research, 2006. **69**(3): p. 562-573.
49. Johnson Jason, L., et al., *Low Tissue Inhibitor of Metalloproteinases 3 and High Matrix Metalloproteinase 14 Levels Defines a Subpopulation of Highly Invasive Foam-Cell Macrophages.* Arteriosclerosis, Thrombosis, and Vascular Biology, 2008. **28**(9): p. 1647-1653.
50. Newby, A.C., *Dual Role of Matrix Metalloproteinases (Matrixins) in Intimal Thickening and Atherosclerotic Plaque Rupture.* Physiological Reviews, 2005. **85**(1): p. 1-31.
51. Hansson, G.K. and A. Hermansson, *The immune system in atherosclerosis.* Nature Immunology, 2011. **12**: p. 204.
52. Colin, S., G. Chinetti-Gbaguidi, and B. Staels, *Macrophage phenotypes in atherosclerosis.* 2014. **262**(1): p. 153-166.
53. Peled, M. and E.A. Fisher, *Dynamic Aspects of Macrophage Polarization during Atherosclerosis Progression and Regression.* Frontiers in Immunology, 2014. **5**: p. 579.
54. Leonard, E.J., et al., *Secretion of monocyte chemoattractant protein-1 (MCP-1) by human mononuclear phagocytes.* Adv Exp Med Biol, 1993. **351**: p. 55-64.
55. Ushach, I. and A. Zlotnik, *Biological role of granulocyte macrophage colony-stimulating factor (GM-CSF) and macrophage colony-stimulating factor (M-CSF) on cells of the myeloid lineage.* Journal of leukocyte biology, 2016. **100**(3): p. 481-489.
56. Cho, K.Y., et al., *The phenotype of infiltrating macrophages influences arteriosclerotic plaque vulnerability in the carotid artery.* J Stroke Cerebrovasc Dis, 2013. **22**(7): p. 910-8.
57. Shaikh, S., et al., *Macrophage subtypes in symptomatic carotid artery and femoral artery plaques.* Eur J Vasc Endovasc Surg, 2012. **44**(5): p. 491-7.
58. Stöger, J.L., et al., *Distribution of macrophage polarization markers in human atherosclerosis.* Atherosclerosis, 2012. **225**(2): p. 461-468.
59. Mosser, D.M., *The many faces of macrophage activation.* J Leukoc Biol, 2003. **73**(2): p. 209-12.
60. Jung, M., et al., *IL-10 improves cardiac remodeling after myocardial infarction by stimulating M2 macrophage polarization and fibroblast activation.* Basic Research in Cardiology, 2017. **112**(3): p. 33.
61. Jablonski, K.A., et al., *Novel Markers to Delineate Murine M1 and M2 Macrophages.* PLOS ONE, 2015. **10**(12): p. e0145342.
62. Sheng, J., et al., *M2 macrophage-mediated interleukin-4 signalling induces myofibroblast phenotype during the progression of benign prostatic hyperplasia.* Cell Death & Disease, 2018. **9**(7): p. 755.
63. Parisi, L., et al., *Macrophage Polarization in Chronic Inflammatory Diseases: Killers or Builders? %J Journal of Immunology Research.* 2018. **2018**: p. 25.
64. Zhang, X. and D.M. Mosser, *Macrophage activation by endogenous danger signals.* The Journal of pathology, 2008. **214**(2): p. 161-178.
65. Mantovani, A., C. Garlanda, and M. Locati, *Macrophage Diversity and Polarization in Atherosclerosis.* Arteriosclerosis, Thrombosis, and Vascular Biology, 2009. **29**(10): p. 1419-1423.
66. Moore, K.J., F.J. Sheedy, and E.A. Fisher, *Macrophages in atherosclerosis: a dynamic balance.* Nature Reviews Immunology, 2013. **13**: p. 709.

67. Williams, J.W., et al., *Macrophage Biology, Classification, and Phenotype in Cardiovascular Disease: JACC Macrophage in CVD Series (Part 1).* Journal of the American College of Cardiology, 2018. **72**(18): p. 2166-2180.
68. Khallou-Laschet, J., et al., *Macrophage plasticity in experimental atherosclerosis.* PLoS One, 2010. **5**(1): p. e8852.
69. Kadl, A., et al., *Identification of a novel macrophage phenotype that develops in response to atherogenic phospholipids via Nrf2.* Circulation research, 2010. **107**(6): p. 737-746.
70. Liao, X., et al., *Krüppel-like factor 4 regulates macrophage polarization.* The Journal of clinical investigation, 2011. **121**(7): p. 2736-2749.
71. de Villiers, W.J. and E.J. Smart, *Macrophage scavenger receptors and foam cell formation.* J Leukoc Biol, 1999. **66**(5): p. 740-6.
72. Kruth, H.S., *Fluid-phase pinocytosis of LDL by macrophages: a novel target to reduce macrophage cholesterol accumulation in atherosclerotic lesions.* Curr Pharm Des, 2013. **19**(33): p. 5865-72.
73. Moore, K.J. and M.W. Freeman, *Scavenger Receptors in Atherosclerosis.* Beyond Lipid Uptake, 2006. **26**(8): p. 1702-1711.
74. Bottalico, L.A., et al., *Transforming growth factor-beta 1 inhibits scavenger receptor activity in THP-1 human macrophages.* J Biol Chem, 1991. **266**(34): p. 22866-71.
75. Pluddemann, A., C. Neyen, and S. Gordon, *Macrophage scavenger receptors and host-derived ligands.* Methods, 2007. **43**(3): p. 207-17.
76. Babaev, V.R., et al., *Reduced atherosclerotic lesions in mice deficient for total or macrophage-specific expression of scavenger receptor-A.* Arterioscler Thromb Vasc Biol, 2000. **20**(12): p. 2593-9.
77. Suzuki, H., et al., *A role for macrophage scavenger receptors in atherosclerosis and susceptibility to infection.* Nature, 1997. **386**(6622): p. 292-6.
78. Babaev Vladimir, R., et al., *Reduced Atherosclerotic Lesions in Mice Deficient for Total or Macrophage-Specific Expression of Scavenger Receptor-A.* Arteriosclerosis, Thrombosis, and Vascular Biology, 2000. **20**(12): p. 2593-2599.
79. Marcovecchio, P.M., et al., *Scavenger Receptor CD36 Directs Nonclassical Monocyte Patrolling Along the Endothelium During Early Atherogenesis.* Arteriosclerosis, thrombosis, and vascular biology, 2017. **37**(11): p. 2043-2052.
80. Hong, C. and P. Tontonoz, *Coordination of inflammation and metabolism by PPAR and LXR nuclear receptors.* Current opinion in genetics & development, 2008. **18**(5): p. 461-467.
81. Andersson, U., et al., *High mobility group 1 protein (HMG-1) stimulates proinflammatory cytokine synthesis in human monocytes.* J Exp Med, 2000. **192**(4): p. 565-70.
82. Newton, K. and V.M. Dixit, *Signaling in innate immunity and inflammation.* Cold Spring Harb Perspect Biol, 2012. **4**(3).
83. Landry, Y.D., et al., *ATP-binding cassette transporter A1 expression disrupts raft membrane microdomains through its ATPase-related functions.* J Biol Chem, 2006. **281**(47): p. 36091-101.
84. Boadu, E. and G.A. Francis, *The role of vesicular transport in ABCA1-dependent lipid efflux and its connection with NPC pathways.* Journal of Molecular Medicine, 2006. **84**(4): p. 266-275.
85. Vaughan, A.M. and J.F. Oram, *ABCG1 redistributes cell cholesterol to domains removable by high density lipoprotein but not by lipid-depleted apolipoproteins.* J Biol Chem, 2005. **280**(34): p. 30150-7.
86. Westerterp, M., et al., *Deficiency of ABCA1 and ABCG1 in Macrophages Increases Inflammation and Accelerates Atherosclerosis in Mice.* Circulation research, 2013. **112**(11): p. 10.1161/CIRCRESAHA.113.301086.

87. Park, J.G., et al., *Evaluation of VCAM-1 antibodies as therapeutic agent for atherosclerosis in apolipoprotein E-deficient mice.* Atherosclerosis, 2013. **226**(2): p. 356-63.
88. Dinarello, C.A., *Interleukin-1 in the pathogenesis and treatment of inflammatory diseases.* Blood, 2011. **117**(14): p. 3720-32.
89. Libby, P., *Interleukin-1 Beta as a Target for Atherosclerosis Therapy: Biological Basis of CANTOS and Beyond.* J Am Coll Cardiol, 2017. **70**(18): p. 2278-2289.
90. Ridker, P.M., et al., *Antiinflammatory Therapy with Canakinumab for Atherosclerotic Disease.* New England Journal of Medicine, 2017. **377**(12): p. 1119-1131.
91. Tanaka, T., M. Narazaki, and T. Kishimoto, *IL-6 in Inflammation, Immunity, and Disease.* 2014. **6**(10).
92. Collaboration, I.R.G.C.E.R.F., et al., *Interleukin-6 receptor pathways in coronary heart disease: a collaborative meta-analysis of 82 studies.* Lancet (London, England), 2012. **379**(9822): p. 1205-1213.
93. Schieffer, B., et al., *Impact of interleukin-6 on plaque development and morphology in experimental atherosclerosis.* Circulation, 2004. **110**(22): p. 3493-500.
94. Davis, N., E. Mor, and R. Ashery-Padan, *Roles for Dicer1 in the patterning and differentiation of the optic cup neuroepithelium.* Development, 2011. **138**(1): p. 127-38.
95. Han, J., et al., *The Drosha-DGCR8 complex in primary microRNA processing.* Genes Dev, 2004. **18**(24): p. 3016-27.
96. Lee, Y., et al., *MicroRNA genes are transcribed by RNA polymerase II.* Embo j, 2004. **23**(20): p. 4051-60.
97. Huang, R.S., et al., *MicroRNA-155 silencing enhances inflammatory response and lipid uptake in oxidized low-density lipoprotein-stimulated human THP-1 macrophages.* J Investig Med, 2010. **58**(8): p. 961-7.
98. Tharanathan, R.N. and F.S. Kittur, *Chitin--the undisputed biomolecule of great potential.* Crit Rev Food Sci Nutr, 2003. **43**(1): p. 61-87.
99. Bueter, C.L., C.A. Specht, and S.M. Levitz, *Innate Sensing of Chitin and Chitosan.* PLOS Pathogens, 2013. **9**(1): p. e1003080.
100. Da Silva, C.A., et al., *TLR-2 and IL-17A in chitin-induced macrophage activation and acute inflammation.* J Immunol, 2008. **181**(6): p. 4279-86.
101. Zhu, Z., et al., *Acidic mammalian chitinase in asthmatic Th2 inflammation and IL-13 pathway activation.* Science, 2004. **304**(5677): p. 1678-82.
102. Kim, L.K., et al., *AMCase is a crucial regulator of type 2 immune responses to inhaled house dust mites.* Proc Natl Acad Sci U S A, 2015. **112**(22): p. E2891-9.
103. Fusetti, F., et al., *Structure of human chitotriosidase. Implications for specific inhibitor design and function of mammalian chitinase-like lectins.* J Biol Chem, 2002. **277**(28): p. 25537-44.
104. Fadel, F., et al., *X-Ray Crystal Structure of the Full Length Human Chitotriosidase (CHIT1) Reveals Features of Its Chitin Binding Domain.* PLOS ONE, 2016. **11**(4): p. e0154190.
105. Renkema, G.H., et al., *Synthesis, sorting, and processing into distinct isoforms of human macrophage chitotriosidase.* Eur J Biochem, 1997. **244**(2): p. 279-85.
106. Renkema, G.H., et al., *Purification and characterization of human chitotriosidase, a novel member of the chitinase family of proteins.* J Biol Chem, 1995. **270**(5): p. 2198-202.
107. Crasson, O., et al., *Human Chitotriosidase: Catalytic Domain or Carbohydrate Binding Module, Who's Leading HCHT's Biological Function.* Scientific Reports, 2017. **7**(1): p. 2768.
108. Ujita, M., et al., *Carbohydrate Binding Specificity of the Recombinant Chitin-binding Domain of Human Macrophage Chitinase.* Bioscience, Biotechnology, and Biochemistry, 2003. **67**(11): p. 2402-2407.

109. Żurawska-Płaksej, E., et al., *Neutrophils as a Source of Chitinases and Chitinase-Like Proteins in Type 2 Diabetes.* PloS one, 2015. **10**(10): p. e0141730-e0141730.
110. Lo, S.M., et al., *Misdiagnosis of Niemann-Pick disease type C as Gaucher disease.* J Inherit Metab Dis, 2010. **33 Suppl 3**: p. S429-33.
111. Schofield, J.P., *Metabolic and molecular basis of inherited disease: paper versus electronic media.* Molecular Medicine Today, 1995. **1**(9): p. 399.
112. Steen, V.D. and T.A. Medsger, *Changes in causes of death in systemic sclerosis, 1972-2002.* Ann Rheum Dis, 2007. **66**(7): p. 940-4.
113. Lee, C.G., et al., *Chitinase 1 is a biomarker for and therapeutic target in scleroderma-associated interstitial lung disease that augments TGF-β1 signaling.* Journal of immunology (Baltimore, Md. : 1950), 2012. **189**(5): p. 2635-2644.
114. Malaguarnera, L., et al., *Chitotriosidase gene expression in Kupffer cells from patients with non-alcoholic fatty liver disease.* Gut, 2006. **55**(9): p. 1313-1320.
115. Correale, J. and M. Fiol, *Chitinase effects on immune cell response in neuromyelitis optica and multiple sclerosis.* Multiple Sclerosis Journal, 2010. **17**(5): p. 521-531.
116. Karadag, B., et al., *Serum chitotriosidase activity in patients with coronary artery disease.* Circ J, 2008. **72**(1): p. 71-5.
117. Fach, E.M., et al., *In vitro biomarker discovery for atherosclerosis by proteomics.* Mol Cell Proteomics, 2004. **3**(12): p. 1200-10.
118. Artieda, M., et al., *Serum Chitotriosidase Activity Is Increased in Subjects With Atherosclerosis Disease.* Arteriosclerosis, Thrombosis, and Vascular Biology, 2003. **23**(9): p. 1645-1652.
119. Kitamoto, S., et al., *Chitinase inhibition promotes atherosclerosis in hyperlipidemic mice.* Am J Pathol, 2013. **183**(1): p. 313-25.
120. McGovern, K.E. and E.H. Wilson, *Role of Chemokines and Trafficking of Immune Cells in Parasitic Infections.* Current immunology reviews, 2013. **9**(3): p. 157-168.
121. Gijsbers, K., et al., *CXCR1-binding chemokines in inflammatory bowel diseases: down-regulated IL-8/CXCL8 production by leukocytes in Crohn's disease and selective GCP-2/CXCL6 expression in inflamed intestinal tissue.* Eur J Immunol, 2004. **34**(7): p. 1992-2000.
122. Bonecchi, R., et al., *Induction of Functional IL-8 Receptors by IL-4 and IL-13 in Human Monocytes.* The Journal of Immunology, 2000. **164**(7): p. 3862.
123. Cao, H., et al., *Leptin promotes migration and invasion of breast cancer cells by stimulating IL-8 production in M2 macrophages.* Oncotarget, 2016. **7**(40): p. 65441-65453.
124. Harrington, J.R., *The Role of MCP-1 in Atherosclerosis.* STEM CELLS, 2000. **18**(1): p. 65-66.
125. Juntang, L., K. Vijay, and L. Xinjie, *Impact of MCP -1 in Atherosclerosis.* Current Pharmaceutical Design, 2014. **20**(28): p. 4580-4588.
126. Boisvert, W.A., et al., *Up-regulated expression of the CXCR2 ligand KC/GRO-alpha in atherosclerotic lesions plays a central role in macrophage accumulation and lesion progression.* The American journal of pathology, 2006. **168**(4): p. 1385-1395.
127. Yue, T.L., et al., *Interleukin-8. A mitogen and chemoattractant for vascular smooth muscle cells*. Vol. 75. 1994. 1-7.
128. Boisvert, W.A., et al., *A leukocyte homologue of the IL-8 receptor CXCR-2 mediates the accumulation of macrophages in atherosclerotic lesions of LDL receptor-deficient mice.* The Journal of clinical investigation, 1998. **101**(2): p. 353-363.
129. Simonini, A., et al., *IL-8 Is an Angiogenic Factor in Human Coronary Atherectomy Tissue.* Circulation, 2000. **101**(13): p. 1519-1526.
130. Koch, A.E., et al., *Interleukin-8 as a macrophage-derived mediator of angiogenesis.* Science, 1992. **258**(5089): p. 1798.

131. Qin, H., et al., *SOCS3 deficiency promotes M1 macrophage polarization and inflammation.* Journal of immunology (Baltimore, Md. : 1950), 2012. **189**(7): p. 3439-3448.
132. Whyte, C.S., et al., *Suppressor of cytokine signaling (SOCS)1 is a key determinant of differential macrophage activation and function.* Journal of Leukocyte Biology, 2011. **90**(5): p. 845-854.
133. Bosurgi, L., et al., *Macrophage function in tissue repair and remodeling requires IL-4 or IL-13 with apoptotic cells.* Science, 2017. **356**(6342): p. 1072.
134. George, J., et al., *Requisite role for interleukin-4 in the acceleration of fatty streaks induced by heat shock protein 65 or Mycobacterium tuberculosis.* Circ Res, 2000. **86**(12): p. 1203-10.
135. King, V.L., S.J. Szilvassy, and A. Daugherty, *Interleukin-4 deficiency decreases atherosclerotic lesion formation in a site-specific manner in female LDL receptor-/- mice.* Arterioscler Thromb Vasc Biol, 2002. **22**(3): p. 456-61.
136. Davenport, P. and P.G. Tipping, *The role of interleukin-4 and interleukin-12 in the progression of atherosclerosis in apolipoprotein E-deficient mice.* The American journal of pathology, 2003. **163**(3): p. 1117-1125.
137. Kitabayashi, A., et al., *Granulocyte colony-stimulating factor downregulates allogeneic immune responses by posttranscriptional inhibition of tumor necrosis factor- alpha production.* Blood, 1995. **86**(6): p. 2220.
138. Rutella, S., et al., *Granulocyte colony-stimulating factor promotes the generation of regulatory DC through induction of IL-10 and IFN-α.* European Journal of Immunology, 2004. **34**(5): p. 1291-1302.
139. Sinha, S.K., et al., *Effects of G-CSF on serum cholesterol and development of atherosclerotic plaque in apolipoprotein E-deficient mice.* International journal of clinical and experimental medicine, 2014. **7**(8): p. 1979-1989.
140. Hasegawa, H., et al., *G-CSF prevents the progression of atherosclerosis and neointimal formation in rabbits.* Biochemical and Biophysical Research Communications, 2006. **344**(1): p. 370-376.
141. Matsumoto, T., et al., *Appropriate doses of Granulocyte-Colony Stimulating Factor Reduced Atherosclerotic Plaque Formation and Increased Plaque Stability in Cholesterol-Fed Rabbits.* Journal of Atherosclerosis and Thrombosis, 2010. **17**(1): p. 84-96.
142. Boesten, L.S.M., et al., *Tumor necrosis factor-α promotes atherosclerotic lesion progression in APOE*3-leiden transgenic mice.* Cardiovascular Research, 2005. **66**(1): p. 179-185.
143. Brånén, L., et al., *Inhibition of Tumor Necrosis Factor-α Reduces Atherosclerosis in Apolipoprotein E Knockout Mice.* Arteriosclerosis, Thrombosis, and Vascular Biology, 2004. **24**(11): p. 2137-2142.
144. Fernando, M.R., et al., *The Pro-Inflammatory Cytokine, Interleukin-6, Enhances the Polarization of Alternatively Activated Macrophages.* PLOS ONE, 2014. **9**(4): p. e94188.
145. Huber, S.A., et al., *Interleukin-6 Exacerbates Early Atherosclerosis in Mice.* Arteriosclerosis, Thrombosis, and Vascular Biology, 1999. **19**(10): p. 2364-2367.
146. Dumitru, C.D., et al., *TNF-α Induction by LPS Is Regulated Posttranscriptionally via a Tpl2/ERK-Dependent Pathway.* Cell, 2000. **103**(7): p. 1071-1083.
147. Li, N., et al., *ERK Is Integral to the IFN-γ–Mediated Activation of STAT1, the Expression of Key Genes Implicated in Atherosclerosis, and the Uptake of Modified Lipoproteins by Human Macrophages.* The Journal of Immunology, 2010. **185**(5): p. 3041.
148. Taganov, K.D., et al., *NF-κB-dependent induction of microRNA miR-146, an inhibitor targeted to signaling proteins of innate immune responses.* Proceedings of the National Academy of Sciences, 2006. **103**(33): p. 12481.
149. Chassin, C., et al., *miR-146a mediates protective innate immune tolerance in the neonate intestine.* Cell Host Microbe, 2010. **8**(4): p. 358-68.

150. Li, Y., et al., *Functions of miR-146a and miR-222 in Tumor-associated Macrophages in Breast Cancer.* Sci Rep, 2015. **5**: p. 18648.
151. Zhai, C., et al., *Selective Inhibition of PI3K/Akt/mTOR Signaling Pathway Regulates Autophagy of Macrophage and Vulnerability of Atherosclerotic Plaque.* PLOS ONE, 2014. **9**(3): p. e90563.
152. Hong, J.Y., et al., *Chitotriosidase inhibits allergic asthmatic airways via regulation of TGF-β expression and Foxp3+ Treg cells.* Allergy, 2018. **73**(8): p. 1686-1699.
153. Cho, S.J., M.D. Weiden, and C.G. Lee, *Chitotriosidase in the Pathogenesis of Inflammation, Interstitial Lung Diseases and COPD.* Allergy, asthma & immunology research, 2015. **7**(1): p. 14-21.
154. Litwiniuk, M., et al., *Hyaluronic Acid in Inflammation and Tissue Regeneration.* Wounds, 2016. **28**(3): p. 78-88.
155. Evanko Stephen, P., C. Angello John, and N. Wight Thomas, *Formation of Hyaluronan- and Versican-Rich Pericellular Matrix Is Required for Proliferation and Migration of Vascular Smooth Muscle Cells.* Arteriosclerosis, Thrombosis, and Vascular Biology, 1999. **19**(4): p. 1004-1013.
156. Bot, P.T., et al., *Hyaluronic acid metabolism is increased in unstable plaques.* European Journal of Clinical Investigation, 2010. **40**(9): p. 818-827.
157. Semino, C.E., et al., *Homologs of the Xenopus developmental gene DG42 are present in zebrafish and mouse and are involved in the synthesis of Nod-like chitin oligosaccharides during early embryogenesis.* Proceedings of the National Academy of Sciences, 1996. **93**(10): p. 4548-4553.
158. Meyer, M.F. and G. Kreil, *Cells expressing the DG42 gene from early Xenopus embryos synthesize hyaluronan.* Proceedings of the National Academy of Sciences, 1996. **93**(10): p. 4543-4547.
159. Rocnik, E.F., B.M. Chan, and J.G. Pickering, *Evidence for a role of collagen synthesis in arterial smooth muscle cell migration.* J Clin Invest, 1998. **101**(9): p. 1889-98.
160. Koyama, H., et al., *Fibrillar collagen inhibits arterial smooth muscle proliferation through regulation of Cdk2 inhibitors.* Cell, 1996. **87**(6): p. 1069-78.
161. Wesley, R.B., 2nd, et al., *Extracellular matrix modulates macrophage functions characteristic to atheroma: collagen type I enhances acquisition of resident macrophage traits by human peripheral blood monocytes in vitro.* Arterioscler Thromb Vasc Biol, 1998. **18**(3): p. 432-40.
162. Fusetti, F., et al., *Crystal Structure and Carbohydrate-binding Properties of the Human Cartilage Glycoprotein-39.* Journal of Biological Chemistry, 2003. **278**(39): p. 37753-37760.
163. Ling, H. and A.D. Recklies, *The chitinase 3-like protein human cartilage glycoprotein 39 inhibits cellular responses to the inflammatory cytokines interleukin-1 and tumour necrosis factor-alpha.* Biochemical Journal, 2004. **380**(3): p. 651.
164. Bigg, H.F., et al., *The Mammalian Chitinase-like Lectin, YKL-40, Binds Specifically to Type I Collagen and Modulates the Rate of Type I Collagen Fibril Formation.* Journal of Biological Chemistry, 2006. **281**(30): p. 21082-21095.
165. Muallem, G. and C.A. Hunter, *ParadYm shift: Ym1 and Ym2 as innate immunological regulators of IL-17.* Nature Immunology, 2014. **15**: p. 1099.
166. Guo, Y., et al., *Elevated plasma chitotriosidase activity in various lysosomal storage disorders.* Journal of Inherited Metabolic Disease, 1995. **18**(6): p. 717-722.
167. Létuvé, S., et al., *Lung chitinolytic activity and chitotriosidase are elevated in chronic obstructive pulmonary disease and contribute to lung inflammation.* The American journal of pathology, 2010. **176**(2): p. 638-649.
168. Di Rosa, M. and L. Malaguarnera, *Chitotriosidase: A New Inflammatory Marker in Diabetic Complications.* Pathobiology, 2016. **83**(4): p. 211-219.
169. Malaguarnera, L., et al., *Potential Role of Chitotriosidase Gene in Nonalcoholic Fatty Liver Disease Evolution.* The American Journal Of Gastroenterology, 2006. **101**: p. 2060.